

**UNIVERSITÀ DEGLI STUDI DI PADOVA**

**DIPARTIMENTO DI INGEGNERIA INDUSTRIALE**  
**Corso di laurea Magistrale in Ingegneria Energetica**

**Tesi di laurea Magistrale in**  
**Ingegneria Energetica**

**Dynamic Model of an Organic Rankine Cycle**  
**System Exploiting Low Grade Waste Heat on**  
**board a LNG Carrier**

*Relatore: Prof. Andrea Lazzaretto*

*Correlatore: Ph.D. Sergio Rech*

*Laureando: Daniele Malandrin*

ANNO ACCADEMICO 2013 – 2014



# SOMMARIO

Questo lavoro presenta il modello dinamico di off-design per un ciclo Rankine a fluido organico (ORC) che sfrutta il calore di scarto a bassa temperatura rilasciato dall'impianto motore di una reale nave metaniera. Il primo passo del lavoro è stato sviluppare il modello di design di ciascun componente dell'impianto ORC. A tal scopo si sono considerati i cicli termodinamici ottimizzati presentati in un precedente lavoro del gruppo di ricerca. Basandosi sui risultati ottenuti nella fase di dimensionamento preliminare, si è costruito il modello dinamico di ciascun componente. Si è scelto l'approccio di soluzione sequenziale, il quale consente di realizzare una modellazione ad oggetti. Ciò significa che ciascun componente dell'impianto ORC è stato modellizzato come un elemento singolo. Di conseguenza, il modello globale del sistema energetico deriva dall'interconnessione dei singoli blocchi, facenti riferimento ciascuno ad un componente reale dell'impianto. I modelli realizzati seguendo questo approccio possono essere facilmente modificati, ed adattati alla simulazione di sistemi energetici diversi dall'originale. Gli scambiatori di calore, evaporatore e condensatore in primis, influenzano fortemente la risposta dinamica dell'intero sistema. Essi sono stati, quindi, oggetto di un lavoro di modellizzazione particolarmente attento, basato sull'applicazione del metodo dei volumi finiti. Le equazioni di bilancio caratterizzanti i modelli sono state risolte in forma differenziale, portando al calcolo delle derivate temporali delle variabili di stato del sistema. Nel modello complessivo, anche le capacità sono state modellizzate come componenti dinamici, mentre per le turbomacchine si sono realizzati modelli stazionari. I modelli sono stati applicati alla simulazione dinamica di due impianti ORC, che recuperano il calore di scarto a bassa temperatura a bordo di una reale nave metaniera. Le simulazioni hanno permesso di valutare la risposta dinamica di un ciclo ORC surriscaldato, con R-134a impiegato come fluido di lavoro, e di un ciclo ORC a vapore saturo operante con R-245fa. Il primo genera una potenza elettrica di circa 405 kW<sub>el</sub>, mentre il secondo produce circa 425 kW<sub>el</sub>. Durante le simulazioni, l'input termico dell'impianto è stato modulato in funzione della velocità di servizio della nave, considerando una leggera (test case A) ed una brusca (test case B) variazione della velocità. I risultati dimostrano che il modello può riprodurre la risposta dinamica dell'impianto ORC durante funzionamento transitorio. Inoltre, sulla base dei risultati ottenuti si è definito un sistema di controllo in grado di evitare il completo riempimento e svuotamento delle capacità presenti nell'impianto.



# ABSTRACT

This work presents an off-design dynamic model of an Organic Rankine Cycle (ORC) exploiting low grade waste heat rejected by the power generating plant of a real Liquefied Natural Gas (LNG) carrier. First step was to develop a design model for the components of the ORC system. This was done starting from the optimal thermodynamic cycle resulting from a previous work of the research group. Basing on the results of the preliminary design process, off-design dynamic model was built. Sequential approach has been choose to numerically solve it, allowing an object-oriented modeling process. Each component of the ORC system was modelled separately, as a single block. Thus, overall model of the energy system derives from the interconnection of blocks referring to real components. Models built in this way can be easily modified and used to simulate different energy systems. Great effort was dedicated to the dynamic modelling of heat exchangers, particularly evaporator and condenser, since their behaviour strongly influences dynamic response of the overall system. Finite volume method was adopted to model heat exchangers. Time derivative of state variables were calculated from differential form of mass and energy balance equations. In the model, also capacities are dynamically modelled, while the models of turbomachinery (feed pump and turbine) are static. Models have been used to simulate the off-design dynamic behaviour of two ORC power plant exploiting low grade waste heat on board a LNG carrier. Simulations investigated a superheated ORC, with R-134a as working fluid, and a saturated ORC with R-245fa as working fluid. The former has an electrical output of about 405 kW<sub>el</sub>, while the latter generates an electrical output of about 425 kW<sub>el</sub>. During simulations, ORC's heat flow input was varied in function of the service speed of the carrier, considering a mild (test case A) and a brutal (test case B) variation of the speed. Results show that the developed model can represent transient response of the ORC, and allow a control system that avoid complete filling or emptying of the capacities to be defined.



# Table of Contents

SOMMARIO .....	1
ABSTRACT.....	3
Table of Contents.....	5
INTRODUCTION.....	9
<b>1 CONCEPTS AND APPLICATIONS OF ORGANIC RANKINE CYCLES.....</b>	<b>11</b>
1.1 Introduction.....	11
1.2 Organic Rankine Cycles working principles.....	11
1.2.1 Simple and regenerative cycles.....	12
1.2.2 Subcritical and Supercritical cycles.....	13
1.3 Working fluids choice in ORC power plants.....	15
1.4 Comparison between water steam Rankine cycle and ORC.....	17
1.5 Main ORC applications.....	21
1.5.1 ORC in WHR applications.....	21
1.5.2 ORC biomass power plants.....	23
1.5.3 ORC application in binary geothermal power plants.....	24
1.5.4 ORC applications in solar power plants.....	26
1.6 Summary.....	27
<b>2 MODELING OF THERMODYNAMIC SYSTEMS.....</b>	<b>29</b>
2.1 Introduction.....	29
2.2 Classification and definition of thermodynamic and fluid systems models	30
2.3 System modeling approaches.....	34
2.3.1 Sequential approach.....	34
2.3.2 Simultaneous approach.....	34
2.3.3 Comparison between Sequential and Simultaneous approaches.....	35
2.4 Review of thermal and energy systems dynamic models.....	35
2.4.1 Dynamic modeling techniques.....	35
2.5 Summary.....	38
<b>3 DYNAMIC MODEL OF AN ORGANIC RANKINE CYCLE SYSTEM.....</b>	<b>39</b>
3.1 Introduction.....	39
3.2 Static model of a counterflow heat exchanger based on the $\varepsilon$ -NTU method	39
3.3 Dynamic models of heat exchangers.....	43
3.3.1 Heat exchanger with no phase change.....	44
3.3.1.1 Internal pipe: organic fluid side.....	45
3.3.1.2 Annulus: water side.....	45
3.3.1.3 Single-phase heat exchange correlations.....	46
3.3.1.4 Simulink® model of single-phase heat exchanger.....	49
3.3.2 Heat exchanger with phase change.....	50

3.3.2.1	Internal pipe: organic fluid side.....	54
3.3.2.2	Phase-change heat flux correlations: evaporation and condensation 55	
3.3.2.3	Simulink® model of heat exchanger with phase change .....	59
3.4	Dynamic models of capacities.....	63
3.4.1	Hot drum .....	63
3.4.2	Cold drum .....	65
3.5	Turbomachinery .....	66
3.5.1	The pump model .....	66
3.5.2	The turbine model.....	69
3.6	Summary.....	71
4	APPLICATION OF THE DYNAMIC MODELS TO AN ICES-ORC COMBINED CYCLE ON BOARD AN LNG CARRIER.....	72
4.1	Introduction.....	72
4.2	Energy system of the current ship .....	72
4.2.1	ICES of the electrical power generating plant: description and energy balance .....	72
4.2.2	Power demands of the current ship .....	76
4.2.3	Operating point of the vessel's energy system.....	78
4.2.4	ICES-ORC combined cycle: integration of the energy systems.....	78
4.2.5	Optimal design operating characteristics.....	81
4.3	Design model of the ORC bottoming ICES with current configuration of the cooling systems. ....	83
4.3.1	Design procedure and specifications of heat exchangers .....	83
4.3.2	Design specification of the capacities .....	90
4.3.3	Design specification of turbomachinery .....	90
4.4	Off-design dynamic model of the ORC bottoming ICES with current configuration of the cooling systems. ....	91
4.5	Summary.....	96
5	OFF-DESIGN DYNAMIC SIMULATIONS.....	97
5.1	Introduction.....	97
5.2	Off-design Hot Composite Curves .....	97
5.3	Test cases for dynamic off-design simulations .....	97
5.3.1	Test Case A: mild variations of service speed.....	98
5.3.2	Test Case B: brutal decrement of service speed .....	100
5.3.3	Control system .....	102
5.4	Simulation results.....	102
5.4.1	R-134a ORC, test case A.....	102
5.4.2	R-134a ORC, test case B.....	105
5.4.3	R-245fa ORC, test case B .....	108
5.5	Summary.....	110
	CONCLUSIONS.....	112
	Results of the work.....	112
	Notes for further works.....	113



References.....115



# INTRODUCTION

Organic Rankine Cycle applies the principle of steam Rankine cycles, but uses organic (e.g. R-134a, R-245fa) and inorganic (e.g. Ammonia  $\text{NH}_3$  and Carbon Dioxide  $\text{CO}_2$ ) working fluids. Evaporator, vapour expander, condenser and pump compose a common plant layout. Simple thermodynamic cycle can be modified passing from a subcritical to a supercritical condition, or by introducing an internal regeneration or a superheating process. Another technological solution is the two-stage ORC system, which operates on two different pressure levels. ORCs systems became a significant energy conversion technology in recent years [1]. Thanks to the low boiling temperature of the working fluid, ORCs plants are a viable solution to convert low temperature heat sources into mechanical or electrical power. In Ref. [1, 2, 3], authors underline the importance of ORCs systems in the WHR application field, and for the exploitation of several renewable energy sources, such as Solar, Geothermal and Biomasses. Several papers in literature deal with the optimization and design process of ORCs plants [4, 5, 6]. In the latter years, also off-design dynamic models were developed in order to evaluate stationary off-design performances and transient behaviour of ORCs systems [7, 8, 9, 10, 11, 12]. In [8] Vaja developed a Simulink® complete library of models of the most widely used components in advanced energy systems. Efforts were focused on creating a flexible, versatile, robust Simulink® library based on physical and rigorous experimental correlations. As can be noted from that work, heat exchangers are the most influencing components on the system's dynamics. Volume discretization approach combined with the finite difference method were used in order to simulate transient behaviour of the plant. This approach was chosen in virtue of its robustness under transient phase. In [9], Manente et al. presented a geothermal plant ORC off-design model, which was built in Simulink® ambient. System dynamics was modelled by adding two capacities, one before vapour expander and the other one after condenser. These storages were analysed using differential forms of mass and energy balances. Other components of the plant were modelled using steady state form of mass and energy balances and performance curves too. An optimal control strategy for the off-design conditions was defined basing on the developed model. Simulations were carried out considering variations in the boundary conditions, like ambient temperature at the air-cooled condenser and brine temperature. Results show that ambient temperature and geofluid inlet temperature at the evaporator strongly influence system's power output. It is well known that heat exchangers strongly influence dynamic behaviour of the entire system. Therefore, an accurate model for these components is necessary to model transient conditions/to obtain significant results from the system's transient simulations. Different methods exist to model heat exchangers. As mentioned before, in [8] discretization method was adopted. In [13], also Quoilin adopted this method in virtue of its numerical robustness during transient simulations. In various other works, Moving Boundary method was adopted [14, 10].

The aim of this work was to create a dynamic model of an ORC energy system exploiting the low grade waste heat on board an LNG carrier. At the same time, efforts have been focused on building up flexible and versatile models of components used in energy systems, as turbomachinery, heat exchangers, and storages, useful to simulate dynamic behaviour of different energy systems. To achieve these goals, sequential

approach has been adopted [15, 16], allowing an object-oriented modeling process. Each component was modelled separately, as a single block, which can be easily modified and then reused to simulate different systems.

As mentioned before, importance of studying ORC systems is related to their capability to exploit several kind of heat sources in the low temperature range. In particular, ORC can represent an interesting solution to recover waste heat rejected by ICEs in the shipping sector. In fact, ICEs on board ships operate for most of the time at steady state, and this allows a better efficiency of the bottoming ORC to be achieved. Even if transient states are not so frequent in the case of ICEs on board a ship, dynamic model of the ORC is still very useful, mainly because of two reasons. First, dynamic simulations allow the transient response of the ORC to be evaluated, giving a useful tool to design an effective control system. Second, dynamic model can be used to evaluate the ORC performance in off-design steady-state conditions reached after transient phases. Furthermore, since the nature of the heat source strongly influences the efficiency of ORC, dynamic models can give useful information to improve the design process of the ORC. In fact, not only nominal conditions could be used to define the design of the ORC. Off-design performance, for a given set of design parameters, could be also considered to refine the choice of the working fluid and the optimal configuration of the ORC, leading to an enhanced effectiveness of the heat recovery.

In this work, Simulink® has been chosen as programming environment because it allows modelling each component very accurately. In fact, user can define each of the model's characteristics, choosing the most proper way (e.g. assumptions, modelling techniques, equations) to describe physical processes. Discretization volume method was adopted to dynamically model heat exchangers, in virtue of its numerical robustness and lower complexity. Two capacities, a hot and a cold drum were added at the plant layout in order to model system dynamics. Pump and turbine were described the former by characteristic flow rate and isentropic maps, the latter with Stodola's correlation and isentropic efficiency maps. No finite difference method is explicitly implemented in the model. All dynamic equations are solved in differential form and then numerically integrated by means of Simulink® integrator blocks. This approach allows modelling the transient behaviour of the energy system with a set of continuous signals representing state variables, instead of a set of discrete values defined by the solution of an algebraic equations system at each time step of the simulation.

As mentioned before, the developed model library has been used to build a dynamic off-design model of a WHR ORC energy system. Basing on the results produced by Soffiato in [17], two configurations characterized by high efficiency have been considered: a saturated cycle using R-245fa and a superheated cycle using R-134a. Dynamic simulations of the energy system have been carried out considering time-variant service speed of the carrier and, accordingly, variable load and heat rejected by the ICEs.

# 1 CONCEPTS AND APPLICATIONS OF ORGANIC RANKINE CYCLES

This chapter exposes basic concepts and various features regarding organic Rankine cycles. Typical configurations and main aspects characterizing ORC systems are presented, comparing this quite recent energy system with traditional water steam cycles. Then, main power production applications of this technology are presented.

## 1.1 Introduction

Rising fuel prices and stringent pollutant emissions regulation are creating a renewed interest in increasing efficiency of traditional energy conversion systems, in developing efficient solutions to exploit renewable energy sources and in enhancing the Waste Heat Recovery (WHR) of industrial processes and traditional power plants. Low grade heat recovery represents one of the viable solutions to achieve these goals.

Various thermodynamic direct cycles and technological solutions have been studied and tested in order to efficiently exploit heat characterized by both low quality and quantity. Kalina cycle, Goswami cycle, open Brayton Joule cycle, Stirling cycle, thermoelectrics, subcritical and supercritical ORC are the most widespread technologies. Among these, ORC systems represent the best compromise between efficiency, flexibility, affordability and cost [18, 3, 19]. First studies on this cycle were carried out during the 70s, while first commercial applications made their appearance during the late 70s and in the 80s. In those years, medium-scale power plant were developed for solar and geothermal applications [13]. Nowadays, the number of ORC plant installed worldwide is steadily increasing [1].

ORC is a traditional Rankine cycle where working fluid is organic. Critical temperature of working fluids in ORC applications is lower than water's critical temperature. As will be explained in the following, using organic components as working fluid determines a substantial differentiation between traditional and ORC plants in terms of temperature and pressure range of application, and efficiency.

## 1.2 Organic Rankine Cycles working principles

In this paragraph working principles of simple and regenerative ORC are presented.

### 1.2.1 Simple and regenerative cycles

As mentioned before, ORCs are based on the concept which characterize traditional Rankine cycle. The cycle is defined by a closed loop composed by four main processes: vaporization, expansion, condensation and compression. Thus, the energy system that carries out this close loop is basically composed by four main components, which are evaporator, vapour expander, condensator and pump. Working fluid is heated and vaporized in the evaporator. Subsequently, it expands in turbine, generating mechanical power. Discharged vapour is then condensed, releasing heat to the cold sink at the condenser. The pressure of the fluid in liquid state is raised by the pump, and pressurized fluid is then send to the evaporator again.

As will be exposed in this chapter, so-called “dry” organic fluids have overhanging saturated vapour line in T-s diagram. In the case of ORC with dry organic working fluid, superheated steam discharged by the turbine can preheat liquid working fluid downstream the pump, before it enters the evaporator [17]. A heat exchanger, called regenerator, is therefore added into the plant layout. Internal regeneration is feasible only if exhausted vapour downstream the turbine has a temperature higher than the subcooled liquid downstream the pump. Effectiveness of so-called regenerative ORC will be discussed in paragraph 1.4.

Typical working principle of a simple and a regenerative ORC are exposed, respectively, in Figure 1.1 and.

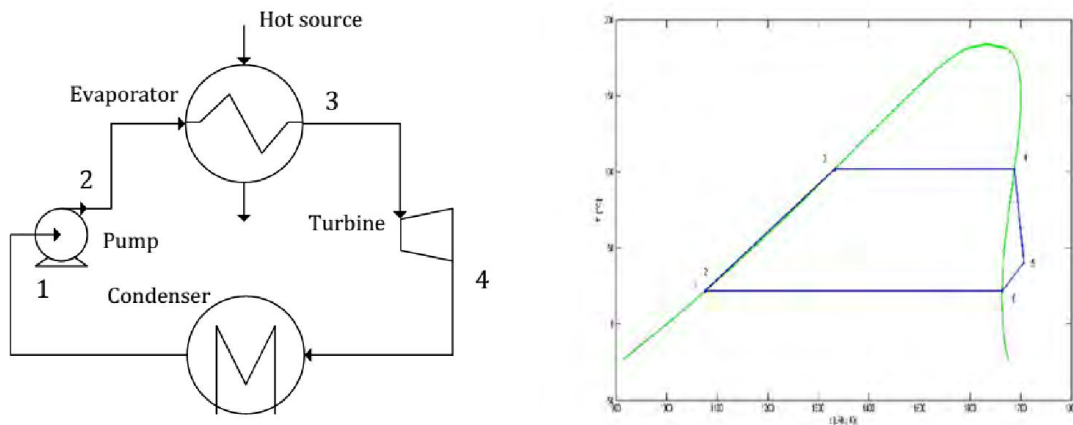


Figure 1.1  
Layout of a simple Rankine cycle, on the left, and corresponding T-s diagram, on the right.

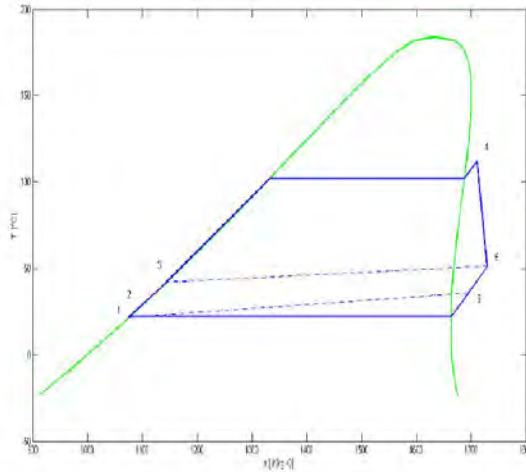
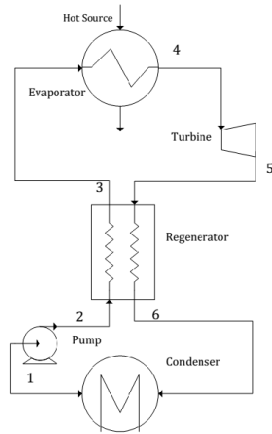


Figure 1.2

Layout of a regenerative Rankine cycle on the left, and corresponding T-s diagram, on the right.

### 1.2.2 Subcritical and Supercritical cycles

Maximum working fluid pressure in ORC can be either greater or lower than its critical pressure value. If the working fluid's critical pressure is relatively low, the pressure of the liquid fluid can be raised by the pump at a supercritical value. Then, working fluid is heated to its supercritical state in a vapour generator. During the heating process of a supercritical Rankine cycle, fluid's properties change progressively without a clear distinction between liquid phase and vapour phase. Conversely, in subcritical Rankine cycles, maximum fluid's pressure does not exceed its critical value. In this case, vaporization takes place in the evaporator, and an isotherm change of phase is clearly recognizable. A qualitative comparison between subcritical and supercritical Rankine cycles is given by Figure 1.3.

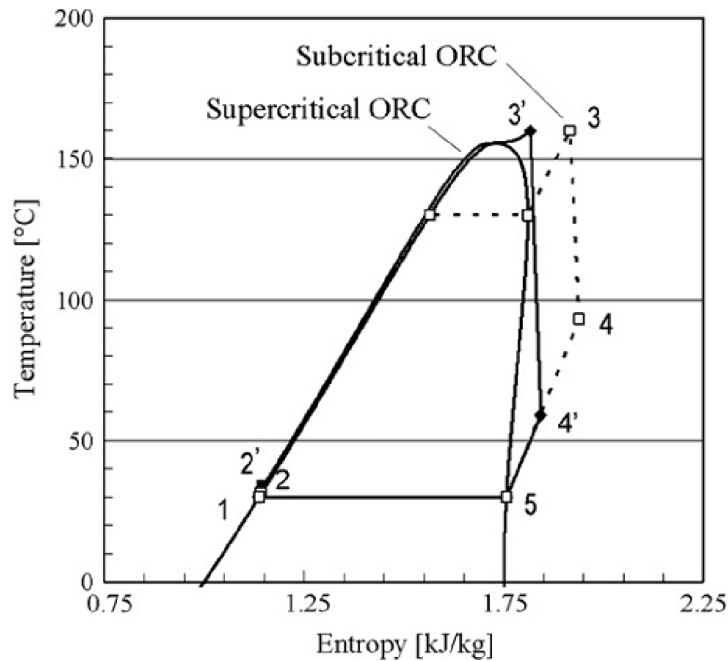


Figure 1.3  
Qualitative comparison between subcritical and supercritical ORC [20].

Shuster et al. [20] investigated the optimization potential in supercritical ORCs. They compared system's efficiency of both subcritical and supercritical ORCs, considering different working fluids and carrying out an exergy analysis of the heat transfer process between working fluid and non-isothermal heat source. Basing on simulation results, they stated that the enthalpy drop during the expansion in supercritical ORCs is greater than in the subcritical one. On the other hand, higher working fluid's pressure must be provided by the pump. However, since pump's additional specific work is much lower respect the additional enthalpy drop in turbine, supercritical cycles shows higher efficiency respect subcritical ones. Furthermore, exergy losses and destruction are lower for supercritical cycles, thanks to the best fitting of the supercritical heating process with the non-isothermal profile of the heat source. As can be noted from Figure 1.4, isothermal evaporation characterizing subcritical ORCs causes an inevitable destruction of energy, which can be reduced by the application of supercritical parameters [20].

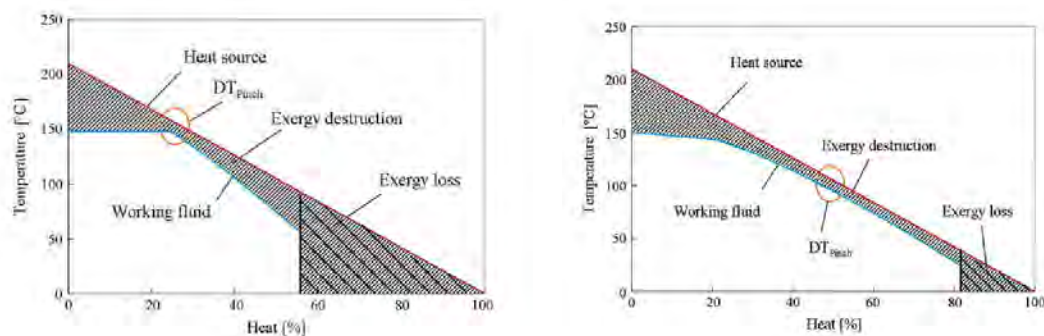


Figure 1.4  
Exergy losses and destruction in subcritical (on the left) and supercritical (on the right) ORC [20].



If on one hand supercritical ORCs allow to achieve higher efficiency, on the other hand the heating process at supercritical pressure involves few drawbacks. Fernández et al. [21] stated that supercritical ORCs adopting siloxanes as working fluid reach maximum thermal efficiency at quite high pressure level: 25 bar for D<sub>4</sub> (cyclic siloxanes) and 50 bar for MM (linear siloxanes). Furthermore, in order to ensure thermal stability, subcritical solutions with lower maximum temperature are preferable [21].

Mikielewicz and Mikielewicz [22] stated that higher thermal efficiency of supercritical ORCs is partially offset by a bigger size of the heat exchanger necessary to evaporate the working fluid. New technological solutions, such as microchannels, must be adopted to enhance the effectiveness of the heat exchange process in supercritical conditions, in order to achieve more compact vapour generators.

### **1.3 Working fluids choice in ORC power plants**

Using organic components, characterized by low temperature boiling point, as working fluid allows exploiting low-grade heat sources, otherwise unusable with traditional water steam Rankine cycles. Several papers present in the open literature deal with the characterization and optimal choice of organic fluids for ORC applications [18]. It is possible to define three categories of organic fluids in function of their saturation vapour curve. As stated in [23] by Hung et al., this feature represents the most crucial characteristic of a working fluid in an ORC, since it affects the fluid applicability, cycle efficiency and the layout of an ORC-based energy system. This is a widely adopted classification criterion [18, 13, 23, 19], which identifies three main categories: wet fluids with negative slopes, dry fluids with positive slopes and isoentropic fluids with nearly vertical saturation vapour curve. Wet fluids (e.g. water, ammonia, R134a) usually have low molecular weights and need to be superheated in order to avoid liquid droplets formation at the end of expansion process. Figure 1.5 reports T-s diagram of few working fluids for ORCs application, and water.

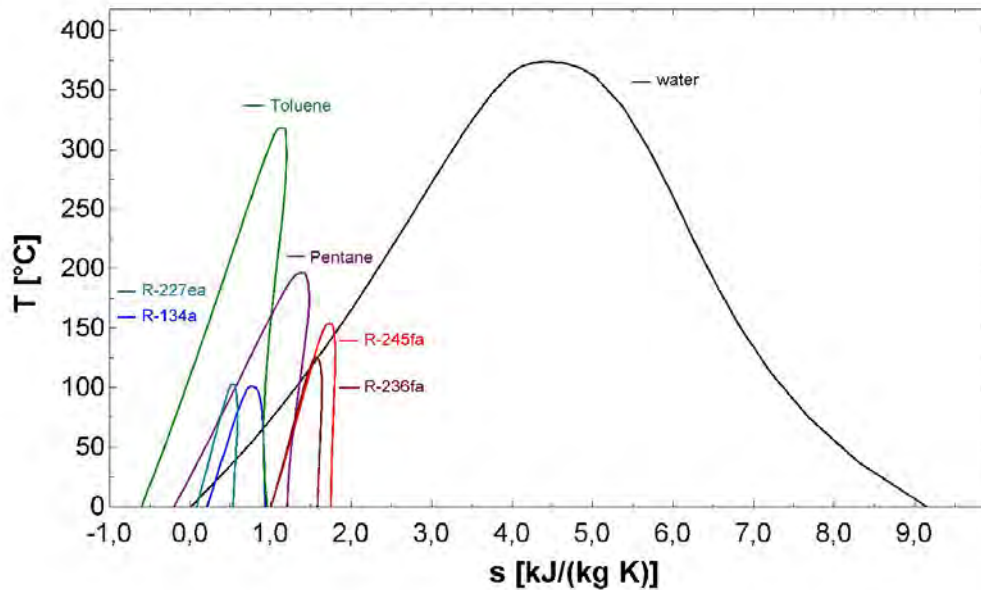


Figure 1.5  
Comparison between  $T$ - $s$  diagram of few working fluids for ORCs application and water.

The nature of the heat source strongly influences the choice of the working fluid in ORC applications. In particular, the temperature level defines the optimal choice for the working fluid. In [24], Wang et al. present a thermal efficiency model based on an ideal ORC to analyse the influence of working fluid properties on the thermal efficiency, optimal operation condition and exergy destruction. Different heat source temperatures were considered, from 340 to 500 K. Results show that the selection of the working fluid helps to maximize the ORC performance if it is carried out considering the temperature level of the heat source, especially in the case of relatively high temperature heat sources. Conversely, in the case of low grade WHR, the difference of optimal net power outputs among various working fluids is small. Particularly, for heat source temperatures below 380 K authors suggested to consider safety, environmental aspects and costs as main features of the ORC working fluid. Figure 1.6 represents the choice criterion, proposed in [24] by Wang et al., to optimize the working fluid selection basing on heat source temperature.

#### Heat source temperature level

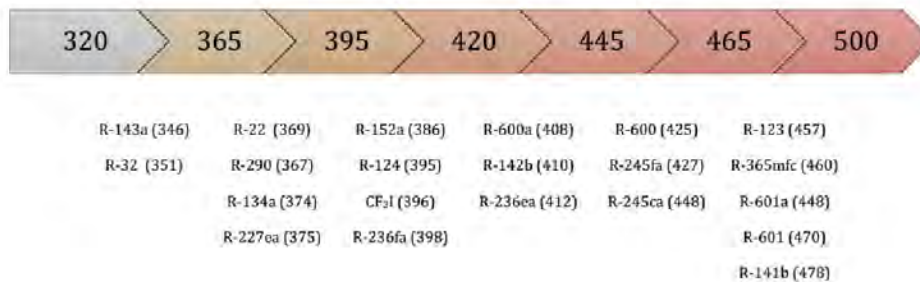


Figure 1.6  
Optimal selection of working fluids corresponding to the heat source temperature level. In brackets, critical temperature of the working fluids. Temperature are expressed in Kelvin [24].

## 1.4 Comparison between water steam Rankine cycle and ORC

Two main differences emerge comparing organic fluids and water T-s diagrams [13]: as stated before, water's saturation vapour has negative slope, while the curve is much more vertical or even positive in the case of organic fluids. Furthermore, entropy difference between saturated liquid and saturated vapour is much bigger for water. Starting from these statements, following observations can be done.

- Pressure and Temperature levels in the evaporator and condenser

Evaporation pressure is about 60–70 bar in traditional water steam Rankine cycles, while in ORC systems it generally does not exceed 30 bar [13]. Low pressures lead to a simpler construction of heat exchangers and storages, and to a safer working condition for the plant. Condensation pressure in ORC systems is generally higher respect traditional water steam cycles. In the latters, condensation pressure is often lower than 0.1 bar absolute, while in ORC systems condenser operates generally at higher pressure values to avoid air infiltrations in the cycle [13]. Critical temperature characterizes condensation pressure of organic fluid: compounds with low critical temperature (as R-245fa, R-134a and R-123a) condense at ambient temperature at a pressure higher than the atmospheric pressure, while fluids with higher critical temperature (as toluene and hexane) condense at ambient temperature with a pressure lower than the atmospheric one. Pressure level at the evaporator and the condenser strongly influence the choice and the design process of turbomachinery to be adopted in the ORC system. As Hung e al. stated in [23], specific enthalpy drop across the turbine is much higher for water-steam mixtures in traditional Rankine cycle than in the case of organic fluids. Thus, a single or two-stage turbine is usually adopted in ORC, whereas a steam turbine with several expansion stages must be used in water steam cycles [23, 1]. Furthermore, low enthalpy drop leads to lower rotating speed and lower tip speed [13]. As a result, turbine shaft can be directly coupled with electrical generator without using gear box, reducing mechanical losses. Lower tip speed reduces mechanical stress on the turbine blades and simplify their design process.

Another difference between water steam cycles and ORC emerges considering temperature level characterizing evaporation process. As can be noted from Figure 1.5, organic fluids have lower critical temperature respect water and, therefore, lower boiling point. This allows ORC recovering heat at a much lower temperature respect traditional water steam cycles. In order to reject condensation heat to the environment, nominal condensation temperature is normally set above 300 K [18]. This solution is generally adopted also in traditional water steam cycles.

- Internal regeneration

Internal regeneration, achieved recovering heat from vapour discharged by the turbine, is a widely used solution to increase thermal efficiency of traditional Rankine cycle. Considering WHR application of ORC systems, regeneration is not always feasible or is not a good solution to improve the cycle efficiency. As Vaja and Gambarotta state in [19], regenerative preheating require a liquid-gas heat exchanger which could be

characterized by a quite critical design process. Furthermore, results reported in [19] and [4] state that, in ORC systems exploiting waste heat, adding the internal heat exchanger would not necessarily improve the cycle's performance.

In [17], Soffiato also stated that internal regeneration could lead to a non-significant increase in cycle's efficiency or, in certain WHR systems, to the impossibility to exploit all the heat available from the hot source. Furthermore, the installation of an internal regenerator could increase significantly the costs related to the system's construction. In summary, while in traditional Rankine cycles internal regeneration is generally a good solution to enhance cycle efficiency, this is not true for ORC systems [23].

- Effectiveness of the superheating

Since the slope of saturation vapour curve in the T-s diagram is negative for water, vapour quality at the end of the expansion process in turbine can be less than unity. This leads to liquid droplets formation, which could damage the turbine and limit its life length. Superheating is therefore necessary in traditional steam Rankine cycles, in order to allow expansion ending in the superheated vapour zone of the T-s diagram. In ORCs, superheat does not always lead to a higher efficiency. Hung et al. [23] stated that the efficiency is not strongly related to turbine inlet temperature and, therefore, increasing superheat in the turbine inlet does not lead to a significant increase in efficiency. This result is expressed by Figure 1.7.

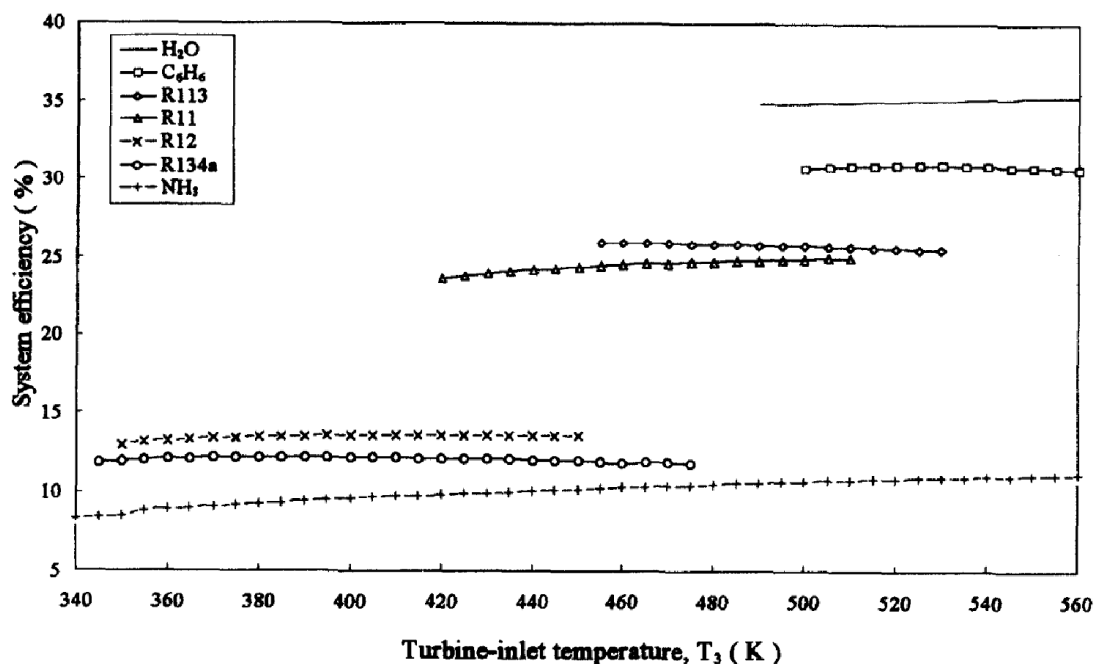


Figure 1.7

Variations of system efficiency with turbine inlet temperature for various working fluids [23].

Chen et al. [18] found that the rate of divergence of constant pressure lines determines the effect of superheating on efficiency. As expressed by Figure 1.8, considering as reference state the saturated vapour condition and given an increment of the degree of superheating, incremental efficiency can be defined by the following:

$$\eta' = \frac{\Delta w}{\Delta q} = 1 - \frac{\Delta h_2}{\Delta h_1} \quad (1.1)$$

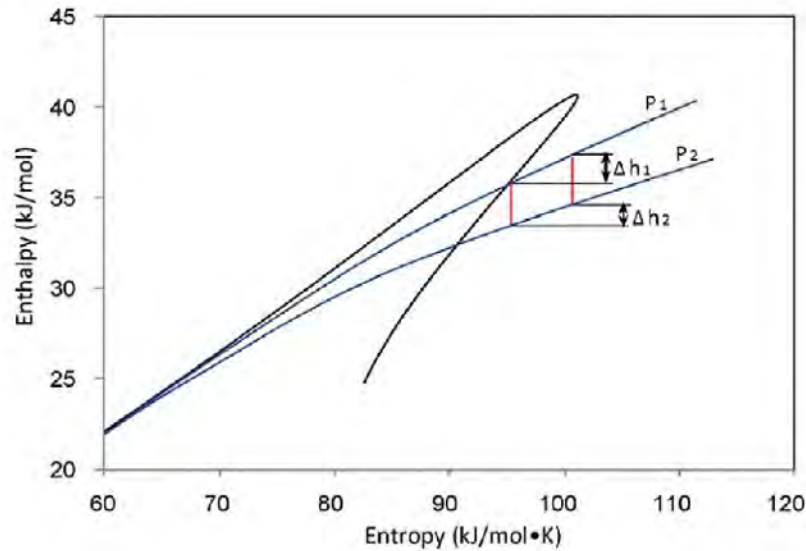


Figure 1.8  
Effect of superheat: enthalpy-entropy diagram of pentane [18].

Considering Equation (1.1) and Figure 1.8, it can be noted that system efficiency increases for wet fluids. Conversely, dry fluids experience a decrement of efficiency. Isoentropic fluids maintain an approximately constant value for high temperatures at the turbine inlet. In summary, in the case of wet fluid superheat is necessary to improve efficiency and to ensure a safe expansion in turbine, while it is not recommended for dry fluids.

- Stability of the fluid and compatibility with materials in contact

Chemical stability and deterioration of the working fluid is not a serious problem in traditional steam water Rankine cycles. Conversely, organic fluids usually suffer chemical deterioration and decomposition at high temperatures [18]. In order to avoid fluid decomposition, maximum operating temperature must be limited within a safe range. Furthermore, working fluid must be compatible with materials in contact and lubricating oil, so it is necessary to adopt non-corrosive organic fluids. In [25], Andersen and Bruno presented the application of ampule testing techniques useful to predict chemical stability of working fluids for ORC applications. Given temperature and pressure conditions, the method allows determining the decomposition reaction rate constant.

- Safety, environmental aspects and costs

Water is a non-toxic and non-flammability fluid. Furthermore, it is characterized by low Global Warming Potential (GWP) and null Ozone Depleting Potential (ODP). Conversely, some organic fluids widely used for refrigeration applications during the past years have been phased out, due to their high environmental impact. For example, fluids such as R-11, R-12 and R-115 belong to this category. Some other organic fluids are being phased out during next years, such as R-21, R-22 and R-123 [18]. In [26], Calm presented toxicity data and exposure limits for refrigerants. He stated that hydrocarbons proposed as replacements for fluorochemicals are generally more toxic, and introduce much higher risk of explosion and flammability.

The ASHRAE refrigerant safety classification is a good indicator of the fluid's toxicity and flammability.

Finally, while water is abundant and cheap, the availability and cost of organic fluids must be taken into account when selecting the working fluid for an ORC application. Working fluids adopted in ORCs are generally expensive [18].

In summary, following aspects emerge by comparing traditional steam water cycles and ORC systems. Advantages and problems characterizing ORCs and water steam cycles are reported in the following table [1, 13, 23]:

<i>Advantages of ORCs</i>	<i>Limits of ORCs</i>
Low pressure and temperature of the evaporation process allow recovering low grade heat.	Lower efficiency.
Superheating is necessary only in the case of wet fluids. Using dry or isentropic fluids superheat is not required, since expansion process ends in the superheated region.	Toxicity, flammability and chemical instability of several refrigerant fluids represent critical issues. An intermediate heat transfer loop could be necessary to limit risks in operational conditions.
Evaporation process needs less heat compared with the vaporization of water.	Higher cost of the working fluid.
Higher fluid density leads to compact devices.	Several organic fluids have high environmental impact.
Pressure and temperature difference between evaporation and condensation processes is smaller. Thus, single or two-stage turbine can be used, reducing costs and design problems.	

*Table 1.1  
Advantages and limits of the ORC system*

<i>Advantages of water steam cycles</i>	<i>Limits of water steam cycles</i>
Higher efficiency.	Desalinization of water is necessary to avoid fouling and corrosion inside plant components.
Water is cheap and abundant, non-toxic, non-flammable and it has low environmental impact.	Need of superheating to avoid droplets formation during expansion process.
Water is characterized by a very good thermal and chemical stability.	Bleed and internal regeneration are necessary to achieve high cycle efficiency. Plant layout is generally complex.
Water is a good energy carrier, by virtue of its high latent and specific heat.	Due to the greater difference between evaporation and condensation pressures, complex multi-stage turbine are necessary.
	Low grade heat is not exploitable with high efficiency.

*Table 1.2  
Advantages and limits of water steam cycles*

Considering the aforementioned aspects, traditional water steam cycles are more profitable in the high power range, with high temperature heat sources. On the other hand, the advantages of organic Rankine cycles are evident in the case of small-scale power plant exploiting low grade heat sources.

## **1.5 Main ORC applications**

The ability to exploit low temperature heat sources, the affordability and the moderate prices of ORC power plant lead to a widespread of this technology, which is now a premier solution to convert low temperature heat sources into power. Various renewable energy sources, such as solar and geothermal, represent exploitable heat sources for ORC applications. At the same time, waste heat rejected by several thermal processes can be recovered to generate electrical power by means of an ORC system. Aim of this paragraph is to present a brief overview of the most important applications of ORC in power generation.

### **1.5.1 ORC in WHR applications**

Waste heat is the unused heat rejected in the environment after a combustion process, a thermal or chemical reaction. Great quantities of heat are rejected at medium and low temperatures by almost all manufacturing activities and thermal engines worldwide. In 2008, US industrial sector alone accounts for one third of total energy

consumptions and greenhouse gasses emissions of the entire country [1]. Among various manufacturing activities, cement industry, refineries, chemical industry, food and beverage processing industry, paper industry and metal industry are characterized by the highest energy demand [1]. In [27], authors stated that global carbon dioxide emissions from the worldwide cement production process alone accounts for 1126 Mton in 1994.

Many of the aforementioned industrial sectors have a high potential for waste heat recovery. In cement manufacturing, combustion gases exiting the kilns preheat air necessary for the combustion process and then are rejected in the atmosphere at about 300 °C. Furthermore, clinker extracted from the kilns at about 1000 °C can heat ambient air at about 200-300 °C. Hot air and combustion gases can be exploited with an ORC system [1].

As Bundela and Chawla state in [27], waste heat rejected in the environment cause essentially two kind of impacts: one related to pollutant components present in exhaust gases or, in general, in the waste heat stream. The second one is given by the destabilizing action of the rejection of heat in the ecosystem.

Any action enhancing system's efficiency, as the waste heat recovery by means of ORCs, allows reducing both kinds of pollution's effects, since it reduces the consumption of primary energy sources (mainly, fossil fuels) which leads to pollutant emissions.

Waste heat recovery can be applied also to Internal Combustion Engines (ICEs). ICEs' thermal efficiency generally does not exceed 30%. This means that the remaining 70% of the energy input is rejected to the ambient through the radiator and the exhaust system.

Research on ORC bottoming ICEs starts in the 70's, after the energy crisis.

In 1976 Patel and Doyle developed one of the first ICE-ORC combined cycles for automotive applications. The system used waste heat of a Mack 676 diesel engine installed on a long haul truck. Since trucks generally operate for long time at near constant engine speed, authors considered these vehicles suitable for ORC WHR applications [28]. The evaporator of the prototype recovered heat from the exhaust stack, while condenser was combined with the truck's radiator. Fluorinol-50 was adopted as working fluid to minimize temperature difference between the working fluid and engine exhaust. Temperature at the inlet of the three stage axial flow turbine was about 343 °C, while condenser outlet temperature was about 70 °C. Test demonstrated a 13% increase in maximum power output and a 15% improvement in fuel consumptions.

A comparison between seven different working fluids for ORC applications was carried out by Marciniak in 1981 [28]. Water, methanol, 2-methyl pyridine/water, Fluorinol-85, toluene, Freon R-11 and Freon R-113 were tested as working fluids for an ORC exploiting waste heat of 600-2400 kW industrial applications, with waste heat temperature between 260 and 590 °C. Scale effect determined a strong decay of costs, from \$1000/kW to \$600/kW.

In 2006, Arias et al. simulated three ORCs suitable for WHR in a hybrid vehicle. Different configuration were considered, including heat recovery from exhaust gases, coolant water and engine block. The highest efficiency, with 7.5% of the waste heat converted in electrical power, was obtained exploiting the heat of the engine block to preheat the working fluid and the heat of exhaust gases to superheat vapour [28].

WHR could increase the efficiency of energy systems adopted in the shipping industry too. However, few works deal with this issue, essentially because of the poor





A European demonstration CHP ORC plant is located in Lienz, Austria. Figure 1.10 represents the first principle energy balance of the plant, whose working principle could be represented by Figure 1.9. It has a nominal electrical capacity of 1000 kW<sub>el</sub> and a nominal thermal capacity of 4400 kW<sub>th</sub>. The plant is grid-connected, and it supplies the town of Lienz with district heat [1]. Net electric efficiency is about 18% in nominal conditions, and about 16.5% at 50% load [29]. Capital costs amount to 2765 €/kW<sub>el</sub>, and electricity production cost is about 0.14€/kWh<sub>el</sub> [29, 1].

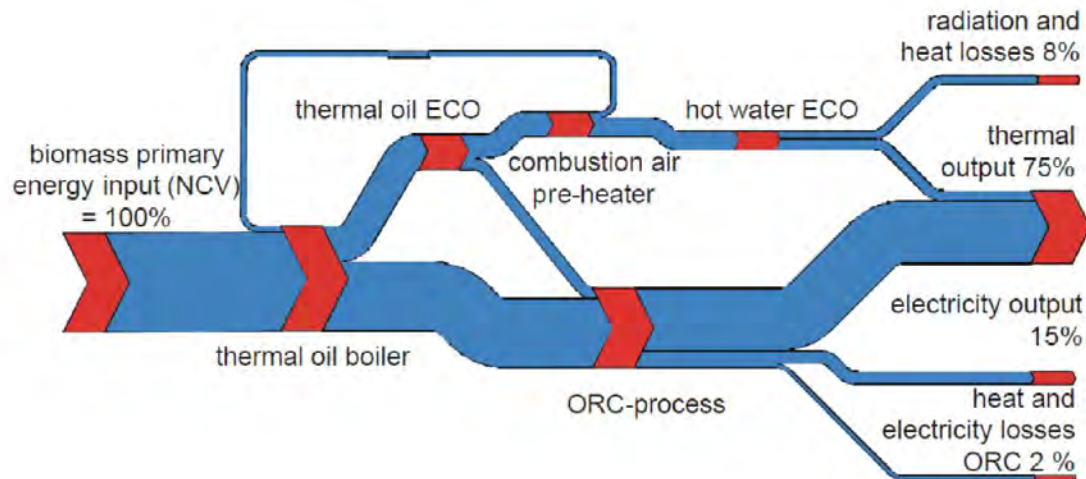


Figure 1.10  
Energy balance of the CHP ORC plant in Lienz [29].

### 1.5.3 ORC application in binary geothermal power plants

The Earth's temperature gradually increases with depth, due to heat generated by decay reactions of minerals and because of endogenous heat deriving from original formation of the planet. Geothermal gradient temperature is not equally distributed: its average value near the Earth's surface is about 30 °C/km, but in certain regions this value can be considerably higher, allowing a simpler and more profitable exploitation of this energy source [30, 1].

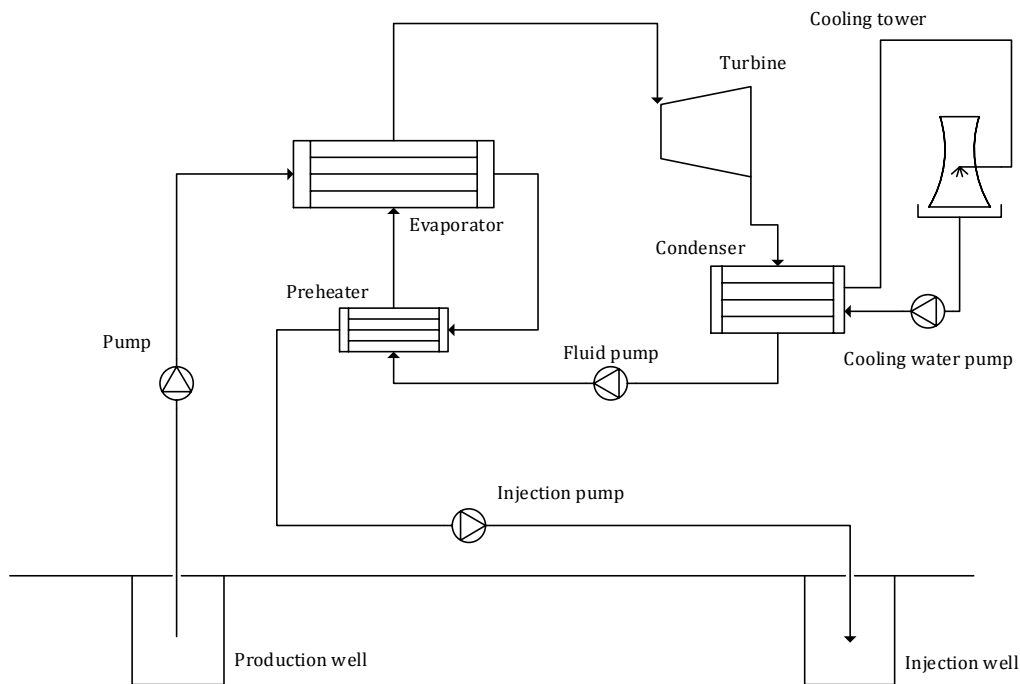
A wide range of temperatures characterizes geothermal sources, and various types of geothermal plants have been developed to achieve an optimal resource utilization. Main types of geothermal plants are reported in Table 1.3.

<i>Type</i>	<i>Resource Temperature [°C]</i>	<i>Utilization Efficiency [%]</i>	<i>Plant cost and complexity</i>
Double -flash	240-320	35-45	Moderate-high
Dry-steam	180-300	50-65	Low-moderate
Single-flash	200-260	30-35	Moderate
Basic binary	125-165	25-45	Moderate-high

*Table 1.3*  
*Classification of geothermal sources and comparison between different power plant solutions [1]*

Nowadays, binary geothermal plants represent a quite high contribute to overall geothermal plant installations worldwide, accounting for about 32% of all geothermal units in operation [1]. In such an energy system, hot geothermal fluid is pumped from the production well to the ORC's evaporator, where it transfers geothermal heat to the working fluid, vaporizing it. A preheater can be introduced to recover residual heat of the geothermal fluid, which is subsequently injected in the ground. Vaporized working fluid expands in turbine producing mechanical or electrical power. Exhaust vapour discharged by the expander is then condensed by means of cooling towers. Working principle of a typical geothermal ORC binary plant is represented by Figure 1.11.

ORCs allow exploiting low grade geothermal sources, though significant energy quantities must be spent to feed both brine and working fluid pumps, considerably reducing system's efficiency [13]. Energy efficiencies are typically in the range 5-15% [1].



*Figure 1.11*  
*Working principle of an ORC binary geothermal power plant.*

As Tchanche et al. stated in [1], various design and optimization criterion are present in the open literature dealing with geothermal binary plants.

Optimal choice of the working fluid can be given by the levelized electricity cost, as suggested by Gawlik and Hassani. Other important indicators, used by various authors in design and optimization calculations, are net power output per mass flow rate, the ratio between total heat transfer area and net power output, thermal and exergy efficiencies. However, a best criterion for optimal design was not found so far [1].

#### 1.5.4 ORC applications in solar power plants

Solar energy must be concentrated in order to generate a relatively high temperature heat source, which can be converted into mechanical power by means of a direct thermodynamic cycle. Nowadays, concentrating solar power plants are well proven, and several technologies are available to track the sun and concentrate its energy. The three main ones are the parabolic dish, the solar tower and the parabolic trough. Parabolic dishes and solar towers are punctual concentrating technologies, and allows reaching higher temperatures. Stirling engines are suitable in the case of small scale plants adopting parabolic dishes concentrators. Traditional steam Rankine cycles, or even combined cycles, are adopted in the case of large scale power plant exploiting heat generated by a solar tower [13].

Parabolic trough plants work in a lower temperature range respect the formers (300-400 °C), and generally, until now, they were coupled with a traditional steam Rankine cycle. However, the following features make ORCs a better solution to be applied in the case of small-scale plants working in the low-medium temperature range [1]:

- a. Low temperature operation: thanks to the low boiling temperature of the working fluid, ORCs are an efficient solution to exploit solar energy in regions with low solar radiation.
- b. Modularity: several small-scale ORC power plant can be combined together in order to build a larger power plant. Thus, a plant characterized by an electrical power of several  $MW_{el}$  can be build.
- c. Reduced capital and O&M costs.

The working principle of a solar plant combining parabolic trough concentration technology and ORC is represented in Figure 1.12.

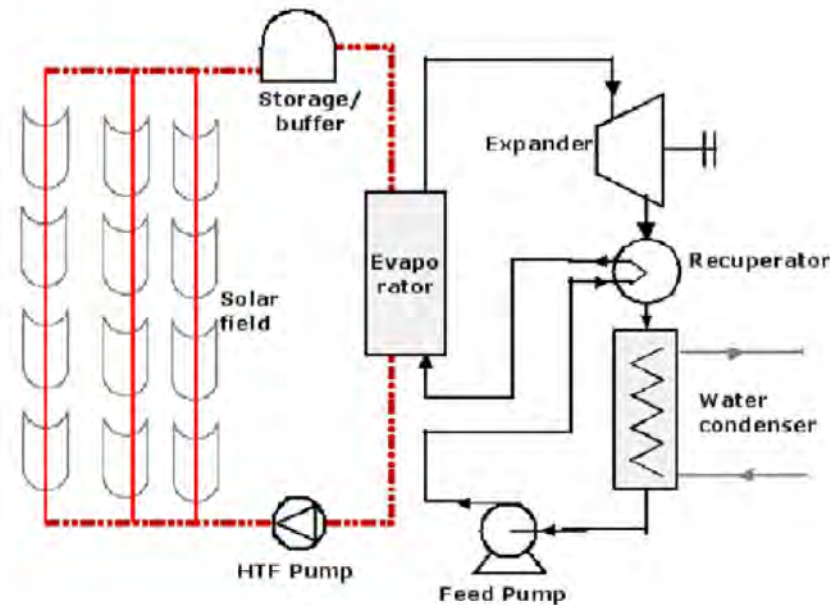


Figure 1.12  
Example of a solar ORC system with parabolic trough solar field [13].

Nowadays, few concentrating solar power plants using ORC are available on the market [13]. Nguyen et al. developed a prototype of low temperature ORC system, characterized by an electrical power output of 1.44 kW<sub>el</sub> and an efficiency of about 4.3%. As authors stated, such a system could be cost-effective in remote areas with high solar radiation [1].

Arizona Public Service operates a 1 MW<sub>el</sub> ORC power plant located at Red Rock in Arizona, USA. Parabolic trough concentrate solar radiation, which heats a mineral oil used as heat transfer medium. n-Pentane was adopted as working fluid for the ORC, which has an efficiency of 12.1%. Overall solar to electricity efficiency is about 20% [13, 1].

In summary, ORCs represent a promising technology to achieve a reduction in capital costs and a higher efficiency of small-scale power plant exploiting solar energy. Such an energy system can be adopted in rural areas for off-grid applications, offering an alternative to Diesel generators [13].

## 1.6 Summary

In this chapter the working principle and basic configurations of ORC were presented. Simple and regenerative configurations were introduced. A comparison between subcritical and supercritical cycles have been carried out, underlying the better compatibility of supercritical cycles with non-isothermal hot sources.

Then, a brief overview of the organic fluids used in ORCs has been presented and a comparison between traditional steam cycles and ORCs has been carried out. ORC emerges as the best solution to exploit low grade heat in small-scale power plants.

Finally, the chapter exposed some applications of ORCs exploiting waste heat of industrial processes and internal combustion engines, and renewable energy sources.

## 2 MODELING OF THERMODYNAMIC SYSTEMS

The aim of this chapter is to present an overview of the basic concepts of the thermal and energy systems modeling. It is important to define what an energy system is and to present which are the suitable ways to describe and analyse it. Sequential and Simultaneous approaches adopted for numerical modeling are described and a comparison between these two approaches is done. Design and off-design models are compared. Finally, a brief energy systems and ORCs modeling review is presented.

### 2.1 Introduction

In a thermodynamic analysis, the system is the portion of universe that is analysed. A well-defined surface separates it from the rest of the universe. Such a surface is known as the control surface or system boundary. When there is a flow of mass through the system boundary, this is called control volume [31].

Particularly, it is possible to define any energy system as a thermodynamic system within which various components allows converting energy from an initial form to a final one. In other words, an energy system is a finite portion of the universe within which energy is converted from a primary source to a final product. It is possible to simulate physical behaviour of real systems by creating a mathematical model of them. Equations and inequalities define the value of system's variable and their validity range respectively.

In order to model a real system it is necessary to define its boundaries. Everything inside boundaries will be considered matter of interest and will be described in the mathematical model. Conversely, space and processes outside boundaries will not be considered. A correct definition of system boundaries it is necessary to include all and only indispensable correlation useful to describe the behaviour of the system. Hence, it is necessary to reach a trade-off between accuracy and complexity of the model. In fact, a restrictive definition of the control surface could lead to an erroneous evaluation of the system's state, whereas broader boundaries involve a major problem complexity [32]. Therefore, the level of detail of the model is a crucial issue, strongly influencing reliability and simulation complexity of the model.

Modular approach is often applied modeling thermal systems, because it *leads to consider the whole system as the result of interconnecting several components* [8]. Single components are mathematically modelled and then connected each other in order to simulate the overall plant behaviour. Links between components may symbolise physical properties (e.g. pressure, temperature, specific enthalpy, density) or exchange quantities (e.g. heat flux, mass flow rate, mechanical work, electrical power). Object-oriented methodologies are based on modular approach. Generally, a set of input values, output variables, a vector of information signals and a vector of state variables characterize each model of the over-mentioned system [8]. Since each of these values

may vary during model simulation, they are generally regarded as time variant signals. In summary, three approaches may be adopted in modeling procedure [8]:

- Synthesis: output variables are fixed, and input variables are known. System state is the unknown quantity.
- Identification: the model of a system is defined with given output variables and a known input array of variables.
- Analysis: The state of the system is defined at an initial time, i.e. state variables are known at time “zero”. Given input variables, output variables are calculated.

The goal of this work is to create an off-design dynamic model of an ORC energy system, which allows to predict physical behaviour of a real plant under given working conditions. Thus, an analysis simulation process will be carried out.

## 2.2 Classification and definition of thermodynamic and fluid systems models

It is hard to find in literature a unique classification of the models used for thermodynamic and fluid system analysis. In [8], Vaja proposes a summary of some classification criteria, discussing characteristics of mathematical models and modeling techniques. In [32], Rech makes a clear distinction between design and off-design prediction models. Finally, in [15, 33] authors expose the basic concepts of numerical techniques of model’s simulation.

Basing on what [8] and [32] report, an arbitrary and maybe not exhaustive summary of classification criteria could be the following:

- a. Geometry
- b. Existence of state parameters
- c. Time dependence
- d. Type of mathematical correlations adopted
- e. Design or working condition model

### d. Geometry

Thermal and fluid systems modeling may be carried out adopting different levels of simplification for the geometry of the system. In the order, zero-dimensional, mono-dimensional, bi-dimensional and tri-dimensional analysis are characterized of an increasing complexity. This issue must be taken into account when choosing which geometry analysis to use. Generally, complexity is directly proportional to the level of detail of the model.

- Three-dimensional analysis: It is used when properties of the system vary in every direction of the three dimensional space. Analytically, a generic property named “P” is expressed as a function of each of the geometric coordinates of the reference system [8]:



$$\frac{dP}{dx_1} \neq 0 \quad \frac{dP}{dx_2} \neq 0 \quad \frac{dP}{dx_3} \neq 0 \quad (2.1)$$

Such a kind of analysis is used when a high level of detail is requested. For example, three-dimensional analysis is generally adopted in the design process of single components [32].

- Two-dimensional analysis: It is possible to simplify the model when particular symmetry conditions characterizes the system in object. If property “P” does not vary significantly along a specific space coordinate, this could be neglected in the model construction. For example, consider the following notation:

$$\frac{dP}{dx_1} = 0 \quad \frac{dP}{dx_2} \neq 0 \quad \frac{dP}{dx_3} \neq 0 \quad (2.2)$$

This approximation will inevitably introduce an error in the simulation process. On the other hand, passing from a three-dimensional to a two-dimensional analysis leads to a significant reduction in computational efforts [32].

- One-dimensional analysis: It is possible to further simplify the geometry of the model if properties of interest vary significantly along only one spatial direction. In such a condition, a one-dimensional approach may be used in the modeling process:

$$\frac{dP}{dx_1} = 0 \quad \frac{dP}{dx_2} = 0 \quad \frac{dP}{dx_3} \neq 0 \quad (2.3)$$

Generally this kind of analysis is not enough accurate to describe a single component physical behaviour. However, in many physical systems the reducing in computational efforts could widely compensate the introduced inaccuracy.

- Zero-dimensional analysis: parameters do not depend on geometric structure of the system [8]:

$$\frac{dP}{dx_1} = 0 \quad \frac{dP}{dx_2} = 0 \quad \frac{dP}{dx_3} = 0 \quad (2.4)$$

In this case, output values are straightforward obtained from input variables by applying characteristic maps (head flow and efficiency characteristic maps in the cases of turbomachineries,  $\varepsilon$ -NTU maps for heat exchangers) or mass, energy and momentum balance equations [32].

It may be noted that the level of detail of the modeling process influences the kind of geometrical analysis to use. For example, to design or improve the performances of a shell-and-tube heat exchanger it could be necessary to model it with a three-dimensional analysis method, in order to describe in a precise way the fluid behaviour and the heat transfer process. Conversely, this approach may be too expensive, in terms

of computational time, if the goal of the model is to describe the global behaviour of a thermal system including the current heat exchanger. In this case, a mono-dimensional analysis may be adopted to describe fluid behaviour inside the pipes, considering fluid properties variation only along the pipe axial direction.

e. Existence of state parameters

The existence of differential equations, which are expressed in terms of state variables time derivative, and algebraic equations, which tie together state variables and other variables of the system, generally characterizes state determined models [8]. Hence, a time dependent vector of state parameters defines the dynamic behaviour of the system. Consequently, output values are calculated as a function of input variables (generally, they are time dependent parameters too) and state parameters for the current instant of time.

Conversely, a not state determined model is not characterized by a set of time variant state variables. Therefore, output variables are calculated only as a function of input variables at the current time. Since no differential equations are introduced, dynamic behaviour of the component is neglected.

f. Time dependence

State properties could be time dependent or not. In the first case, their time derivative is not null:

$$\frac{dP}{dt} \neq 0 \quad (2.5)$$

Such a condition characterize a so-called Dynamic model. Therefore, system behaviour is state determined [8]. Conversely, a Steady-State (or Stationary) model is characterized by null state properties time derivative:

$$\frac{dP}{dt} = 0 \quad (2.6)$$

g. Type of mathematical correlation adopted

Nature of correlations adopted in the modeling process in order to calculate state and output variables define two main categories of models [8]:

- Black box models, within which physical behaviour of the system is described essentially using empirical correlations. Physically based equations use is limited. Pump model represents a typical example of a black box model. Output values (e.g. volumetric flow rate or mass flow rate) are calculated as a

function of input variables (e.g. pressure head) by means of characteristic maps, generally based on experimental data or manufacturer's data.

- White box models, within which conservation equations define correlations between system variables. In the analysis of energy systems, thermodynamic and fluid dynamic models are widely used. In the first case conservation of energy and mass, equation of state and equation describing the physical process define the time variation of thermodynamic variables. In the second case, mass and energy balance equations, momentum and moment of momentum balance equations are necessary to model time variation of cinematic variables [8].
- Grey box models. In this case, physical behaviour of the component is described both by conservation equations and by empirical correlations.

#### h. Design and off-design model

Design model defines the size of the system and its performance for a given working condition, which coincides with nominal working condition, while off-design model can describe the performance of a given system in different operational conditions. As mentioned above, nominal conditions characterizing the design point model generally refers to maximum load of the system. Off-design model may cover a certain range of operational points. Generally, it describes the performance of the system at partial loads.

Building up design-point and off-design models, a crucial issue is the proper definition of the equation system that describes the physical system. The greater is the number of equations adopted, the greater is the mathematical complexity of the solution process. Moreover, variables need a proper definition too in order to solve the system in the right way. In general, it is possible to consider a system composed by  $j$  equations, with  $k$  corresponding to the global number of variables ( $k > j$ ). Therefore, the number of independent variables must be equal to  $k - j$ . Once the value of independent variables is properly defined, the system can be solved and it is possible to calculate the value of the dependent variables. In both kind of models, variables are not necessary different, but different quantities may be considered as dependent or independent variables [32]. In design models, size variables (mass flow rate, heat exchanger area) are considered as dependent. Conversely, in off-design models they are generally imposed as independent parameters, and performance variables (thermal or electrical efficiency, electrical power) are considered as dependent quantities. Referring to time-dependence classification criterion, off-design models could be differentiated in static and dynamic. In the first one, a partial load stationary condition is assumed, and the system is described by an algebraic equation system. Thus, mass and energy balance equations are expressed in algebraic form, with no differential terms. On the other hand, dynamic off-design models describe system dynamics adopting differential forms of the over mentioned balance equations. Thus, it is possible to describe not only specific partial load operational conditions, but also the transient that leads from one to another partial load state. This could be very useful in the case of energy systems that experience fast or significant load variations, as in the case of power plant bottoming main energy systems, the first exploiting waste heat from the latter.

## 2.3 System modeling approaches

Any thermal system could be described by a flow sheet representing the flow of the information among single components. Each of these components model physical processes by means of proper mathematical equations. Thus, describing the behaviour of the overall system requires the solution of a certain number of equations. In this chapter, two of the most widely adopted approaches for the model resolution process are briefly described and compared.

### 2.3.1 Sequential approach

Sequential resolution method result from the simplest calculations carried out even without using computer. It is associated to the modular modeling approach for thermal systems. Each component could be modelled by a block containing equations that describe physical phenomena. Output values are calculated from the input to the module, and this implies both a positive and a negative characteristic of the modular approach. In fact, if this is clearly a straightforward and intuitive resolution process, on the other hand it does not allow to a simple handling of recirculation and design specifications [15]. In summary, each component of the flow sheet is described by a sequence of calculations that requires inputs values and state parameters values in order to determine output quantities. Following the structure of the flow sheet, modules are linked together in order to model overall thermal system. Links among components represent mass flow rate, thermodynamic properties, heat exchange, and work. It may be noted that input and output quantities of physical and modelled system could not match [8].

### 2.3.2 Simultaneous approach

Simultaneous resolution method is based on the pure mathematical description of the investigated system. It is not necessary to define modules that evaluate output values from input quantities and state parameters: system flow sheet does not influence equations hierarchy and the resolution approach. The functional and state relationships necessary to describe fully the modelled thermal system define, in most of the cases, a nonlinear equation system. A solution approach that solves simultaneous nonlinear equation is then instituted [15]. Even if the basic concept of this approach seems quite simple, its implementation is not always immediate, and the solution technique could be often very complicated. In fact, it is possible to have a high number of nonlinear equations to solve. Another problem is that the system configuration could not lead to a solution. Furthermore, starting values are viable to solve the problem and their identification can also be a complicated task to be performed [15]. On the other hand, simultaneous resolution method allows to handle design specifications and on the outputs and in any intermediate streams.

### **2.3.3 Comparison between Sequential and Simultaneous approaches**

Both of the aforementioned methods have positive and negative peculiarities, and it is hard to define a better approach in a general way. From time to time, the choice of the resolution approach must fall on the method that allows defining and solving the mathematical model of the system in the easier and more effective way. In [15], Boehm makes a comparison between Sequential and Simultaneous approach. Sequential approach appears slightly preferable to Simultaneous approach. In fact, it allows defining subroutines associated with real components of the modelled system and, therefore, it simplifies the creating process of versatile modules associated to components widely used in thermal systems. This is a significant benefit if flexibility and versatility are considered as main peculiarities of the developing model. In some cases, Simultaneous approach could be preferable in virtue of its independence from the flow sheet of the system and its higher computational efficiency. On the other hand, a lack of flexibility affects this method. In fact, a model build up with simultaneous approach cannot be easily adapted for systems with different configuration.

In this work, Sequential approach has been adopted to create a dynamic off-design model of an ORC system. Modular-Sequential method was chosen in order to create flexible modules describing some of the most widely used components of energy systems. Subroutines can be easily modified in order to be suitable for a wide range of models and test cases.

## **2.4 Review of thermal and energy systems dynamic models**

This paragraph reports a brief literature review of thermal and energy systems dynamic modeling. In particular, papers dealing with numerical and object-oriented modeling of thermal systems have been taken into account.

### **2.4.1 Dynamic modeling techniques**

Importance of dynamic models and simulations is rapidly growing in recent years, due to the increasing need to simulate and analyse unsteady operation of complex systems. In fact, knowing dynamic response of a specific system undergoing a change in operational or boundaries conditions allows improving preliminary design stage and control strategy. This led to a high level of accuracy and sophistication of recent modeling and simulation techniques. Many solutions to model heat exchange processes and turbomachineries have been developed. In the following, basic concepts and methodologies characterizing the framework within which this work is included are presented.

As mentioned in paragraph 2.2, simultaneous and sequential approaches are widely used in system's modeling. The choice of the approach to follow is not always straightforward, because both the first and the latter have positive peculiarities and

drawbacks. However, in almost all the papers considered in this review a modular sequential approach was adopted in virtue of its flexibility.

Many of the works that have been considered in the preliminary part of this thesis deal with the development of a flexible and reusable library of modular dynamic components, which can be used to predict dynamic behaviour of different energy systems.

In [16] and [34], authors present a dynamic modeling software for energy systems called SimECS, developed at the Delft University of Technology. This software is based on a modular and causal paradigm: systems are formed by components which in turn are formed by predefined modules characterized by causal interaction. Physical relations and conservation laws are at the base of implemented equations. System is described by an algebraic and differential equations system. The choice of the modular modeling approach mainly derives from its flexibility. In fact, changes to the system configuration can be easily made by just replacing components accordingly to the modelled plant's structure. In this first part of the work, composed by two papers, authors present elementary modules composing the modeling software SimECS. Fluid flow module, fluid thermal resistive module, solid thermal storage module, solid rotational storage module are presented. These elements are subsequently used to build up the dynamic model of a steam cycle and simulation results have been validated with experimental data. To be noted that bilateral coupling principle [16] must be taken into account when connecting resistive and storage components or modules, in order to assure the well-posedness of the mathematical problem and to avoid algebraic loops. In the second part of the work, various simECS components are presented: heat exchangers, the axial impulse turbine, the pump. These components have been used to build a dynamic model of a biomass fired power plant with an electrical power output of about 0.6 MW. Steady state and dynamic calculations have been carried out, simulating a step increase of pump rotational speed and flue gas mass flow rate starting from design point conditions.

Casella et al. present in [7] a software library of modular reusable dynamic models of ORC components developed in MODELICA®. The work aims to provide an environment and a methodology to test the dynamic response of ORC power systems for stationary applications as well as heat recovery from mobile engines. In this case, quite strong simplifications were applied to heat exchanger models. Heat transfer coefficient on working fluid side of the evaporator was neglected, considering overall heat transfer coefficient essentially influenced only by the low heat transfer coefficient on the flue gas side. A control system was implemented, controlling turbine inlet temperature by acting on the turbopump rotational speed. The model has been validated carrying out a comparison between simulation results and experimental data.

Object-oriented sequential modeling approach also characterizes Vaja's work, presented in [8]. In this case, a wide object oriented library of models for the dynamic simulation of energy systems has been developed. Author's efforts were focused on building up a flexible Simulink® library of components. Subsequently, they have applied to the dynamic modeling of combined ICE-ORC power plants. Methodologies and building process of each component have been precisely exposed. Heat exchangers have been modelled adopting a discrete volume approach, while turbomachineries characteristic maps have been defined by means of general equations. Differential equation system describing the whole model was solved adopting finite difference method.

In some other cases, specific models have been developed to study the response of a particular ORC power plant.

In [13] and [35], Quoilin et al. present a dynamic model of an ORC energy system. In this case, the model was developed to study the system's reaction to transient conditions and to define and compare different control strategies. Furthermore, two studies of small scale ORC energy systems are proposed in [13]. As in [8], also in these works a finite volume approach was adopted to develop heat exchangers dynamic models. Pump and vapour expander dynamic models are also presented. MODELICA® was chosen as programming ambient.

In [9], Manente et al. present a Simulink® off-design model of an Organic Rankine Cycle exploiting geothermal heat. The model was used to find the optimal operating parameters to maximize the electricity production when changes in ambient temperature and geofluid temperatures occur. Sequential approach was adopted. Dynamic behaviour of the system was simulated by adding two capacities in the plant layout. The first one was placed downstream the evaporator, while the second one was placed downstream the condenser. Capacities were modelled by unsteady form of mass and energy balance equations. Heat exchangers were modelled adopting the log mean temperature difference method. Characteristic maps of the heat exchangers were defined by using Aspen Shell & Tube Exchanger®.

The aim of this work is to develop an off-design dynamic model of an ORC system exploiting low grade waste heat of ICE on board an LNG carrier. However, using a sequential modular approach, components can be easily modified and reused to describe dynamic response of different energy plants. Thus, different configuration (saturated or superheated cycle) or different working fluid can be simulated by simply modifying part of the subroutines or by adding/replacing components of the system's model. Final result, therefore, is similar to the one given by the development of a library of models.

Since a dynamic model has to be defined, leading dynamics of the analysed system must be identified and accurately modelled. Heat exchangers and capacities are the components which mostly influence system dynamics, in virtue of their thermal and mass inertia. In order to describe dynamic behaviour of heat exchangers, different techniques have been analysed. As reported in the open literature, moving boundaries and discretization techniques are the most widely adopted ones. In [10] Wei et al. present a MODELICA® dynamic model for an ORC, to be used for the design of control and diagnostic systems. Both moving boundaries and discretization approaches were implemented and compared in terms of accuracy, complexity and computing speed. The model has been validated making a comparison between simulation results and experimental data. From the validation procedure emerges that while both models have good accuracy, moving boundaries is faster and, therefore, more suitable for control design applications.

In [14], Jensen applied moving boundaries technique to model evaporators and condensers in refrigeration systems. He presents a new general moving boundary model and a new average void model, the latter taking into account the influence of the slip and the inlet and outlet quality. Furthermore, a new discretized model was developed and compared with the one based on moving boundary approach. Experimental data validated both the new discretized and the new moving boundary models.

Moving boundary and discretization techniques seem to give similar results in terms of accuracy. However, as reported in [13], moving boundaries models are generally less accurate and less robust through start-up and load-variation transients.

Considering robustness and accuracy main features of a dynamic model, discretization technique was chosen in this work.

About capacities, Åström et al. developed a drum boiler dynamic model based on unsteady form of mass and energy balance equations, which is exposed in [36]. The model was built with a nested structure: a simple dynamic model based on mass and energy balance equations was subsequently improved by taking into account the distribution of steam in risers and drum, in order to accurately describe dynamic behaviour of liquid level in the drum boiler. However, in order to model a simple capacity, within which liquid and vapour coexist in saturation conditions, the simplest model is sufficient. In this work, hot drum and cold drum has been modelled taking inspiration from [36].

Since leading dynamics of the modelled energy systems are related to capacities and heat exchangers, and since an overall view on the system's dynamics is aimed to be analysed, simple not state determined models were considered for turbomachineries. As reported in [8], characteristic head and efficiency maps for a single stage radial pump have been described in an analytical form, easily modifiable and replaceable with more accurate maps provided by pump's manufacturer. Analogously, Stodola's semi empirical correlation has been adopted to evaluate turbine's mass flow rate, while efficiency was provided by specific equation expressed in function of cinematic ratio. In other works, like [9] and [10], authors used characteristic maps of pump and turbine to develop mathematical models derived from manufacturer's data. Since no manufacturer's data are available, in this work simple characteristic maps for turbomachineries have been implemented, as Vaja exposed in [8]. However, it should be noted that the pump and turbine models exposed in this thesis are easily modifiable and, therefore, more accurate characteristic maps can be implemented on a later time.

## 2.5 Summary

In this chapter, classification criteria and approaches to system modeling were presented. Classification takes into account geometry, the existence of system parameters, time dependence and type of mathematical correlations adopted. Furthermore, a distinction between design and off-design models has been presented, focusing on the choice of independent and dependent variables in both cases. A comparison between Simultaneous and Sequential approaches has been carried out, underlying positive peculiarities and drawbacks of both the approaches. Finally, a brief overview of the open literature dealing with modeling approaches and techniques is reported.



## 3 DYNAMIC MODEL OF AN ORGANIC RANKINE CYCLE SYSTEM

In the previous chapters, an overview on ORCs technology and modelling methodologies has been presented, trying to give a brief and comprehensive description of the knowledge applied in the modelling process. The aim of this chapter is not only to introduce the dynamic off-design model of the current ORC energy system, but also to expose the methodology adopted to develop these flexible and easy to modify models.

### 3.1 Introduction

This section reports the complete set of models developed in order to describe the dynamic behaviour of an ORC power plant. As authors suggest in [8, 13], since leading dynamics of the heat exchangers are much slower than those of pump and turbine, the latter can be described as static components. Therefore, not all the components described in this work were modelled considering their real dynamic behaviour. Dynamic models of hot drum, cold drum, preheaters, condenser and evaporator have been developed. Conversely, pump and turbine were considered as static components. A static model was developed for superheater, in virtue of the slight enthalpy increase occurring in this component.

The following paragraphs present each of the models built to describe the behaviour of the current ORC energy system, particularly focusing on methodology, simplifying assumptions and governing equations.

### 3.2 Static model of a counterflow heat exchanger based on the $\epsilon$ -NTU method

This paragraph describes a static model for a counterflow heat exchanger. It has been developed to be used in those cases when dynamic behaviour of the modelled heat exchange process is considered negligible. The model is based on the  $\epsilon$ -NTU method, where  $\epsilon$  expresses the effectiveness of the heat exchanger. Compared to dynamic models presented in the previous paragraphs of this chapter, this static model is significantly faster. In fact, since dynamics of the heat exchange process is neglected, the component can be described by means of an algebraic equation system, which requires minor calculation time. To be noted that input values request by this static model are the same of the ones required by the dynamic models, thus they can be switched quite readily. Input quantities are listed below:

- i. Mass flow rate of both fluids.
- ii. Inlet temperature of both fluids.
- iii. Pressure of both fluids.

Output values can be any of the quantities calculated during simulation. Main values are:

- i. Outlet temperature of both fluids.
- ii. Effectiveness of the heat exchanger.
- iii. Heat exchanged.

This static model refers to a pipe in pipe configuration with perfect countercurrent. Fluids flowing in the internal pipe and in the annulus are considered in single-phase state. No phase-change is considered. Gnielinski correlation was adopted to evaluate Nusselt number of both fluids. See equations from (3.16) to (3.19). Heat exchanger performance parameters and output values are evaluated applying the  $\varepsilon$ -NTU method [37, 38]. Considering a hot fluid and a cold fluid flowing along the two heat exchanger sides, it is possible to define heat exchanger effectiveness with the following equation:

$$\varepsilon = \frac{\dot{C}_h(T_{hin} - T_{hout})}{\dot{C}_{min}(T_{hin} - T_{cin})} \quad (3.1)$$

Or by the following one:

$$\varepsilon = \frac{\dot{C}_c(T_{cout} - T_{cin})}{\dot{C}_{min}(T_{hin} - T_{cin})} \quad (3.2)$$

In (3.1), (3.2) and in the following equations, subscripts  $h$  and  $c$  identify, respectively, hot and cold fluid.  $\dot{C}_h$  and  $\dot{C}_c$  express, respectively, hot and cold fluid heat capacity rates, determined by the product of mass flow rate and constant pressure specific heat:

$$\dot{C} = \dot{m} \cdot c_p \quad (3.3)$$

Minimum heat capacity rate is determined comparing hot and cold fluid value of this quantity:

$$\dot{C}_{min} = \min\{\dot{C}_h, \dot{C}_c\} \quad (3.4)$$

As reported in [38], the number of transfer units  $NTU$  can be calculated using the following equation:

$$NTU = \frac{K_e A_e}{\dot{C}_{min}} \quad (3.5)$$

With usual definition for symbols  $K_e$  and  $A_e$ .

For a pipe in pipe heat exchanger with perfect countercurrent, effectiveness is given by:

$$\varepsilon = \frac{1 - \exp[-NTU(1-C_r)]}{1 - C_r \exp[-NTU(1-C_r)]} \quad \text{if } C_r < 1 \quad (3.6)$$

$$\varepsilon = \frac{NTU}{1 + NTU} \quad \text{if } C_r = 1$$

With  $C_r$  given by the ratio between heat capacity rates:

$$C_r = \frac{\dot{C}_{min}}{\dot{C}_{max}} \quad (3.7)$$

Finally, overall heat exchanged can be calculated with the following equation, considering the definition of effectiveness given by (3.1) and (3.2):

$$q = \dot{C}_{min}(T_{hin} - T_{cn}) \quad (3.8)$$

To be noted that an iterative solution process is necessary, since thermodynamic properties of both fluids should be evaluated at an average temperature characterizing heat exchange process. Such a temperature value is not calculable straightforward, because outlet temperature of both fluids are unknown variables of the equation system. However, by setting outlet temperature of both fluids equal to respective inlet temperatures, the model is able to calculate a first approximation value of both the hot and cold flows outlet temperatures. For clarity, a scheme of the iterative solution process is reported below.

- 1) Heat exchange area, pipe length and diameters of the heat exchanger are parameters set in the preliminary design phase. Furthermore, inlet temperature, mass flow rates and pressure of both the hot and cold fluid are input values of the model. A proper value is set for the tolerance parameter *error*, which defines the convergence of the system solution.
- 2) First calculation: outlet temperature of both fluids is set equal to the inlet temperature. An approximate average temperature is then calculated:

$$\bar{T}_H \bar{T}_c$$

- 3) It is now possible to calculate average thermodynamic properties of both fluids during the heat exchange process. Convective coefficients are evaluated.
- 4) Using equations from (3.1) to (3.8),  $\epsilon$ -NTU method is applied to calculate heat exchanged  $q$  during the process.
- 5) Knowing the heat exchanged, outlet temperature of both the hot and cold fluid are calculated.
- 6) A new value for the average temperature of both fluids is calculated.
- 7) A comparison between new and previous values of average temperature of both fluid is carried out. Two conditions may occur:
  - a) Absolute value of the difference between new and previous values of  $\bar{T}_h$  and  $\bar{T}_c$  exceeds *error's* value. In this case, calculation starts again from step 3), using average temperatures calculated at step 6).
  - b) Absolute value of the difference between new and previous values of  $\bar{T}_h$  and  $\bar{T}_c$  does not exceed *error's* value. In this case, a convergence of the solution is reached and, therefore, calculation terminates. Output values are set equal to those values obtained at the end of the previous iteration step. Main output variables of the model are the followings:

$$q, \bar{T}_h, \bar{T}_c, T_{h,out}, T_{c,out}$$

Table 3.1 defines parameters, input and output variables of the model. Table 3.2 presents the equation system.

INPUT PARAMENTERS	heat exchange area, geometry (diameters, pipe length, no. of pipes)
INPUT VARIABLES	$[T_{in}, p, \dot{m}]_{hc}$ : inlet temperature, pressure and mass flow rate of both fluids ( $H, C$ )
OUTPUT VARIABLES	$q, \bar{T}_h, \bar{T}_c, T_{h,out}, T_{c,out}$

Table 3.1  
Input and output variables of the static counterflow heat exchanger model.

1	$q^t = \varepsilon^t (\dot{m}^t c_p^t)_{min} (T_{Hin}^t - T_{Cin}^t)$	Overall variables: 10
2	$q^t = \dot{m}_{HC}^t c_{pH}^t (T_{Hin}^t - T_{Hout}^t)$	Independent variables: 7
3	$q^t = \dot{m}_{CC}^t c_{pC}^t (T_{Cout}^t - T_{Cin}^t)$	Dependent variables: 3

Table 3.2  
Equation system of the static model of counterflow heat exchanger.

Auxiliary equations: empirical correlation for the calculation of convective coefficients and fluid's thermodynamic properties library.

### 3.3 Dynamic models of heat exchangers

This section reports the description of the heat exchangers distinguishing between single phase and two-phase heat exchange process. In both cases, a discrete volume approach was used in order to model the heat exchange process. It was necessary a preliminary design process to define geometry and size of each heat exchanger. For sake of simplicity, a counterflow tube in tube configuration was choose. In order to limit the heat exchanger length, a suitable number of pipes in parallel configuration was considered. Fluids behaviour and heat exchange process are considered identical in each of the single pipes.

The following assumptions were considered in the modelling process [8]:

- Head losses are neglected for both fluids along the pipe. Accordingly, the application of momentum balance equation results unnecessary and, therefore, it is not applied to the block referring to each lumped volume.
- Without any phase change, both fluids are considered as incompressible. Therefore, mass balance equation is not applied to the block referring to each lumped volume and no mass accumulation is considered for both the fluids.
- Thermal capacitance of the metal pipe has been neglected.
- Axial conductive heat flux has been neglected for both fluids.
- Since external pipe is considered ideally insulated, heat losses to the environment are null.
- Only convective heat flux between fluids and pipe has been considered.
- Lumped cinematic and thermodynamic properties are considered in each of the discretisation volumes.

An elementary block was created in order to describe the fluid dynamics and heat transfer processes that occur in each of the discretization volumes. It contains energy balance equations and heat transfer correlations for both the water and the organic fluid side. Mass balance equations are implemented in the case of phase change on the organic fluid side of the heat exchanger.

The following sections present the different typologies of heat exchanger models developed in this work, focusing on the heat transfer correlations and the balance

equations adopted. A flexible dynamic model for single phase and two-phase heat exchangers is described in the following. A simplified static model for super-heater is then presented.

### 3.3.1 Heat exchanger with no phase change

In this kind of heat exchanger both fluids does not undergo any phase change. Under this hypothesis, heat exchange process occurs between a gas and a liquid, two liquid or two gases. The counterflow pipe in pipe heat exchanger has been uniformly split in a proper number of finite elements. Each of these elements represent a finite portion of the heat exchanger and an elementary block describes physical process occurring in the considered finite volume. Blocks are linked together, in order to allow input and output variables exchange. The discretization adopted leads to a two dimensional model. In fact, the variation of state parameters is assessed not only along axial direction, but also along radial direction. Mean values of the thermodynamic and cinematic properties of both fluids characterize the state of the lumped volumes. State variables of each lumped volume are considered as input variables for the following block, consistently with the direction of the fluid outflow.

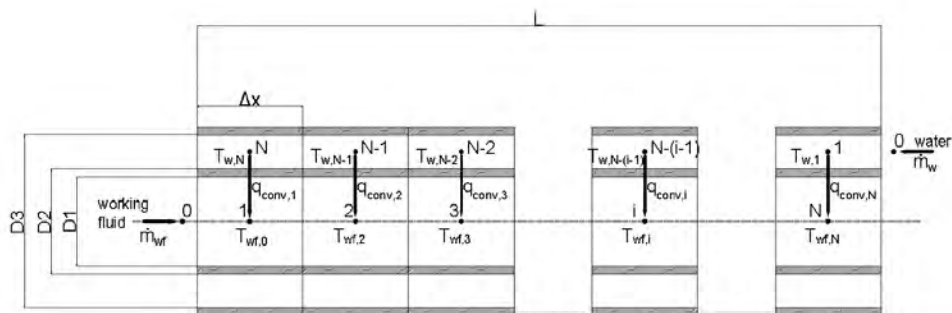


Figure 3.1  
Discretization of pipe in pipe counterflow heat exchanger with no phase-change.

As mentioned in chapter 3, variable state define the behaviour of the system during simulation. In single-phase heat exchangers, pressure and absolute temperature are adopted as state variables.

In the following paragraphs, the main equations adopted in each elementary block corresponding to a discretization volume of the heat exchanger are presented.

### 3.3.1.1 Internal pipe: organic fluid side

Since no phase change occurs on organic fluid side, mass flow rate is considered as a constant value. Organic fluid exchange heat with the water flowing in the annulus. In the case of preheaters and super heater, organic fluid receive heat from the hot water, while in condenser it released condensation heat to the cooling seawater. The following provides the energy balance equation applied to the control volume  $i$  at time  $t$  in the case of heating process of the organic fluid:

$$\dot{m}_{wfi}^t \bar{c}_{pwfi}^t (T_{wfi-1}^t - T_{wfi}^t) + q_{conv i}^t = \bar{\rho}_{wfi}^t V_{wf} \bar{c}_{pwfi}^t \frac{dT_{wfi}^t}{dt} \quad (3.9)$$

The only unknown of the previous equation is the time derivative of the temperature of the organic fluid. In fact:

- Working fluid mass flow rate  $\dot{m}_{wfi}$  was imposed as a constant value, defined by turbo machinery present in the system (pump or vapour expander).
- Since temperature and pressure of the working fluid at time  $t$  are known, mean value of specific density  $\bar{\rho}_{wfi}$  and heat capacity at constant pressure for the working fluid  $\bar{c}_{pwfi}$  are defined using thermodynamic properties tables [39]
- The number of discretization volumes adopted defines the control volume of the elementary block on the working fluid side of the heat exchanger  $V_{wf}$ .
- Temperature of both fluids flowing in the heat exchanger at the current time  $t$  are define from initial state conditions (if  $t=0$ ) or from integration process at the previous time step ( $t>0$ ).
- Global heat transfer coefficient, temperature of both fluids flowing in the heat exchanger at the current time  $t$  and heat exchange area of the control volume  $i$  allow to determine heat exchanged  $q_{conv i}$ .

Rearranging the terms, it is possible to explicit the unknown quantity:

$$\frac{dT_{wfi}^t}{dt} = \frac{\dot{m}_{wfi}^t \bar{c}_{pwfi}^t (T_{wfi-1}^t - T_{wfi}^t) + q_{conv i}^t}{\bar{\rho}_{wfi}^t V_{wf} \bar{c}_{pwfi}^t} \quad (3.10)$$

A numerical integration process then determines the temperature of the working fluid at time step  $t+1$ . This calculation is carried out using the integration block implemented in Simulink®. In order to evaluate the state system during the simulation, proper initial condition for the temperature of water must be considered.

### 3.3.1.2 Annulus: water side

Water flowing in the annulus exchanges heat with the working fluid flowing in the internal cylinder. In preheaters, evaporator and super heater water is the hot source

and it is cooled by the working fluid during preheating, evaporating and superheating processes. Conversely, seawater is the cold sink of the system and it is heated by working fluid during its condensation. No phase change occurs on water side of any heat exchanger. Thus, mass flow rate entering and leaving each of the elementary control volumes are the same and mass balance equation is redundant as mentioned before for the internal pipe. Energy balance equation in the case of heating process of organic fluid is given by the following, similar to that reported for the internal pipe:

$$\dot{m}_{wi}^t \bar{c}_{pwi}^t (T_{wi-1}^t - T_{wi}^t) - q_{conv,i}^t = \bar{\rho}_{wi}^t V_w \bar{c}_{pwi}^t \frac{dT_{wi}^t}{dt} \quad (3.11)$$

The only unknown is the time derivative of the water temperature in the current discretization volume. Rearranging the terms, the following explicit equation form is obtained:

$$\frac{dT_{wi}^t}{dt} = \frac{\dot{m}_{wi}^t \bar{c}_{pwi}^t (T_{wi-1}^t - T_{wi}^t) - q_{conv,i}^t}{\bar{\rho}_{wi}^t V_w \bar{c}_{pwi}^t} \quad (3.12)$$

With a similar meaning of the terms respect previous equations.

A numerical integration process then determines the temperature of the fluid at time step  $t+1$ . This calculation is carried out using the integration block implemented in Simulink®. Proper initial condition for the temperature of the working fluid must be considered, in order to evaluate the state system during the simulation.

### 3.3.1.3 Single-phase heat exchange correlations

For sake of simplicity, thermal dynamic behaviour of the wall pipe was not considered in the current model. Heat flux exchanged between fluids flowing in the heat exchanger has been evaluated by calculating global heat transfer coefficient of each discretization volume, considering:

- Convective heat flux between fluid in the inner pipe and the pipe wall.
- Heat flux resistance of the pipe wall.
- Convective heat flux between fluid in the annulus and the pipe wall.

Two different heat flux correlations have been used, in order to distinguish between liquid and gaseous single-phase fluxes. Sieder & Tate correlation was used for the liquid single-phase state, to take into account effects of the organic fluid viscosity on the heat exchange process [40]. Gnielinski correlation has been used for the gaseous single-phase state [38].



- Sieder & Tate correlation

Single-phase organic fluid flows in the inner pipe, with inner diameter  $D_1$  and outer diameter  $D_2$ . Reynolds number is given by the following:

$$Re_{1f} = \frac{4\dot{m}_{1f} D_1}{\pi D_1^2 \mu} \quad (3.13)$$

In the case of turbulent flow, Nusselt number can be evaluated using Sieder & Tate correlation [38, 40]:

$$Nu_{1f} = 0.023 Re_{1f}^{0.8} Pr_{1f}^{0.33} \left( \frac{\mu}{\mu_p} \right)^{0.14} \quad (3.14)$$

The terms in brackets represents the ratio between fluid viscosity evaluated at the fluid temperature and at the pipe wall temperature. An iterative calculation process is necessary to determine this term. In the design model of the heat exchangers, a rigorous iterative solution has been carried out. In the dynamic off design model, the iterative resolution process has been approximate imposing a constant value for  $\left( \frac{\mu}{\mu_p} \right)$ , set basing on the results of a sensitivity analysis.

The convection coefficient is calculated from the next correlation:

$$\alpha_{1f} = \frac{Nu_{1f} \lambda}{D_1} \quad (3.15)$$

- Gnielinski correlation

Single-phase water at liquid state flows in the annulus, defined by internal diameter  $D_2$  and external diameter  $D_3$ . Single-phase organic fluid at gaseous state in the inner pipe. In these cases, Gnielinski correlation has been adopted to determine convective heat transfer coefficient between single-phase flow and the pipe wall. Reynolds number is expressed by the following:

$$Re_{1f} = \frac{4\dot{m}_{1f} D_h}{\pi(D_3^2 - D_2^2)\mu} \quad (3.16)$$

Where  $D_h$  represents the hydraulic diameter of the conduct, defined by:

$$D_h = \frac{4A}{P} \quad (3.17)$$

Nusselt number in turbulent flow can be calculated using Gnielinski correlation [38]:

$$Nu_{1f} = \frac{\left(\frac{f}{8}\right) (Re_{1f} - 1000) Pr}{1 + 127 \left(\frac{f}{8}\right)^{1/2} (Pr^{2/3} - 1)} \quad (3.18)$$

With the following expression adopted to define friction factor  $f$ :

$$f = (0.79 \ln Re_{1f} - 164)^{-2} \quad (3.19)$$

Convection coefficient is calculated from the usual correlation, given by equation (3.15).

- Overall heat transfer coefficient

Thermal resistances associated to the convective heat transfer process are evaluated from convection coefficients. Given the cylindrical geometry of the pipe, and setting external area as reference to calculate overall heat transfer coefficient, the following correlations are used to determine, respectively, the thermal resistance related to convection in the internal pipe and in the annulus [37]:

$$R_{ip} = \frac{D_2}{D_1} \frac{1}{\alpha} \quad (3.20)$$

$$R_a = \frac{1}{\alpha} \quad (3.21)$$

Thermal resistance of the pipe wall can be calculated from the following [37]:

$$R_p = \frac{D_2}{2\lambda} \ln \left( \frac{D_2}{D_1} \right) \quad (3.22)$$

Finally, overall heat transfer coefficient referred to external area can be calculated from next equation:

$$K_e = \frac{1}{R_{ip} + R_p + R_a} \quad (3.23)$$

Finally, it is possible to evaluate the heat flux exchanged in the discrete volume  $i$ . Since the heat exchanger has been discretized in a number of finite volumes, log mean temperature difference has been approximated with the temperature difference between fluids in each discretization volume. Thus, considering the heating process of the organic fluid, heat flux in the volume  $i$  is given by the following approximated equation:

$$q = K_e A_e (T_w - T_{wf}) \quad (3.24)$$

Following Table 3.3 presents the equation system that describe the behaviour of a discrete volume of the single-phase heat exchanger.

1	$\dot{m}_{wfi}^t \bar{c}_{pwfi}^t (T_{wfi-1}^t - T_{wfi}^t) + q_{conv}^t = \bar{\rho}_{wfi}^t V_{wfi} \bar{c}_{pwfi}^t \frac{dT_{wfi}^t}{dt}$	Overall variables: 19
2	$\dot{m}_{wi}^t \bar{c}_{pwi}^t (T_{wi-1}^t - T_{wi}^t) - q_{conv}^t = \bar{\rho}_{wi}^t V_w \bar{c}_{pwi}^t \frac{dT_{wi}^t}{dt}$	Independent variables: 16
3	$q_{conv}^t = K_{ei}^t A_{ei} (T_w^t - T_{wf}^t)$	Dependent variables: 3

Table 3.3  
Equation system of the dynamic model of heat exchanger with no phase change..

Auxiliary equations: empirical correlation for the calculation of convective coefficients and fluid's thermodynamic properties library.

### 3.3.1.4 Simulink® model of single-phase heat exchanger

Specific subroutines were developed to model heat exchange and other physical processes occurring in finite volumes. Simulink® model of a single phase heat exchanger presents the following structure.

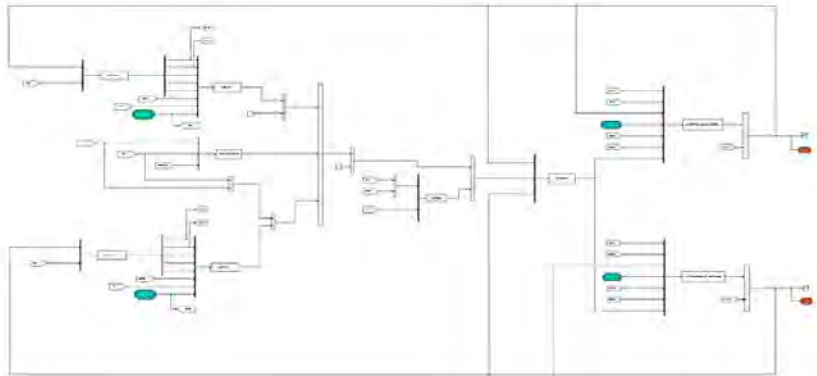


Figure 3.2  
Simulink ® single-phase heat exchanger elementary block layout

The elementary block built to model single phase heat exchange in each finite volume of the heat exchanger presents:

- Subroutines built to evaluate thermodynamic properties and convection coefficient of water flowing in the annulus at the current simulation time  $t$  are located on the upper left of the figure.
- Pipe wall thermal resistance calculation block.
- Subroutines built to evaluate thermodynamic properties and convection coefficient of the working fluid flowing in the internal pipe at the current simulation time  $t$  are located on the lower left of the figure.

As mentioned before, the dynamic effect of the pipe wall has been neglected. Heat exchanged is then calculated and used as input value for the energy balance equation applied to the control volume:

- Subroutine built to evaluate time derivative of water temperature in the discrete volume at the current time  $t$  is located on the upper right of the figure.
- Subroutine built to evaluate time derivative of the working fluid temperature in the discrete volume at the current time  $t$  is located on the lower right of the figure.

Finally, temperature of both fluids is calculated with a numerical integration process from time derivatives.

### 3.3.2 Heat exchanger with phase change

A dynamic model for condenser and evaporator is here presented. The structure of the model is similar to the one adopted for heat exchanger with no phase change, but in this case it is considered the possibility for the working fluid to evaporate or

condense. Evaporator and condenser are key elements in defining the dynamic behaviour of the investigated energy system. Thus, a rigorous dynamic model of heat exchangers is essential to describe dynamic behaviour of the system during transient states. On the other hand, modelling physical phenomena occurring during phase – change is quite complicated and not straightforward. As mentioned before, different approaches can be adopted to represent dynamics in evaporator and condenser. Moving boundaries and lumped volumes are the most widely used methods adopted for this purpose [8, 14, 10, 11, 13]. In this work, finite volume approach was chosen in virtue of its numerical robustness and accuracy [8, 13]. As in the case of heat exchanger with no phase–change, straight pipe in pipe configuration, with multiple pipes in parallel, was adopted. The pipe has been split into  $N$  longitudinal discrete volumes.

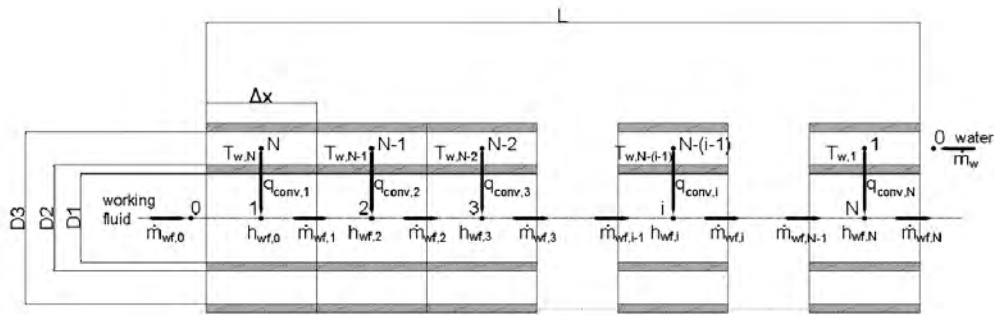


Figure 3.3  
Discretization of pipe in pipe counterflow heat exchanger with phase-change.

Again, an elementary block was built in Simulink® in order to represent all physical phenomena occurring within each discrete volume. Respect to the analogous block adopted for the heat exchanger with no phase change, two main differences emerge:

- A differential mass balance equation is now applied to each control volume. In fact, a brutal change in the specific density occurs during evaporation and condensation. Thus, it is necessary to calculate outflow mass flow rate of each control volume, knowing inflow mass flow rate and time derivative of density of the working fluid undergoing the phase – change. To be noted that numerical issue can affect calculation of time derivative of evaporating (condensing) working fluid.

Next figure represent the variation of density in function of vapour quality for R134a, at 2013.2 [kPa], during evaporation process. It is possible to note that for low vapour qualities, i.e. at the beginning of the phase – change process, the curve is very steep. Figure 3.4 reports the derivative of density as a function of vapour quality. Derivative of density can reach very high values, negative in the case of vaporization or positive in the case of condensation. This could lead to numerical instabilities and, therefore, to a failure in the simulation. In [13], Quoilin suggests the truncating of the vapour quality-derived density. For example, in the case of R134a, the truncation value was set equal to -1500. The choice of the truncating value derived from an analysis of

the behaviour of the working fluid adopted in the investigated ORC system during condensation and evaporation.

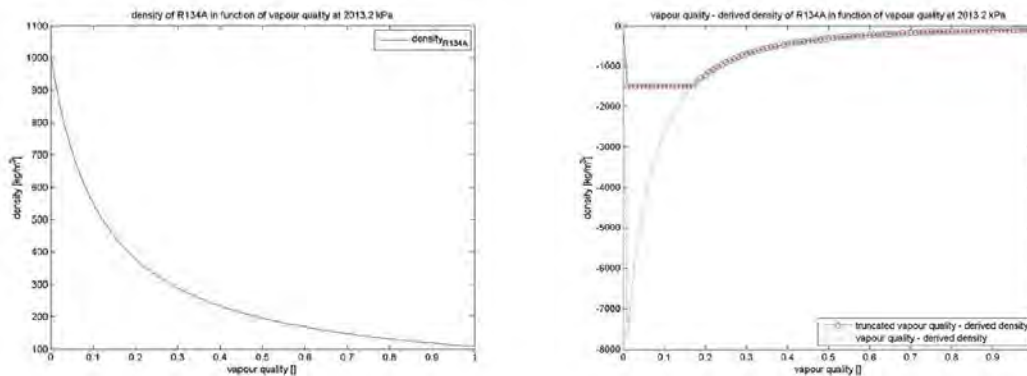


Figure 3.4

Qualitative trend of density and vapour quality-derived density of refrigerant R134A. In the right hand figure, truncation has been applied to density derivative.

- In order to describe with sufficient accuracy the phase change process occurring along the evaporator, Chen empirical correlation has been adopted [8, 41, 42]. Cavallini-Zecchin correlation has been chosen to calculate convective coefficient during condensation [43, 44]. Linearization between single phase (liquid and vapour) and two-phase convective heat exchange coefficient was introduced, as suggested by Vaja and Quoilin respectively in [8] and [13]. To be noted that, in general, working fluid enters the evaporator in sub cooled liquid state, and leaves the heat exchanger in a slight superheated state. Conversely, working fluid generally enters condenser in superheated vapour state, and leaves the heat exchanger in a slight sub cooled liquid state. In order to model the change in the convection coefficient passing from single-phase to two-phase condition, enthalpy has been adopted as state variable of the working fluid, instead of temperature. Under the hypothesis of constant pressure along the heat exchanger, enthalpy allows to uniquely define the physical state of the working fluid and, therefore, its quality. Correlation adopted to evaluate convection coefficient has been chosen basing on the quality of the working fluid in each discrete volume. Convection coefficient for evaporating-condensing fluid has been calculated with the over mentioned empirical correlations for a vapour quality of the working fluid included between  $\Delta x$  and  $(1 - \Delta x)$ , where  $\Delta x$  is the linearization parameter. This means that, for the evaporator:

- i. For  $x < 0$  (sub cooled liquid condition), Sieder & Tate correlation for single-phase state is adopted to calculate convective coefficient.
- ii. For  $0 < x < \Delta x$ , the heat convection coefficient derived from the linearization between Sieder & Tate's single phase coefficient and the value of Chen's heat exchange coefficient for the nucleate boiling in straight vertical pipes calculated setting vapour quality equals to  $\Delta x$ .
- iii. For  $\Delta x < x < (1 - \Delta x)$ , pure Chen's correlation is adopted without any modification.

- iv. For  $\Delta x < x < 1$ , the heat exchange coefficient derived from the linearization between the value of Chen's heat exchange coefficient for the nucleate boiling in straight vertical pipes calculated setting vapour quality equals to  $(1-\Delta x)$  and Gnielinski single-phase coefficient calculated considering saturated vapour state.
- v. For  $x > 1$ , Gnielinski correlation is used to calculate convection coefficient of single-phase vapour. For sake of simplicity, superheated vapour is approximated as saturated vapour.

Analogous considerations are valid for the condenser:

- i. For  $x < 0$  (sub cooled liquid condition), Sieder & Tate correlation for single-phase state is adopted to calculate convective coefficient.
- ii. For  $0 < x < \Delta x$ , the heat convection coefficient derived from the linearization between Sieder & Tate's single phase coefficient and the value of convective coefficient for condensation in horizontal smooth pipes, calculated with Cavallini-Zecchin correlation setting vapour quality equals to  $\Delta x$ .
- iii. For  $\Delta x < x < (1-\Delta x)$ , pure Cavallini-Zecchin correlation is adopted without any modification.
- iv. For  $\Delta x < x < 1$ , the heat exchange coefficient derived from the linearization between the value of Cavallini-Zecchin convection coefficient calculated setting vapour quality equals to  $(1-\Delta x)$  and Gnielinski single phase coefficient calculated considering saturated vapour state.
- v. For  $x > 1$ , Gnielinski correlation is used to calculate convection coefficient of single-phase vapour. For sake of simplicity, superheated vapour is approximated as saturated vapour.

Figure 3.5 and Figure 3.6 represent, respectively, results of the over mentioned linearization process in the case of evaporator and condenser, comparing convection coefficients during vaporization and condensation process with and without applying linear interpolation for vapour qualities included in ranges  $0 < x < \Delta x$  and  $\Delta x < x < 1$ .

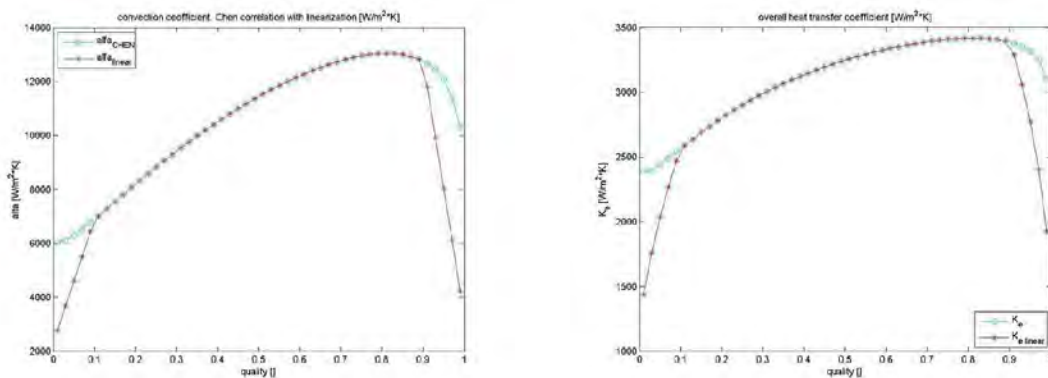


Figure 3.5

Chen's convective coefficient for nucleate boiling and overall heat transfer coefficient of the evaporator expressed in function of vapour quality. Red line represents linearized coefficients.

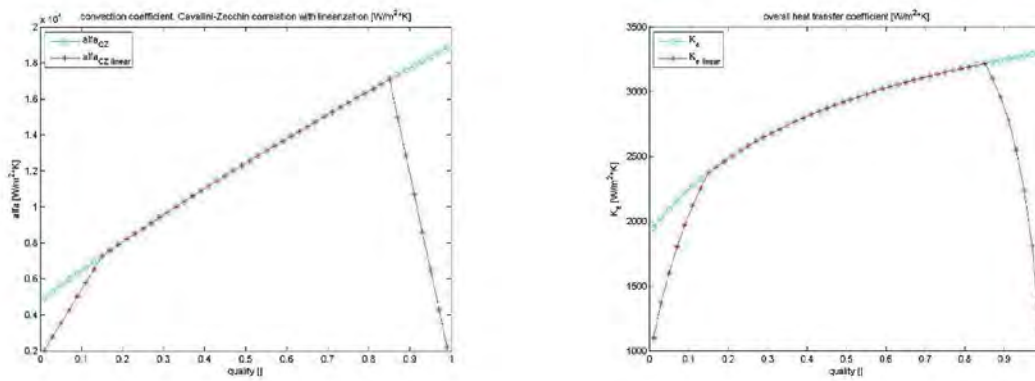


Figure 3.6

*Cavallini-Zecchin's convective coefficient for condensation and overall heat transfer coefficient of the condenser expressed in function of vapour quality. Red line represents linearized coefficients.*

Next paragraphs are focused on cardinal equations considered for the internal pipe, since equations adopted to model the annulus are identical to those reported in paragraph 3.3.1.2.

### 3.3.2.1 Internal pipe: organic fluid side

Organic fluid experiences phase change in evaporator and condenser. Considering the case of an evaporator, heat transferred from the hot source rises the enthalpy of the working fluid, that undergoes preheating, vaporizing and, eventually, superheating processes. Conversely, in the case of condenser, working fluid is cooled by refrigerant water flowing in the annulus. The heat rejected to the cold sink has the effect of cooling superheated (or saturated) vapour, then to condense it and, eventually, to sub cool it. During phase change, density undergoes a remarkable variation, and mass flow rate leaving each discrete volume could be considerably different from the entering one. Thus, mass flow rate in condenser and evaporator can no longer be considered as a constant value, as in the case of heat exchanger with no phase change. In order to determine mass flow rate leaving each discrete volume, differential mass balance equation has been implemented in each elementary block. Mass balance for control volume  $i$  at time simulation  $t$  is expressed by the following:

$$\dot{m}_{wfi-1}^t - \dot{m}_{wfi}^t = V_{wf} \frac{\partial \rho_{wfi}^t}{\partial t} \quad (3.25)$$

Rearranging the terms, mass flow rate leaving control volume  $i$  can be expressed by:

$$\dot{m}_{wfi}^t = \dot{m}_{wfi-1}^t - V_{wf} \frac{\partial \rho_{wfi}^t}{\partial t} \quad (3.26)$$



Mass flow rate  $\dot{m}_{wfi}^t$ , leaving control volume  $i$  and entering the following volume  $i+1$ , is necessary to solve energy balance equation applied to the current volume  $i$ . In summary, mass flow rate leaving a control volume defines the mass flowing within the control volume, and it is used as reference quantity to solve energy balance equation for the control volume  $i$  at time simulation  $t$ , that is expressed by the following differential equation [8]:

$$q_{conv}^t + \dot{m}_{wfi-1}^t h_{wfi-1}^t - \dot{m}_{wfi}^t h_{wfi}^t = V_{wf} \frac{d(\rho_{wfi}^t h_{wfi}^t - p_{wfi}^t)}{dt} \quad (3.27)$$

Neglecting time derivative of pressure, expressed by the term  $\frac{dp_{wfi}^t}{dt}$  [8], right hand term can be expressed as following:

$$V_{wf} \frac{d(\rho_{wfi}^t h_{wfi}^t - p_{wfi}^t)}{dt} = V_{wf} \left( \rho_{wfi}^t \frac{dh_{wfi}^t}{dt} + h_{wfi}^t \frac{d\rho_{wfi}^t}{dt} \right) \quad (3.28)$$

Substituting this new form in the energy balance equation and rearranging the terms, it is possible to explicit the unknown:

$$\frac{dh_{wfi}^t}{dt} = \frac{1}{\rho_{wfi}^t} \left( \frac{q_{conv}^t + \dot{m}_{wfi-1}^t h_{wfi-1}^t - \dot{m}_{wfi}^t h_{wfi}^t}{V_{wf}} - h_{wfi}^t \frac{\partial \rho_{wfi}^t}{\partial t} \right) \quad (3.29)$$

A numerical integration process then determines the enthalpy of the fluid at time step  $t+1$ . This calculation is carried out using the integration block implemented in Simulink®. In order to evaluate the state system during the simulation, proper initial condition for the temperature of working fluid must be considered.

### 3.3.2.2 Phase-change heat flux correlations: evaporation and condensation

During evaporation and condensation, thermodynamic properties of the working fluid vary significantly, strongly influencing the values of mass flow rate and convection coefficient along the heat exchanger. Thus, a volume discretization is useful to define local lumped values for thermodynamic properties of the working fluid, allowing the calculation of local mass flow rate and convection coefficient. As mentioned in the previous paragraphs, Chen and Cavallini-Zecchin empirical correlations has been used, respectively, to evaluate convective coefficient during evaporation and condensation. Cardinal equations are reported in the following.

- Chen's correlation for boiling heat transfer to saturated fluids in convective flow

Chen proposes a quite simple and straightforward correlation describing convection coefficient during evaporation with nucleate boiling. Fluid is assumed flowing in a smooth vertical pipe. Accordingly to [42, 41], Nusselt number is given by the sum of the contributes of evaporation in forced convection  $Nu_{DC}$  and nucleate boiling  $Nu_{DB}$  (see figure for a qualitative comparison between the two contributes):

$$Nu = Nu_{DC} + Nu_{DB} \quad (3.30)$$

First term on the right hand side of the equation can be expressed by the following:

$$Nu_{DC} = 0.023 Re_l^{0.8} Pr_l^{0.4} F \quad (3.31)$$

With  $Re_l$ , representing Reynolds number of the liquid phase, given by:

$$Re_l = \frac{4\dot{m} (1-x)}{\pi D \mu_l} \quad (3.32)$$

$D$  represents the hydraulic diameter. In the case of pressurized liquid flowing within a cylindrical pipe, it coincides with the internal pipe diameter.

$Pr_l$  expresses the Prandtl number of the liquid phase. It can be evaluated, as well as any other thermodynamic property, from Refprop database [39].  $F$  is an empirical factor taking into account the characteristics of the fluid flow. It is calculated from the Martinelli's factor  $X_{tt}$ :

$$X_{tt} = \left(\frac{1-x}{x}\right)^{0.9} \left(\frac{\rho_v}{\rho_l}\right)^{0.5} \left(\frac{\mu_l}{\mu_v}\right)^{0.1} \quad (3.33)$$

$$F = 235 \left( \frac{1}{X_{tt}} + 0.213 \right)^{0.736} \quad \text{if } X_{tt} < 10 \quad (3.34)$$

$$F = 1 \quad \text{if } X_{tt} > 10$$

$Nu_{DB}$  is expressed by the following empirical correlation:

$$Nu_{DB} = 0.001225 Ja^{0.24} Pr_l^{0.21} \left( \frac{D \Delta p}{\sigma} \right)^{0.5} \left( \frac{\rho_l D^2 \Delta p}{\mu_l^2} \right)^{0.25} \quad (3.35)$$

$S$  is an empirical factor, which dampens nucleate boiling contribution with increasing two-phase Reynolds number:

$$S = \frac{1}{1 + 25310^{-6} Re_{2f}^{117}} \quad (3.36)$$

Where  $Re_{2f}$  can be expressed by the following:

$$Re_{2f} = Re_l F^{125} \quad (3.37)$$

Jacob number  $Ja$  is expressed by:

$$Ja = \frac{c_l \Delta T_w}{h_{sat}} \quad (3.38)$$

Where  $c_l$  represents specific heat of the working fluid in constant pressure conditions,  $h_{sat}$  gives the difference between saturated vapour and saturated liquid specific enthalpies, i.e. the latent heat of vaporization of the working fluid. Finally,  $\Delta T_w$  represents the difference between pipe wall temperature and fluid saturation temperature. The term  $\sigma$  expresses surface tension of the working fluid, while  $\Delta p$  gives the difference between saturation pressure of the working fluid at the pipe wall temperature and hydrostatic pressure of the fluid [8]:

$$\Delta p = p(T_w) - p(T_{wf}) \quad (3.39)$$

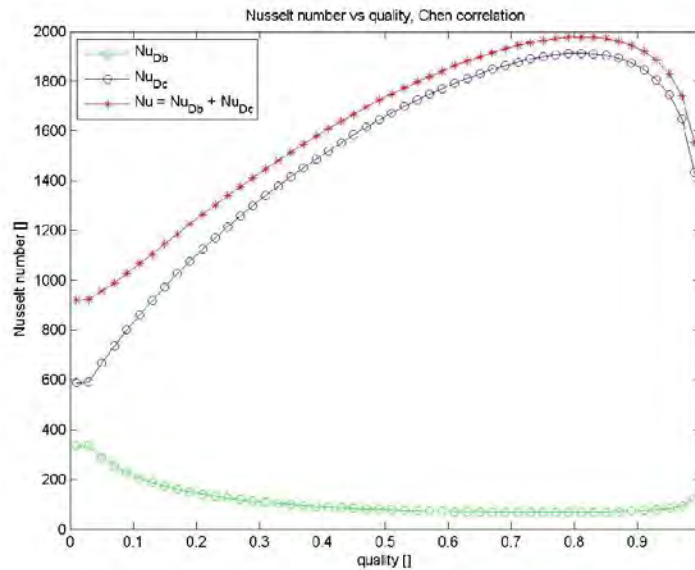


Figure 3.7  
Overall Nusselt number  $Nu$ , vaporization in forced convection term  $Nu_{Dc}$  and nucleate boiling term  $Nu_{Db}$  expressed as a function of vapour quality

- Cavallini-Zecchin's correlation for heat transfer in forced convection condensation

Cavallini-Zecchin's empirical correlation has been chosen to describe condensation process. This correlation allows calculating heat transfer coefficient in forced convection condensation, and it is based on the Dittus-Boelter equation form. Cardinal equations composing Cavallini-Zecchin condensation model are reported in the following.

Nusselt number is given by [40]:

$$Nu = 0.05 Re_{eq}^{0.8} Pr_l^{0.33} \quad (3.40)$$

Where, as usual,  $Pr_l$  expresses Prandtl number for the liquid phase. Equivalent Reynolds number is given by the following equation [40]:

$$Re_{eq} = G (1 - x) + Gx \left( \frac{\rho_l}{\rho_g} \right)^{0.5} \quad (3.41)$$

Where  $G$  expresses specific mass flow rate, calculated as the ratio between overall mass flow rate and flow section of the pipe and  $x$  gives vapour quality. Equivalent Reynolds number can be calculated by the following expression:

$$Re_{eq} = \frac{G_{eq} D}{\mu_l} \quad (3.42)$$

Where  $\mu_l$  represents dynamic viscosity of the working fluid at the liquid state.

To be noted that, as in the case of evaporation, different empirical models to describe condensation are available in the open literature. In [45], author compares different two-phase condensation heat transfer models basing on the comparison of the boundary condition. Cavallini-Zecchin's correlation presents high deviation from reference value of convective coefficient for saturated liquid conditions. On the other hand, in [44] authors underline the good prediction capacity of this correlation in the case of flow condensation of R-134a inside a vertical smooth pipe. However, as mentioned before, linearization has been implemented to evaluate convective coefficient for two-phase state near to saturation conditions, limiting the over mentioned drawback.

For both evaporation and condensation, once Nusselt number is calculated, it is possible to evaluate convection coefficient with the usual equation:

$$\alpha = \frac{Nu \lambda_l}{D} \quad (3.43)$$

Following Table 3.4 reports the equation system that describe the behaviour of a discrete volume of the heat exchanger with phase-change:

1	$\dot{m}_{wfi-1}^t - \dot{m}_{wfi}^t = V_{wf} \frac{\partial \rho_{wfi}^t}{\partial t}$	Overall variables: 18
2	$\frac{dh_{wfi}^t}{dt} = \frac{1}{\rho_{wfi}^t} \left( \frac{q_{conv,i}^t + \dot{m}_{wfi-1}^t h_{wfi-1}^t - \dot{m}_{wfi}^t h_{wfi}^t}{V_{wf}} - h_{wfi}^t \frac{\partial \rho_{wfi}^t}{\partial t} \right)$	Independent variables: 14
3	$\dot{m}_{wi}^t \bar{c}_{pwi}^t (T_{wi-1}^t - T_{wi}^t) - q_{conv,i}^t = \bar{\rho}_{wi}^t V_w \bar{c}_{pwi}^t \frac{dT_{wi}^t}{dt}$	Dependent variables: 4
4	$q_{conv,i}^t = K_{ei}^t A_{ei} (T_w^t - T_{wf}^t)$	

Table 3.4  
Equation system of the dynamic model of heat exchanger with phase change.

Auxiliary equations: empirical correlation for the calculation of convective coefficients and fluid's thermodynamic properties library.

### 3.3.2.3 Simulink® model of heat exchanger with phase change

As in the case of heat exchanger with no phase change, an elementary block containing all the subroutines necessary to describe heat exchange and mass transport

phenomena was developed in Simulink® ambient. Each finite volume of the discretization adopted is modelled by an elementary block that contains:

- Implementation of the over mentioned state equations for the working fluid undergoing phase change: (3.26) and (3.29). Compared to the case of single-phase heat exchanger, mass balance equation has been added to the block, in order to model density variation during evaporation and condensation.
- Implementation of state equations describing heat transfer and mass transport phenomena characterizing the fluid that does not experience phase change and flows in the annulus. In this case, no difference exist respect the heat exchanger with no phase change.
- To note that a control subroutine is necessary to choose the proper correlation to use in order to calculate convective coefficient for the working fluid during phase-change. It has been implemented in an *m-Sfunction*, using vapour quality as input parameter for the decision process.

The dynamic effect of the pipe wall has been neglected. Heat exchanged is calculated and, subsequently, used as input value for the energy balance equation applied to the control volume on annulus and internal pipe side:

- Subroutine built to evaluate time derivative of water temperature in the discrete volume at the current time  $t$  is located on the upper right of the figure.
- Subroutine built to evaluate time derivative of the working fluid specific enthalpy in the discrete volume at the current time  $t$  is located on the upper right of the figure.

Finally, temperature and specific enthalpy of both fluids are calculated with a numerical integration process from time derivatives.

Referring to Figure 3.8, which reports the layout of the elementary block adopted to model phase-change heat exchanger, colours indicate the specific application of each block or subroutine. It is possible to classify blocks and subroutines in the following categories:

- Light blue coloured blocks identify the annulus side of the heat exchanger. Two main clusters of blocks are present: *m-Sfunction* used to evaluate thermodynamic properties of the fluid, using pressure and temperature as input variables, and convection coefficient compose the first one, on the left. Thermal resistance is calculated and then used to evaluate overall heat exchange coefficient. The second one, on the right, is composed by the block that solves equation (3.10) and the following integration block used to evaluate the temperature of the fluid flowing in the annulus. Temperature signal is then used as input value for the following simulation time step.
- Blocks in magenta identify geometry and material of the metal pipe. These parameters allow determining thermal resistance related to conduction.
- Yellow blocks identify the internal pipe side of the heat exchanger. From left to right it is possible to identify the following *m-Sfunctions* and blocks:
  - i. *m-Sfunction* used to evaluate thermodynamic properties of the working fluid undergoing phase-change. Input parameters are pressure and specific enthalpy.

- ii. *m-Sfunction* used to calculate truncated value of vapour quality-derived density of the working fluid.
  - iii. Mass balance equation block, solving equation (3.26).
  - iv. *m-Sfunction* calculating convection coefficient and thermal resistance of the working fluid during phase-change.
  - v. Block that solves (3.29), and the following integration block used to determine specific enthalpy of the working fluid flowing in the internal pipe. Specific enthalpy signal is then used as input value for the calculations of the consecutive simulation step.
- Blue blocks identify the calculation of the overall heat transfer coefficient.
  - Lilac blocks identify the calculation of the heat exchanged in the investigated instant of the simulation.
  - Light green blocks set initial values for the state variables of both fluids.
  - Cyan coloured blocks identify output quantities of the elementary block, while orange blocks identify input variables.
  - Finally, red coloured blocks represent the calculation of temperature difference existing between the fluids flowing in the heat exchanger. This calculation is useful to evaluate potential violations of Pinch Point during transient phases.

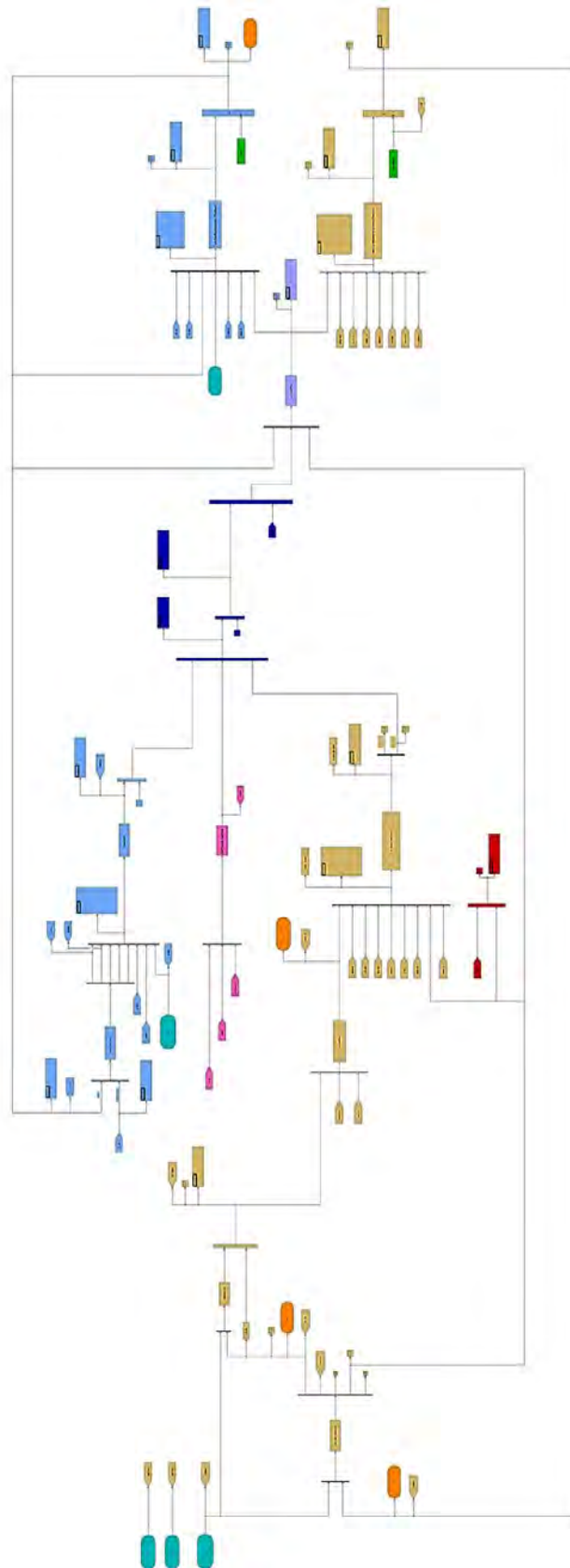


Figure 3.8  
Simulink® phase-change heat exchanger elementary block layout.



### 3.4 Dynamic models of capacities

Dynamic models of capacities are here exposed. A hot drum have been placed downstream the evaporator, while a cold drum was located downstream the condenser. Both the capacities have been modelled applying unsteady form of energy and mass balance equations. The methodology and the numerical modeling process is presented in the following paragraphs.

#### 3.4.1 Hot drum

In order to provide saturated vapour to superheater, or directly to the expander in the case of saturated vapour cycle, a hot drum is placed downstream of evaporator. It collects vapour exiting evaporator and releases saturated steam at the outflow duct, ensuring a unitary vapour quality entering superheater or vapour expander, even during transient phases. Hot drum consists of a tank within which liquid and vapour coexist in saturation conditions, with liquid laying on the bottom and vapour that occupies the remaining volume. Outflow duct is supposed to be on the upper side of the tank, and allows sucking up saturated vapour. Pressure characterizing evaporation process is provided by enthalpy, mass and volume balance equations applied to the control volume of the hot drum. Thus, input quantities of the current component are mass flow rates entering (from the evaporator), leaving (defined by the vapour expander), and specific enthalpy of the entering flow. Main output variables are specific enthalpy of the flow leaving the storage, pressure and liquid volume inside the hot drum. Under the hypothesis of saturation conditions existing within the hot drum, thermodynamic properties of liquid and vapour leaving the storage are known from database [39]. Pressure and vapour quality are considered as input variables for the evaluation of fluid properties. As mentioned before, differential form of energy and mass balance equations allow the gross dynamic behaviour of a hot drum to be described [36]. In fact, combining two over mentioned equations with volume algebraic balance equation it is possible to evaluate all leading dynamics of the system, particularly the alteration of pressure and liquid volume within the storage. These parameters are set as state variables of the model, and their time derivatives define the unknown quantities of the algebraic equations system describing the hot drum. In [36], Åström and Bell present a nonlinear dynamic model for natural circulation drum-boilers. Authors' efforts were dedicated to building up a simple but effective dynamic model, structured as a nesting of a second-, a third, a fourth-order model [15]. It is interesting to note that the structure of this model allows state variables of models to be computed separately, with different grades of accuracy. In this work, the second-order model was taken as reference to build up a dynamic model of the hot drum. Pressure and liquid volume has been set as state variables of the model. Differential form of the mass balance equation adopted in the current model is given by:

$$\frac{d}{dt} [\rho_v^t V_v^t + \rho_l^t V_l^t] = \dot{m}_{in}^t - \dot{m}_{out}^t \quad (3.44)$$

Where subscripts  $l$  and  $v$  indicate, respectively, liquid and vapour fluid within the hot drum. Under the hypothesis of null heat exchange with the environment, energy balance equation applied to the control volume of the hot drum can be expressed by the following:

$$\frac{d}{dt} [\rho_v^t u_v^t V_v^t + \rho_l^t u_l^t V_l^t] = \dot{m}_{in}^t h_{in}^t - \dot{m}_{out}^t h_{out}^t \quad (3.45)$$

Rearranging the terms and expressing internal energy  $u$  as  $h - pv$ , (3.45) becomes:

$$\frac{d}{dt} [\rho_v^t h_v^t V_v^t - \rho_l^t h_l^t V_l^t - p^t V_{tot} + m_{hd} c_p T_m^t] = \dot{m}_{in}^t h_{in}^t - \dot{m}_{out}^t h_{out}^t \quad (3.46)$$

Terms  $m_{hd}$ ,  $c_p$  and  $T_m$  express, respectively, overall mass of the hot drum, its specific heat and averaged temperature. To be noted that metal temperature  $T_m$  is strongly correlated to changes in the temperature of saturated vapour [36]. Furthermore, simulations with more accurate models show that, in steady state conditions, wall temperature is close to saturation temperature of the vapour and temperature differences are small dynamically [36]. Thus, it is possible to approximate wall temperature of the hot drum with saturation temperature of the vapour, which is strictly related to pressure existing within the storage.

Finally, overall volume of the hot drum is given by the sum of liquid and vapour volume:

$$V_t = V_l^t + V_v^t \quad (3.47)$$

Equations (3.44), (3.46) and (3.47) combined with saturated steam tables constitute equation system describing the hot drum dynamics. Referring to the notation adopted in [36], cardinal equations can be rearranged in the following form:

$$\begin{cases} a_{11} \frac{dV_l}{dt} + a_{12} \frac{dp}{dt} = b_1 \\ a_{21} \frac{dV_l}{dt} + a_{22} \frac{dp}{dt} = b_2 \end{cases} \quad (3.48)$$

Where equation coefficients represent the following terms:

$$\left\{ \begin{array}{l} a_{11} = \rho_l - \rho_v \\ a_{12} = V_v \frac{d\rho_v}{dp} + V_l \frac{d\rho_l}{dp} \\ a_{21} = \rho_l h_l - \rho_v h_v \\ a_{22} = V_v \left( h_v \frac{d\rho_v}{dp} + \rho_v \frac{dh_v}{dp} \right) + V_l \left( h_l \frac{d\rho_l}{dp} + \rho_l \frac{dh_l}{dp} \right) - V_t + m_{hd} c_p \frac{dT_v}{dp} \\ b_1 = \dot{m}_{in} - \dot{m}_{out} \\ b_2 = \dot{m}_{in} h_{in} - \dot{m}_{out} h_{out} \end{array} \right. \quad (3.49)$$

State variables  $\frac{dV_l}{dt}$  and  $\frac{dp}{dt}$  are calculated solving the equation system. State variables are subsequently evaluated by means of a numerical integration process, using integrator block provided by Simulink®. Once pressure and liquid volume are determined, vapour volume can be evaluated by difference from total volume of the storage using equation (3.47). Considering a cylindrical shaped hot drum, liquid level can be determined dividing liquid volume by the hot drum base area. Since saturation condition is considered within the storage, thermodynamic properties of liquid and vapour are defined by pressure and quality null or unitary respectively. To be noted that outflow specific enthalpy  $h_{out}$  is defined by equilibrium condition existing within the hot drum, and it is calculable considering pressure calculated from (3.48) and unitary quality [39]. Hot drum is a state determined component. Proper initial conditions for liquid volume and pressure must be set. Furthermore, it is necessary to define dimensions and material of the hot drum. The equation system is given by the following Table 3.5:

1	$a_{11}^t \frac{dV_l^t}{dt} + a_{12}^t \frac{dp^t}{dt} = b_1^t$	Overall variables: 15
2	$a_{21}^t \frac{dV_l^t}{dt} + a_{22}^t \frac{dp^t}{dt} = b_2^t$	Independent variables: 13
		Dependent variables: 2

Table 3.5  
Equation system of the dynamic model of hot drum.

Auxiliary equations: fluid's thermodynamic properties library.

### 3.4.2 Cold drum

Cold drum is placed downstream the condenser. It collects liquid exiting the latter and releases saturated liquid at the outflow duct, ensuring a null vapour quality entering the pump, even during transient phases. Cold drum consists of a tank within which liquid and vapour coexist in saturation conditions, with liquid laying on the bottom and vapour that occupies the remaining volume. Outflow duct is supposed to be on the lower side of the tank, and allows saturated liquid to be sucked up. Cold drum has been modelled adopting the same structure and subroutine previously described

for the hot drum. However, it must be noted that, in this case, outflow specific enthalpy is determined by pressure existing within the cold drum and null vapour quality. As for the hot drum case, proper initial condition for the state variables, material and geometrical specifications for the tank must be set. Equation system is defined once again by Table 3.5.

### 3.5 Turbomachinery

The model of a dynamic, single stage, radial pump and the model of a single stage, axial impulse turbine are here presented. Since the dynamic response of these components is much faster than the one that characterizes heat exchanger and storages, a steady-state model was built for both the pump and the turbine. Thus, time behaviour of both the pump and the turbine has been described as a sequence of stationary condition, according to quasi-steady approach.

#### 3.5.1 The pump model

The model of a dynamic single stage radial pump is here presented. Such a kind of machine was chosen considering its wide application in ORC energy systems [8]. The aim of this work is to build up an effective and versatile dynamic model of an ORC system, therefore also the pump model has been developed considering as main features flexibility and reliability. This component is described by characteristic maps reporting head and efficiency as functions of mass flow rate. In order to develop a generic and flexible model, characteristic maps can easily be modified introducing new look-up tables of the considered machine. This operation does not modify the structure of the model, which maintains its input and output variables unchanged. In first analysis, simple characteristic maps have been implemented using proper analytical forms, as will be explained in this paragraph.

First, flow rate characteristic map, defining the relationship between head and processed flow rate, has to be defined. Turbomachinery widely known theory states that flow rate characteristic can be described as a function of volumetric flow rate and rotational speed [8, 46]. However, referring to inflow fluid density, it is possible to define also a mass flow rate characteristic. With this assumption, it is possible to express head of the pump  $y$  by the following [8]:

$$y = \frac{y_{dp} - y_{0dp}}{\dot{m}_{dp}^2} \dot{m}^2 + y_{0dp} \quad (3.50)$$

where  $y_{dp}$  and  $y_{0dp}$  express, respectively, pump head in nominal conditions and pump head at nominal rotational speed when no flow rate is allowed. Similarly, pump isentropic efficiency can be expressed as a function of mass flow rate and rotational speed. As in the case of flow rate characteristic, efficiency is plotted as a function of

mass flow rate considering a fixed rotational speed. Thus, different parametric curves are plotted considering a different rotational speed for each one. With this assumptions, efficiency is given by [8]:

$$\eta = -\frac{\eta_{dp}}{\dot{m}_{dp}^2} \dot{m}^2 + 2 \frac{\eta_{dp}}{\dot{m}_{dp}} \dot{m} \quad (3.51)$$

Turbomachinery similarity laws allow scaling head and efficiency characteristic maps in function of varying rotational speed [46]. Mass flow rate varies linearly with the ratio between operational and nominal rotational speed, while pump head varies with square value of the over mentioned ratio. Efficiency does not undergo any modification. In summary, following equations describe the scaling process of pump head and mass flow rate in function of rotational speed for two generic working condition *A* and *B*:

$$\dot{m}_B = \dot{m}_A \left( \frac{\omega_B}{\omega_A} \right) \quad (3.52)$$

$$y_B = y_A \left( \frac{\omega_B}{\omega_A} \right)^2$$

Figure 3.9 and Figure 3.10 show, respectively, flow and efficiency characteristics for different rotational speed.

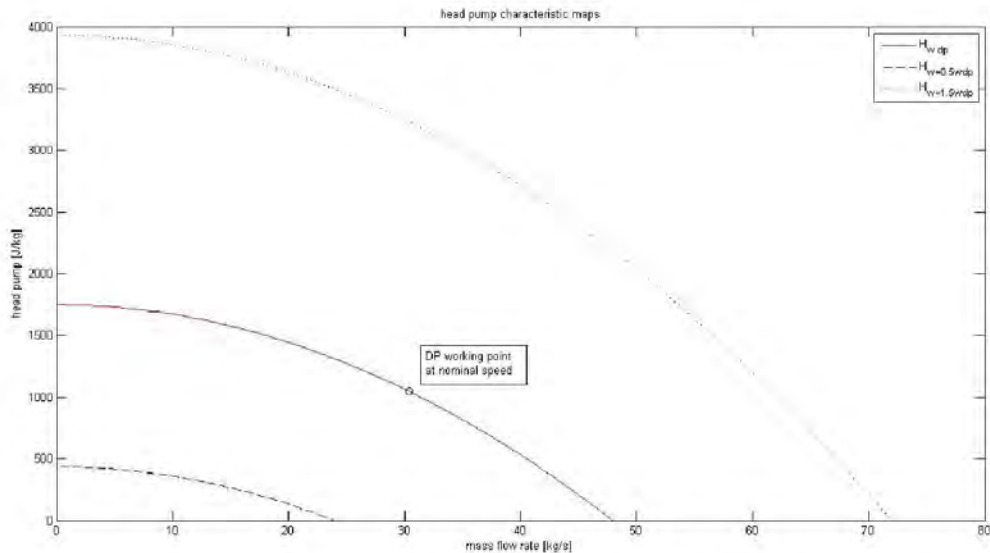


Figure 3.9  
Pump flow rate characteristics for different rotational speed. Black circle represent design point working condition at nominal speed

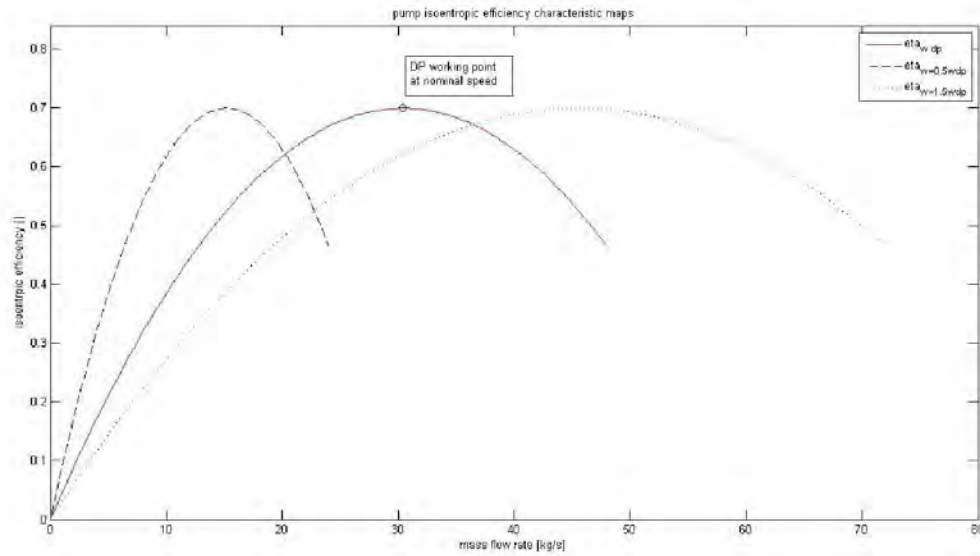


Figure 3.10  
Pump efficiency characteristics for different rotational speed. Black circle represent design point working condition at nominal speed

Input values for the pump model are upstream and downstream pressure levels, and inflow thermodynamic properties, which are provided by the previous cold drum component. As mentioned before inflow density has been taken as reference for the computing process. Since pressure gap existing between inflow and outflow ducts of the pump are known, it is possible to determine mass flow rate flowing in the component from (3.50). Once mass flow rate is calculated, pump efficiency is evaluated using equation (3.51). Real outflow thermodynamic properties can be determined, knowing pressure and specific enthalpy. Thus, mass flow rate and thermodynamic properties of the exiting flow are main output quantities of this component. Equation system of the model is reported in the following Table 3.6.

1	$y^t = \frac{y_{dp} - y_{\alpha dp}}{\dot{m}_{dp}^2} (\dot{m}^t)^2 + y_{\alpha dp}$	Overall variables: 10
2	$\eta^t = -\frac{\eta_{dp}}{\dot{m}_{dp}^2} (\dot{m}^t)^2 + 2 \frac{\eta_{dp}}{\dot{m}_{dp}} \dot{m}^t$	Independent variables: 7
3	$\eta^t = \frac{h_{2is}^t - h_1^t}{h_2^t - h_1^t}$	Dependent variables: 3

Table 3.6  
Equation system of the pump model.

Auxiliary equations: fluid's thermodynamic properties library.

### 3.5.2 The turbine model

In this paragraph the model of an impulse turbomachinery was chosen in virtue of its wide use in ORC energy systems. Thus, a model of a single stage, axial impulse turbine has been developed [8]. As for the previously described pump model, a quasi-steady approach was adopted.

Similarly to the pump model, turbine must provide mass flow rate as a function of pressure gap existing between inflow and outflow ducts. Mass flow rate can be evaluated, knowing inlet and outlet pressure, using Stodola's equation [34, 8]:

$$\dot{m}_T = K \sqrt{\rho_{in} p_{in} \left[ 1 - \left( \frac{1}{\varepsilon_T} \right)^2 \right]} \quad (3.53)$$

where  $\varepsilon_T$  represent the vapour expansion ratio and  $K$  is defined as the product between the coefficient of discharge and the equivalent nozzle cross area at the inlet [8]. Since inlet thermodynamic properties are provided by the superheater (or the hot drum, in the case of a saturated vapour cycle),  $\rho_{in}$  and  $p_{in}$  are known quantities. Constant coefficient  $K_T$  has been determined rearranging (3.53) and considering nominal working conditions:

$$K_T = \frac{\dot{m}_{dp}}{\sqrt{\rho_{indp} p_{indp} \left[ 1 - \left( \frac{1}{\varepsilon_{Tdp}} \right)^2 \right]}} \quad (3.54)$$

Isoentropic efficiency has been represented by a generic characteristic map, which can be easily modified with a more accurate one. Non-dimensional flow number has been used as input value to define a non-dimensional value for the isentropic efficiency of the expansion process. Following equation provide non-dimensional flow number:

$$\varphi_T = \sqrt{\frac{1 - \left( \frac{1}{\varepsilon_T} \right)^2}{1 - \left( \frac{1}{\varepsilon_{Tdp}} \right)^2}} \quad (3.55)$$

Non-dimensional isentropic efficiency is given by Figure 3.12, where it is expressed as a function of flow number  $\varphi_T$ . Isoentropic efficiency is finally calculated as the product between non-dimensional value and nominal value. As reported in [8], Stodola's semi empirical correlation has general validity and can describe also the condition of choking. Figure 3.11 reports a representation of turbine mass flow rate calculated using equations (3.53) and (3.54). To be noted that, both in the case of mass flow characteristic and efficiency characteristic, influence of rotational speed of the shaft can be neglected [8]. For sake of simplicity, mechanical-electrical efficiency was considered constant.

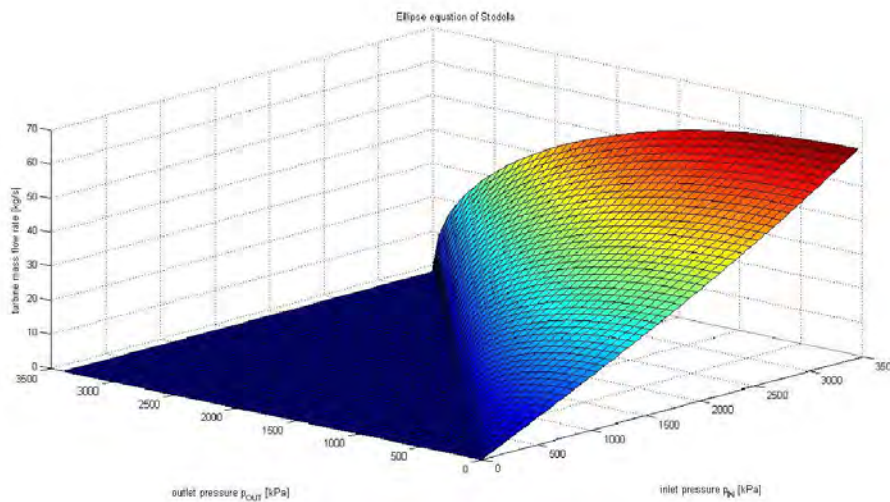


Figure 3.11  
Graphic representation of equation (3.53): turbine mass flow rate provided by Stodola's equation given the pressure at evaporator ( $p_{IN}$ ) and condenser ( $p_{OUT}$ ).

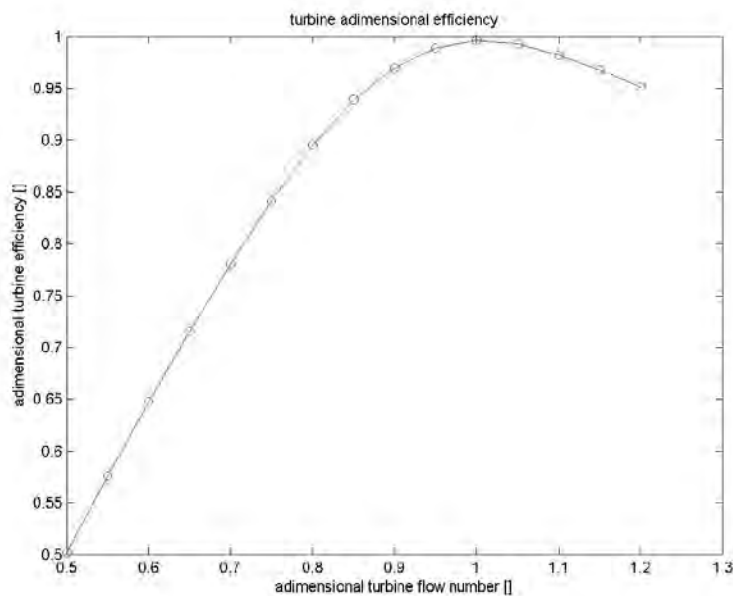


Figure 3.12  
Non-dimensional isentropic efficiency characteristic curve adopted for the turbine dynamic model.

Inputs for the turbine model are inflow and outflow pressures. Furthermore, in order to evaluate inflow density and real thermodynamic properties of the discharged flow, inflow density and specific enthalpy are also requested as input quantities. Output variables are mass flow rate, thermodynamic properties of the discharged fluid, electrical power output. Computing process is straightforward: knowing evaporator pressure, condenser pressure and inflow thermodynamic properties, and equation (3.53) allows calculating mass flow rate. Similarly, isentropic efficiency is obtained



from characteristic curve reported in Figure 3.12 and equation (3.55). Following Table 3.7 reports equation system of this component.

1	$\dot{m}^t = K_T \sqrt{\rho_{in}^t p_{in}^t \left[ 1 - \left( \frac{1}{\varepsilon_T^t} \right)^2 \right]}$	Overall variables: 9
2	$\eta^t = f(\varphi(\varepsilon_T^t, \varepsilon_{Tdp}^t), \eta_{dp})$	Independent variables: 6
3	$\eta^t = \frac{h_2^t - h_1^t}{h_{2is}^t - h_1^t}$	Dependent variables: 3

Table 3.7  
Equation system of the turbine model.

Auxiliary equations: fluid's thermodynamic properties library.

### 3.6 Summary

In this chapter, dynamic models of the most common components of modern energy systems were presented. Efforts has been focused on building up flexible and versatile dynamic models of heat exchangers, even characterized by phase change, turbomachinery and capacities. Particular attention was spent to develop an accurate model of heat exchange process during phase change, which strongly influences system dynamics. These components will be used to describe dynamic behaviour of an ORC system during transient phases, but it should be noted that their structure is flexible and this allows them to be used in various applications.

# 4 APPLICATION OF THE DYNAMIC MODELS TO AN ICES-ORC COMBINED CYCLE ON BOARD AN LNG CARRIER

## 4.1 Introduction

The aim of this chapter is to present the design and off-design model of the optimal ORC solutions proposed by Soffiato [17, 47].

Initially, ICES and cooling systems are briefly described, presenting their operation and performance in design and off-design conditions. Then, optimal design solutions for the ORC developed by Soffiato [47] are exposed. Two of them, a superheated ORC with R-134a as working fluid and a saturated ORC with R-245fa as working fluid, have been taken into account to develop the model of the ORC. Design model of the components of both the investigated systems are presented, exposing the followed design methodology and design specifications. Finally, the off-design dynamic model of both the ORCs is presented.

## 4.2 Energy system of the current ship

Following paragraphs present the energy system of the investigated ship, which is composed by four Dual Fuel Diesel Electric Engines. Two of them have an electrical power output of 5500 kW<sub>el</sub>, while the other two have an electrical power output of 11000 kW<sub>el</sub>. The cooling system is feed with fresh water and it is composed by a low temperature and a high temperature circuit.

Quantity and quality of the heat rejected by ICES must be evaluated to define the amount of heat exploitable by the bottoming ORC. Thus, a first principle balance is applied to the ICES system, and three configurations for the ICES-ORC combined cycle are introduced. Once a configuration for the combined cycle is chosen, optimal design operating characteristics of the bottoming ORC are presented, taken into account six different working fluids.

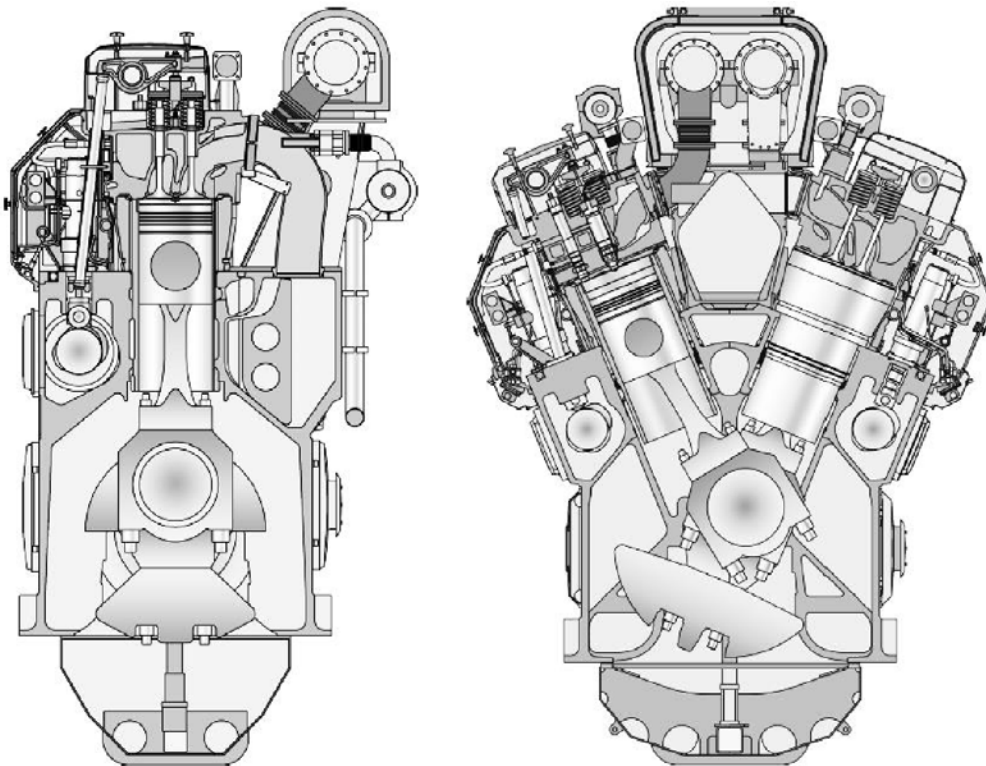
### 4.2.1 ICES of the electrical power generating plant: description and energy balance

Four Dual Fuel Diesel Electric engines (DFDE) supply electrical demand of the current ship. Two of them are Wärtsilä 12V50DF type, while the other two are Wärtsilä

6L50DF type. All the engines are four-stroke turbocharged inter-cooled ones and they can be fuelled either with heavy fuel oil or with natural gas. If natural gas is adopted to fuel the engines, a small quantity of light fuel oil is required as well as pilot injection. The 12V50DF type is a twelve cylinders V engine, and the 6L50DF type is a six cylinders in-line engine. The pumps of the cooling system are of the engine driven type [17]. Table 4.1 and Figure 4.1 report, respectively, main characteristic and schematic cross section of the ICEs of the ship.

	<i>Unit</i>	6L50DF	12V50DF
<i>Mechanical output</i>	kW	5700	11400
<i>Cylinder bore</i>	mm	500	500
<i>Stroke</i>	mm	580	580
<i>Engine speed</i>	rpm	500	500
<i>Mean piston speed</i>	m/s	9.7	9.7
<i>Mean effective pressure</i>	bar	20	20
<i>Electrical output</i>	kW	5500	11000
<i>Generator efficiency</i>	%	96.49	96.49

*Table 4.1  
Main characteristic of the Diesel generator engines [17].*



*Figure 4.1  
From left to right, cross section of the 6L50DF in-line engine and of the 12V50DF V engine [17].*

In [17], Soffiato performed a first law energy balance of both the 6L50DF and 12V50DF engines. System's boundaries included the conversion from mechanical to electrical power, as can be seen in Figure 4.2. ISO conditions were considered, so the

reference temperature is 25°C, the total barometric pressure is 1 bar and the relative humidity of the air is equal to 30%. The charge air coolant is 25°C.

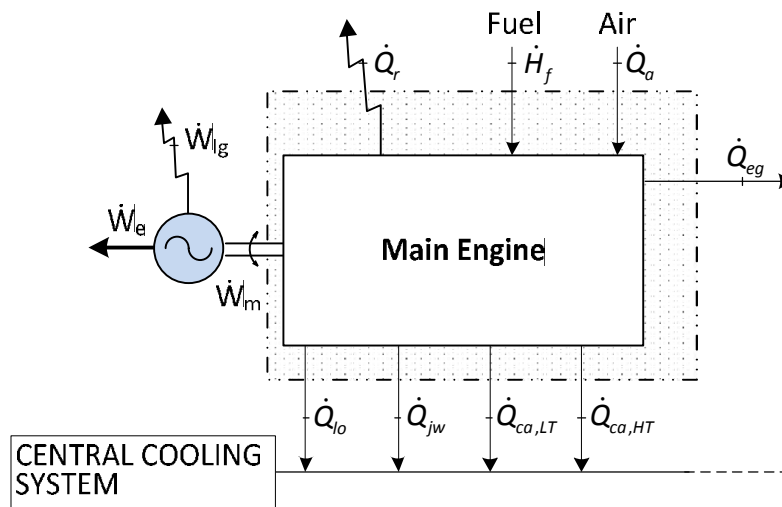


Figure 4.2  
Schematic representation of the ICE's control volume and of its energy balance [17].

$$\dot{H}_f + \dot{Q}_a = \dot{W}_e + \dot{Q}_{lo} + \dot{Q}_w + \dot{Q}_{ca,HT} + \dot{Q}_{ca,LT} + \dot{Q}_{eg} + \dot{Q}_r + \dot{W}_{lg} \quad (4.1)$$

Referring to Figure 4.2 and equation (4.1), symbols have the following meaning [17]:

- $\dot{H}_f$ : energy flow rate related to the fuels,
- $\dot{Q}_a$ : energy flow rate of the air,
- $\dot{W}_e$ : electric power,
- $\dot{Q}_{lo}$ : heat flow rate rejected to the lubricating oil,
- $\dot{Q}_w$ : heat flow rate rejected to the jacket water,
- $\dot{Q}_{ca,HT}$ : heat flow rate at the high temperature charge air cooler,
- $\dot{Q}_{ca,LT}$ : heat flow rate at the low temperature charge air cooler,
- $\dot{Q}_{eg}$ : heat flow related to the exhaust gas,
- $\dot{Q}_r$ : radiation and convection losses,
- $\dot{W}_{lg}$ : electric generation losses.

Once the energy balance of each engine is performed, it is necessary to quantify the temperature level of the fresh water cooling system. For each engine, it is composed of the low temperature circuit LT and of the high temperature one HT. In the HT circuit, cooling water passes through the cylinder jackets and heads, and then it enters the first stage of the charge air cooler. In the LT circuit, cooling water passes through the second stage of the charge air cooler and then it cools lubricating oil. In the following, Figure 4.3 reports a schematic representation of the cooling system of main ICEs, and Table 4.2 collects the values of the main parameters characterizing the cooling system.



Par.	Unit	Wärtsilä 6L50DF					Wärtsilä 12V50DF				
		100	90	85	75	50	100	90	85	75	50
$T_{w1}$	°C	74	74.6	75	76	78	76	76.4	76.6	77	78
$T_{w2}$	°C	79.4	78.3	78.6	79.5	81.0	80.1	79.8	79.9	80.5	81.0
$T_{w3}$	°C	83	82.2	82	82	82	85	83.3	83	83	82
$T_{w7}$	°C	36	36	36	38	38	36	36	36	36	36
$T_{w8}$	°C	45	43.7	43.1	43.9	41.4	45	43.7	43.1	41.9	39.4
$T_{w9}$	°C	54.2	52.6	51.9	52.6	49.7	54.2	52.6	51.9	50.6	47.2
$T_{a2}$	°C	187.0	177.6	170.5	151.9	113.1	183.3	176.8	169.6	151.9	113.1
$T_{a3}$	°C	97.8	95.2	94.1	91.1	79.3	96.3	94.9	93.7	91.1	79.6
$T_{a4}$	°C	44	44.6	45	46	50	45	44.2	44	45	51
$T_{eg2}$	°C	390	397	409.7	441	438	390	397	409.7	441	438
$T_{lo1}$	°C	76	75.4	75.3	75.1	73.6	76	75.4	75.3	75.1	73.6
$T_{lo2}$	°C	61	61	61	61	61	61	61	61	61	61
$\dot{m}_{lo}$	kg/s	18.1	18.1	18.1	18.1	18.1	36.2	36.2	36.2	36.2	36.2
$\dot{m}_{w1}$	kg/s	31.5	42.7	42.6	41.3	41.7	82.1	93.9	93.2	82.6	83.4
$\dot{m}_{w7}$	kg/s	13.3	13.3	13.3	13.3	13.3	26.6	26.6	26.6	26.6	26.6
$\dot{m}_a$	kg/s	9.15	8.27	7.78	6.9	5.26	18.3	16.64	15.67	13.81	10.52
$\dot{m}_{eg2}$	kg/s	9.4	8.5	8.0	7.1	5.4	18.8	17.1	16.1	14.2	10.8
$p_{bar}$	bar	1.028	1.028	1.028	1.030	1.031	1.015	1.015	1.015	1.016	1.016
$p_{a2}$	[bar-g]	2.4	2.14	2	1.7	1	2.3	2.16	2	1.6	0.9
$p_{w1}$	bar	3.15	3.15	3.15	3.15	3.15	3.15	3.15	3.15	3.15	3.15
$p_{w7}$	bar	3.15	3.15	3.15	3.15	3.15	3.15	3.15	3.15	3.15	3.15

Table 4.2  
Summary of the operating parameters for the two types of engines [17].

#### 4.2.2 Power demands of the current ship

Engines on board the vessel must provide mechanical power necessary to cover the mechanical and electrical power demand given by propulsion, auxiliary systems and other needs. As Soffiato states in [17], power demands of the ship can be expressed as a function of service speed  $V_s$ . Equations (4.2) and (4.3) **Errore. L'origine riferimento non è stata trovata.** give the overall electrical power demand of the vessel for the laden and the ballast voyage respectively.

$$\dot{W}_{eladen} = 855833V_s^3 - 4731250V_s^2 + 87060416V_s - 5349187500 \quad (4.2)$$

$$\dot{W}_{eballast} = 847917V_s^3 - 4476750V_s^2 + 823652083V_s - 506033125 \quad (4.3)$$

Average speed kn	Hours %	Hours -	$W_e$ kW	12V50DF No.1 kW	6L50DF No. 2 kW	6L50DF No. 3 kW	12V50DF No.4 kW	Load %
7.5	3.5	117.1	2823	0	0	2823	0	51
8.5	0.0	0.0	3517	-	-	-	-	-
9.5	1.3	43.8	4395	0	0	4395	0	80
10.5	3.7	125.2	5478	0	0	5478	0	100
11.5	6.2	211.8	6789	0	0	0	6789	62
12.5	5.3	180.6	8350	0	0	0	8350	76
13.5	11.4	386.6	10180	0	0	0	10180	93
14.5	10.5	357.7	12304	0	0	4101	8202	75
15.5	22.6	766.4	14741	0	0	4914	9827	89
16.5	14.2	483.3	17514	0	4378	4378	8757	80
17.5	9.6	326.5	20711	0	5178	5178	10355	94
18.5	4.3	146.6	24315	9726	0	4863	9726	88
19.5	7.3	248.1	28302	9434	4717	4717	9434	86

Table 4.3  
Operating profile of the engines, laden voyage [17].

Average speed kn	Hours %	Hours -	$W_e$ kW	12V50DF No.1 kW	6L50DF No. 2 kW	6L50DF No. 3 kW	12V50DF No.4 kW	Load %
6.5	0.7	22.3	2112	0	0	2112	0	38
7.5	0.0	0.0	2617	-	-	-	-	-
8.5	0.0	0.0	3276	-	-	-	-	-
9.5	0.0	0.0	4110	-	-	-	-	-
10.5	0.5	14.7	5139	0	0	5139	0	93
11.5	6.2	192.8	6385	0	0	0	6385	58
12.5	7.4	232.3	7867	0	0	0	7867	72
13.5	14.2	444.1	9607	0	0	0	9607	87
14.5	5.6	175.5	11624	0	0	3875	7749	70
15.5	17.9	561.4	13939	0	0	4646	9293	84
16.5	34.5	1079.8	16573	8287	0	0	8287	75
17.5	10.1	317.5	19607	9804	0	0	9804	89
18.5	3.0	94.0	23027	9211	0	4605	9211	84

Table 4.4  
Operating profile of the engines, ballast voyage [17].

Given the service speed of the vessel, data reported in Table 4.3 and Table 4.4 allow determining the working engines and their load.

### 4.2.3 Operating point of the vessel's energy system

Since four different engines compose the energy system of the current vessel, the selection of a certain value for the electrical power that has to be generated is not sufficient to define the heat flows that are exploitable by the recovery system. Not all the engine-generators are kept in operation, except in the case of high power demand. Therefore, various solutions could be adopted to fulfil electrical power demand, keeping in operation different engines which could be working at different load. However, this could leave to a quite complicated resolution process.

In order to overcome these complications, Soffiato proposed to consider the operating profile of the vessel and the engines, here proposed again in Table 4.3 and Table 4.4, to define the ICE's control strategy and their operating point [17]. The operating point that has been selected for the design calculations is presented in Table 4.5. The choice takes into consideration the observations on the distribution profile of the sea speed [17], and it allows the calculation of the thermal flows related to the exhaust gas and the thermal flows rejected to the cooling system of the engines.

$W_e$	12V50DF no.1	6L50DF no.2	12V50DF no.3	6L50DF no.4	<i>Load</i>
kW	kW	kW	kW	kW	%
23375	9350	0	4675	9350	85

Table 4.5  
Operating point for the engines in design point condition [17].

### 4.2.4 ICEs-ORC combined cycle: integration of the energy systems

In [17], Soffiato presented three different configurations for the cooling system of the engines, which are listed in the following:

1. First configuration represents the current layout of the cooling system. In this case, ORC absorbs heat from two heat sources, at different temperature level, from each engine in operation: water HT circuit and water LT circuit (see paragraph 4.2.1).
2. In the second configuration, LT cooling circuit is split into two parts. Lubricating oil exchange heat directly with the ORC working fluid, while water LT circuit passes only through the second stage charged air cooler. Thus, three thermal sources at three different temperature level are available for the ORC: water HT circuit, which does not undergo any modification respect to the first case, lubricating oil cooling circuit and water LT circuit.



3. Third case proposes a new design for the cooling system. In this new configuration, ORC recovers heat from lubricating oil, charged air and jacket water.

In this work, the first configuration has been considered. Figure 4.4 reports a schematic representation of the current cooling system of the ship. It can be noted how ORC recovers heat from water HT circuit through heat exchanger  $HE_1$ , and from water LT circuit through heat exchanger  $HE_2$ . It is important to note that Figure 4.4 refers to the operation of all the working engines for the considered operating point. This means that the parameters characterizing the heat sources of the ORC must be calculated considering contributes of each of the operating engines. Mass and energy equations adopted for this purpose are defined in the following.

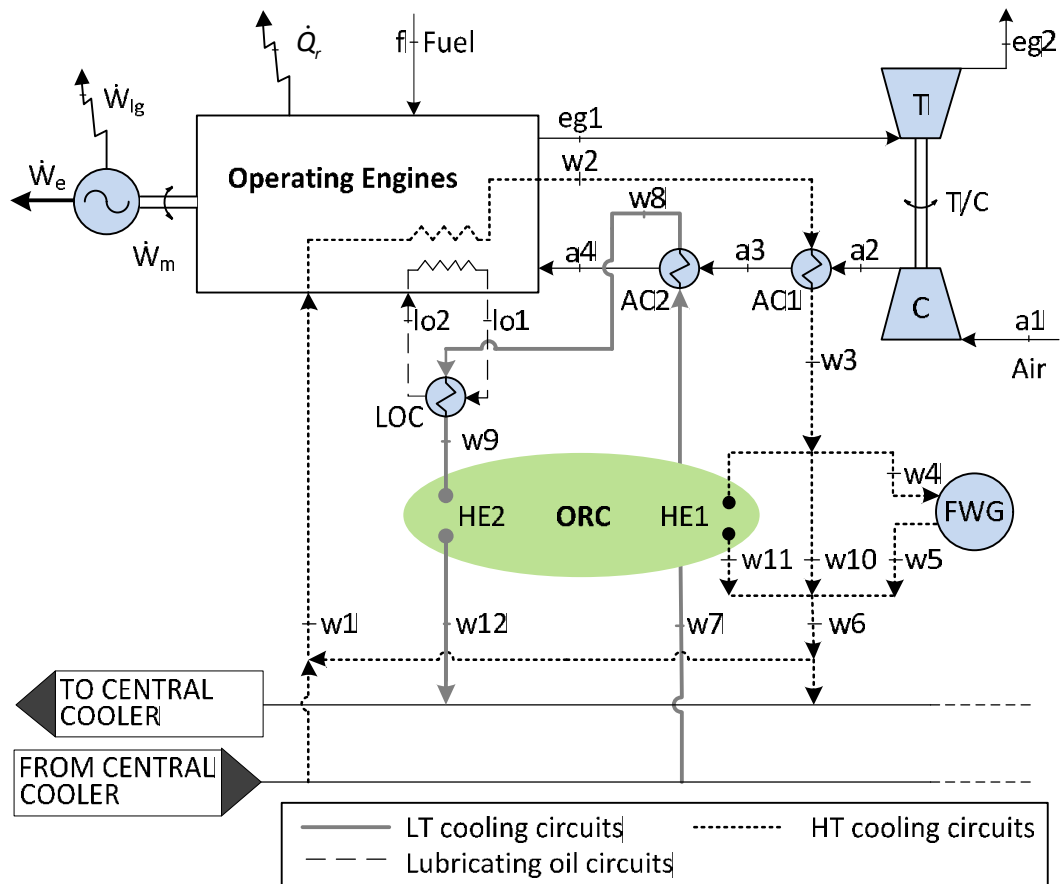


Figure 4.4  
Schematic representation of the current cooling system, first configuration [17].

Regarding the HT circuit, the value of the specific enthalpy  $h_{w3}$  can be calculated considering the mixing of the flows coming from the operating engines. Subscripts  $A$  and  $B$  refer, respectively, to Wärtsilä 6L50DF and Wärtsilä 12V50DF. Equations (4.4) and (4.5) allows the calculation of  $h_{w3}$ . Temperature  $T_{w3}$  can be evaluated knowing  $h_{w3}$  and the pressure of water at the same state.

$$\dot{m}_{w1A} h_{w3A} + 2\dot{m}_{w1B} h_{w3B} = (\dot{m}_{w1A} + 2\dot{m}_{w1B}) h_{w3} \quad (4.4)$$

$$h_{w3} = \frac{\dot{m}_{w1A} h_{w3A} + 2\dot{m}_{w1B} h_{w3B}}{\dot{m}_{w1A} + 2\dot{m}_{w1B}} \quad (4.5)$$

Water temperature  $T_{w1}$  can be calculated following the same procedure, replacing  $h_{w3}$  with  $h_{w1}$ . Mass flow rate of the water collected at the outlet of the HT circuit is given by the following mass balance equation:

$$\dot{m}_{w1} = \dot{m}_{w1A} + 2\dot{m}_{w1B} \quad (4.6)$$

Water mass flow rate feeding the fresh water generator can be calculated by the following:

$$\dot{m}_{w4} = \frac{KV_d}{\Delta T} \quad (4.7)$$

where  $K$  and  $\dot{V}_d$  are, respectively, a constant parameters and the capacity of the fresh water generator [17].  $\Delta T$  is inlet-outlet temperature difference of the feeding water,  $(T_{w4} - T_{w5})$ . Following equations were defined to allow the calculation of mass flow rate  $\dot{m}_{w10}$ :

$$\dot{m}_{w10} h_{w3} + \dot{m}_{w4} h_{w5} = (\dot{m}_{w10} + \dot{m}_{w4}) h_{w1} \quad (4.8)$$

$$\dot{m}_{w10} = \dot{m}_{w4} \frac{h_{w1} - h_{w5}}{h_{w3} - h_{w1}} \quad (4.9)$$

The following mass balance gives the mass flow rate of the water of the HT circuit:

$$\dot{m}_{w11} = \dot{m}_{w1} - \dot{m}_{w10} - \dot{m}_{w4} \quad (4.10)$$

In summary, equations (4.5) and (4.9) define mass flow rate and temperature of the hot water entering the heat exchanger HE1, which exchanges heat with the bottoming ORC.

Considering now LT circuits, following energy and mass balance equations allow the calculation of temperature  $T_{w9}$  and mass flow rate  $\dot{m}_{w7}$ .

$$h_{w9} = \frac{\dot{m}_{w7A} h_{w9A} + 2\dot{m}_{w7B} h_{w9B}}{\dot{m}_{w7A} + 2\dot{m}_{w7B}} \quad (4.11)$$

$$\dot{m}_{w7} = \dot{m}_{w7A} + 2\dot{m}_{w7B} \quad (4.12)$$

Equations (4.11) and (4.12) define mass flow rate and inlet temperature of the hot water entering the heat exchanger HE<sub>2</sub>, which exchanges heat with the bottoming ORC.

Considering data presented in Table 4.2, equations from (4.4) to (4.12) allow the definition of the hot composite curve of the current configuration. Table 4.6 and Figure 4.5 report data characterizing the HCC.

Source	$\dot{Q}$	$T_{max}$	$T_{min}$	$\dot{m}$	pressure
	kW	°C	°C	kg/s	bar
HT circuit	5367.3	82.8	76.3	196.36	3.15
LT circuit	4406	51.9	36	66.5	3.15

Table 4.6  
Main parameters of HT and LT hot water circuit [17].

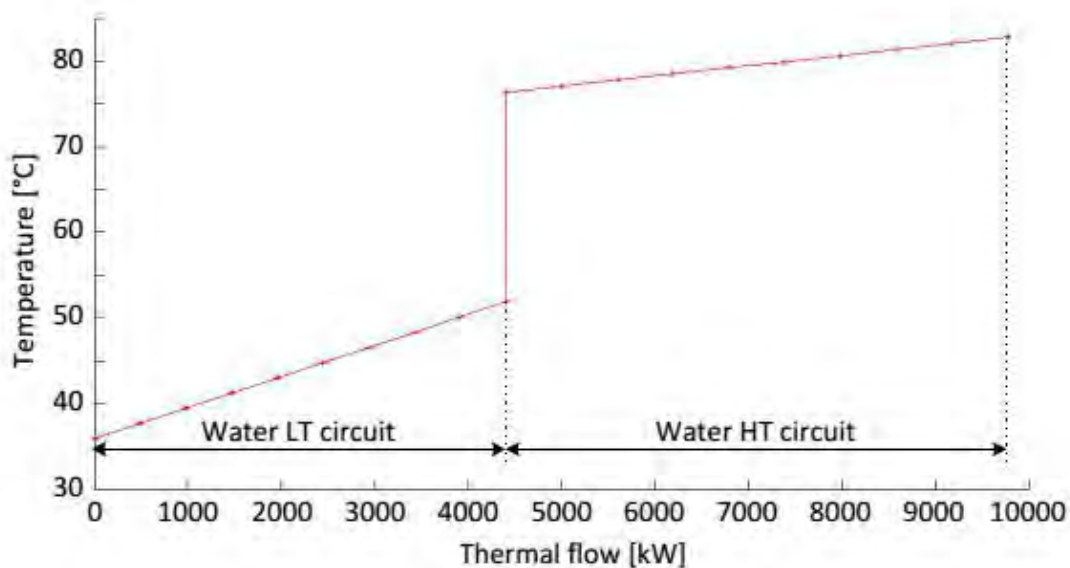


Figure 4.5  
Hot composite curve of the available heat [17].

#### 4.2.5 Optimal design operating characteristics

Considering a simple ORC bottoming the Hot Composite Curve (HCC) reported in Figure 4.5, Soffiato et al. obtained the following results [47], which define optimal design solutions for the bottoming ORC for six different working fluids. As can be noted from Table 4.7, only two of them need to be superheated: R-134a and R-125.

Fluid	unit	R-134a	R-125	R-236fa	R-245ca	R-245fa	R-227ea
$p_{ev}$	bar	20.132	35.197	9.327	4.054	5.695	14.288
$p_{con}$	bar	7.702	15.685	3.210	1.217	1.778	5.284
$T_{con}$	°C	30.0	30.0	30.0	30.0	30.0	30.0
$\Delta T_{sup}$	°C	5.0	8.0	0.0	0.0	0.0	0.0
$T_5$	°C	72.8	72.8	67.8	67.4	67.5	68.2
$T_6$	°C	34.1	34.8	41.3	40.9	39.2	41.0
$\chi$	-	1.02	1.05	1.07	1.05	1.05	1.09
sub/sup	-	sub	sub	sub	sub	sub	sub
$w_{exp}$	kJ/kg	14.968	8.923	12.395	17.153	16.133	9.547
$w_{pump}$	kJ/kg	1.658	2.651	0.722	0.328	0.469	1.044
$w_{net}$	kJ/kg	13.310	6.273	11.672	16.825	15.664	8.503
$q_{absorbed}$	kJ/kg	192.525	117.742	166.239	227.523	213.729	128.443
$q_{con}$	kJ/kg	177.385	110.212	153.118	208.760	196.226	118.775
$\dot{m}_{wf}$	kg/s	30.388	51.517	35.450	25.372	27.109	44.699
$W_{net}$	kW	404.5	323.1	413.8	426.9	424.6	397.1
$\eta_{th}$	%	6.91	5.33	7.02	7.39	7.33	6.62
$\eta_t$	%	4.14	3.31	4.23	4.37	4.34	4.06
F	%	59.9	62.1	60.3	59.1	59.3	61.4
VR	-	2.801	2.657	3.136	3.323	3.234	3.153
SF	m	0.433	3.881	0.656	0.906	0.777	0.578
$\dot{Q}_{absorbed}$	kW	5850.4	6065.5	5893.2	5772.7	5749.0	5998.1
$\dot{Q}_{absorbed}$	kW	5390.4	5677.6	5428.0	5296.6	5319.5	5546.6

Table 4.7

Optimized operating characteristics for the simple ORC, first configuration of the cooling systems [17].

Green-shaded cells highlight working fluids that have been chosen for the simulation campaign: R-134a and R-245fa. The possibility to simulate two different configurations of the power plant (R-134a needs to be superheated, while superheating process is not necessary for R-245fa), both of them characterized by a high efficiency, led to this choice.

### **4.3 Design model of the ORC bottoming ICEs with current configuration of the cooling systems.**

This paragraph presents the design model of heat exchangers and design parameters of the components used to model ORC systems. Optimized operating characteristics obtained by Soffiato [17] have been used to design preheater, evaporator, superheater and condenser. Capacities were sized considering mass flow rate characterizing ORC.

#### **4.3.1 Design procedure and specifications of heat exchangers**

A pipe in pipe counterflow configuration have been considered for each of the heat exchangers adopted in the current energy system. In order to limit pipe length, both the water and the working fluid mass flow rates were split in several, identical pipes. In the following, procedure and main results of the design process of each heat exchanger are presented. To be noted that pipe in pipe configuration leads to high values of heat exchange areas. However, such a kind of heat exchanger was selected in virtue of its simplicity.

- Low temperature pre-heater

ORC low temperature preheater recovers heat from the water LT circuit, rising the temperature of the working fluid. Figure 4.6 reports the flow chart of the methodology adopted to develop the low temperature preheater design model. Independent variables are set starting from the findings of Soffiato et al. [47]. Since no phase-change occurs during heat exchange process, Gnielinski's and Sieder & Tate correlations were adopted to evaluate, respectively, convective coefficients of water flowing in the annulus, and working fluid within the internal pipe (see paragraph 3.3.1). An iterative procedure was necessary to determine the effect of the pipe wall temperature on the value of the convective coefficient of working fluid. Overall heat exchanger was modelled considering a single lumped volume for both the water and the working fluid side. Control volume of the model corresponds to the physical boundaries of the real component. Following Table 4.8 reports main design characteristics and working parameters in nominal conditions of low temperature preheaters of both the R-134a and R-245fa ORCs.

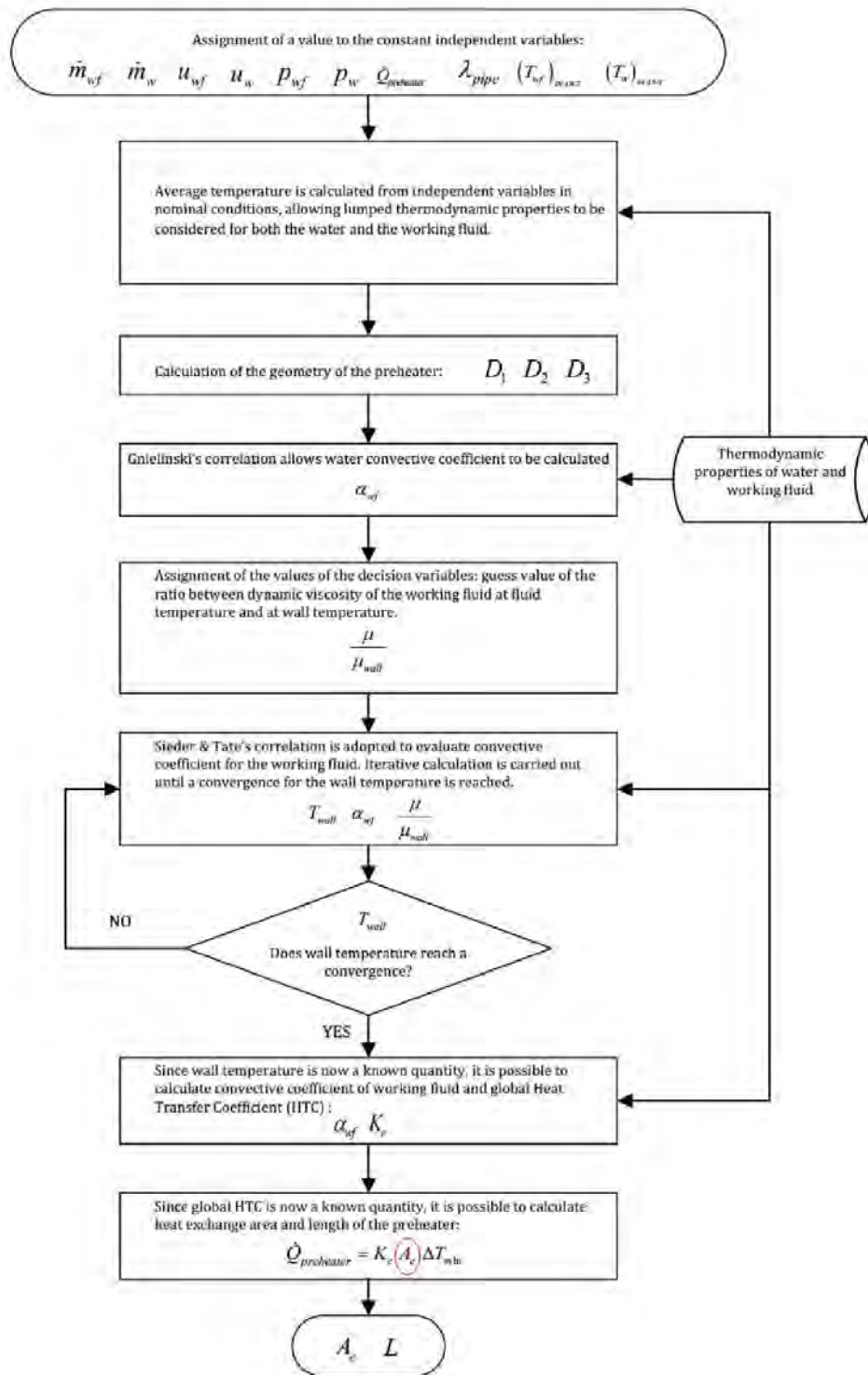


Figure 4.6  
 Flow chart representing the design methodology of low temperature preheater.

<i>Parameter</i>	<i>unit</i>	R-134a	R-245fa
Single pipe length	m	2.845	3,28
Number of pipes	/	200	150
Internal diameter, inner pipe (D <sub>1</sub> )	m	0.0091	0.0094
External diameter, inner pipe (D <sub>2</sub> )	m	0.0131	0.0124
Internal diameter, outer pipe (D <sub>3</sub> )	m	0.0196	0.0210
Heat exchange area, referred to D <sub>2</sub>	m <sup>2</sup>	23.4	19.125
Hot water overall mass flow rate	kg/s	66.5	66.5
Working fluid overall mass flow rate	kg/s	30.388	27.109
Working fluid inlet temperature	°C	31.05	30.24
Working fluid outlet temperature	°C	41.9	41.9
Hot water inlet temperature	°C	51.9	51.9
Hot water outlet temperature	°C	50.17	50.36
Working fluid pressure	bar	20.132	5.695
Hot water pressure	bar	3.15	3.15

Table 4.8

*Design characteristics and working parameters in nominal conditions for low temperature pre-heater.*

- High temperature pre-heater and evaporator

Water of the HT circuit pass through ORC superheater (in the case of R-134a) first. Then, water leaves the superheater and enters the evaporator. The latter allows the preheating of the working fluid, until it reaches saturation conditions, and its vaporization. ORC with R-245fa as working fluid is a saturated vapour cycle. Thus, superheater is not necessary in this case: water HT circuit enters directly the evaporator. For both the ORC configurations, separate design processes have been carried out to size the high temperature preheater and the evaporator. Methodology adopted to develop the high temperature preheater design model is identical to the one exposed in Figure 4.6. Methodology followed to develop design model of evaporator is quite elaborated, and it is briefly described in Figure 4.7. Independent variables are set starting from the findings of Soffiato et al. [47], and an arbitrary number of lumped volumes is set to define the spatial discretization of the heat exchanger. Overall vaporization heat flow in nominal condition is uniformly split considering the over mentioned spatial discretization, therefore it is assumed that each volume exchanges identical heat flow. Starting from an initial guess value assumed for the global Heat Transfer Coefficient (HTC, see ref. [37]), an iterative solution procedure was implemented. This is composed by an outer iterative cycle, based on the value of HTC, and an inner cycle based on the pipe wall temperature. Sizing process of each lumped volume terminates when the value of both these quantities converges to a stable value. Subsequently, linearization procedure exposed in paragraph 3.3.2 was followed to define a smooth transition from single-phase to two-phase convective coefficients. Results of this first step of the design process were used in a second moment to define a new spatial discretization of the evaporator, with lumped volumes characterized by an equal size. Table 4.9 presents main design characteristics and working parameters in nominal conditions for evaporators of R-134a and R-245fa ORCs.

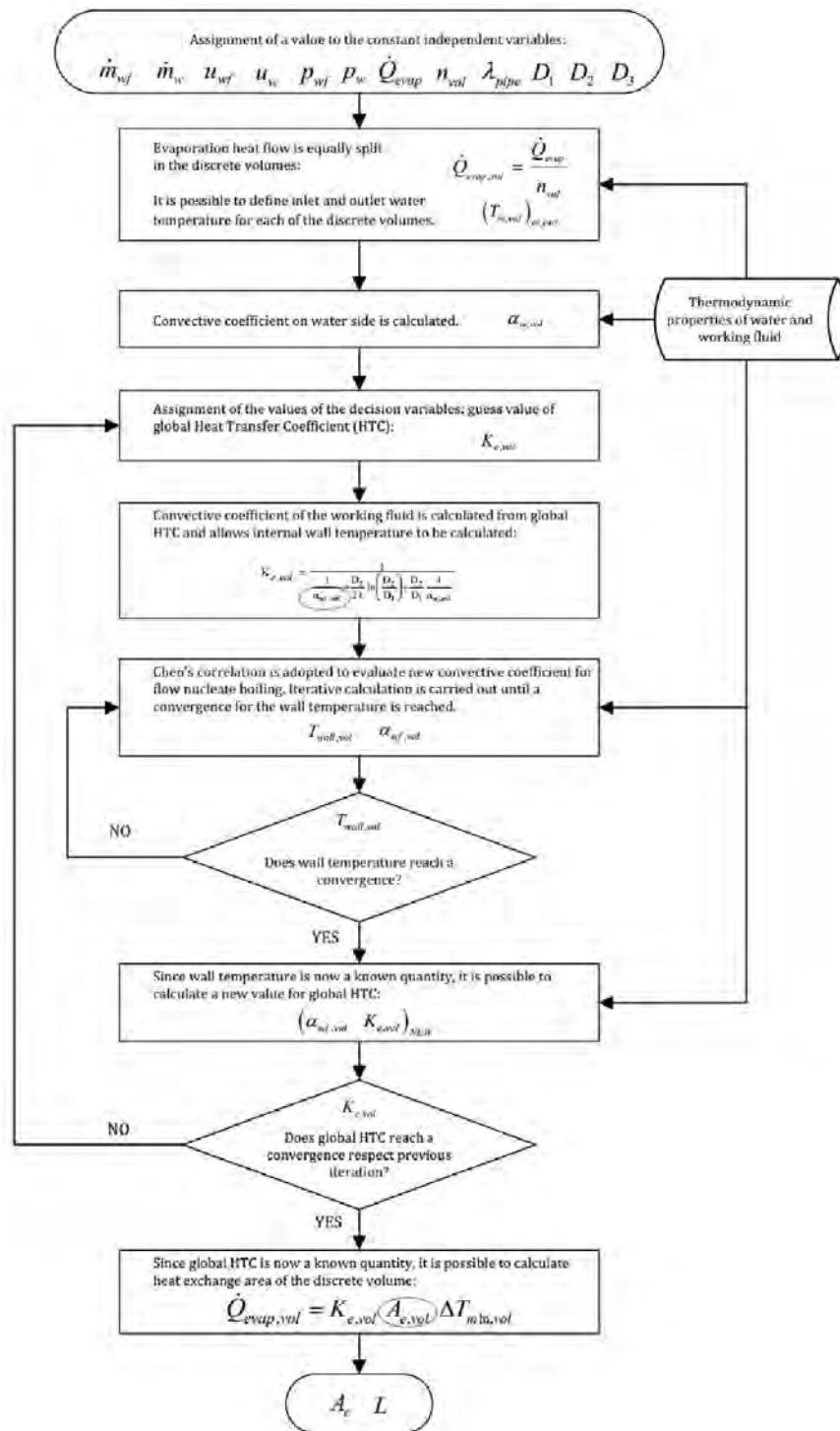


Figure 4.7  
 Flow chart representing the design methodology of evaporator.



<i>Parameter</i>	<i>unit</i>	R-134a		R-245fa	
		Pre HT	Ev HT	Pre HT	Ev HT
Single pipe length	m	5.4	13.65	4.545	15.26
Number of pipes	/	200	200	200	200
Internal diameter, inner pipe (D <sub>1</sub> )	m	0.0095	0.0095	0.0083	0.0083
External diameter, inner pipe (D <sub>2</sub> )	m	0.0135	0.0135	0.0113	0.0113
Internal diameter, outer pipe (D <sub>3</sub> )	m	0.0287	0.0287	0.0277	0.0277
Heat exchange area, referred to D <sub>2</sub>	m <sup>2</sup>	45.66	115.82	32.26	108.34
Hot water overall mass flow rate	kg/s	196.36	196.36	196.36	196.36
Working fluid overall mass flow rate	kg/s	30.388	30.388	27.109	27.109
Working fluid inlet temperature	°C	41.9	67.8	41.9	67.5
Working fluid outlet temperature	°C	67.8	67.8	67.5	67.5
Hot water inlet temperature	°C	77.31	82.0	76.96	82.3
Hot water outlet temperature	°C	75.79	77.31	75.79	76.96
Working fluid pressure	bar	20.132	20.132	5.695	5.695
Hot water pressure	bar	3.15	3.15	3.15	3.15

Table 4.9

*Design characteristics and working parameters in nominal conditions for high temperature pre-heater and evaporator.*

- Superheater, R-134a ORC

Superheater is necessary when the working fluid has a saturated vapour curve characterized by negative slope, as in the case of R-134a. Figure 4.8 reports the flow chart of the methodology adopted to develop the design model. Independent variables are set starting from the findings of Soffiato et al. [47]. Since no phase-change occurs during heat exchange process, Gnielinski's correlation were adopted to evaluate, respectively, convective coefficients of water flowing in the annulus, and vaporized working fluid within the internal pipe (see paragraph 3.3.1). Overall heat exchanger was modelled considering a single lumped volume for both the water and the working fluid side. Control volume of the model corresponds to the physical boundaries of the real component. Following Table 4.10 reports main design characteristics and working parameters in nominal conditions of superheater of R-134a ORC.

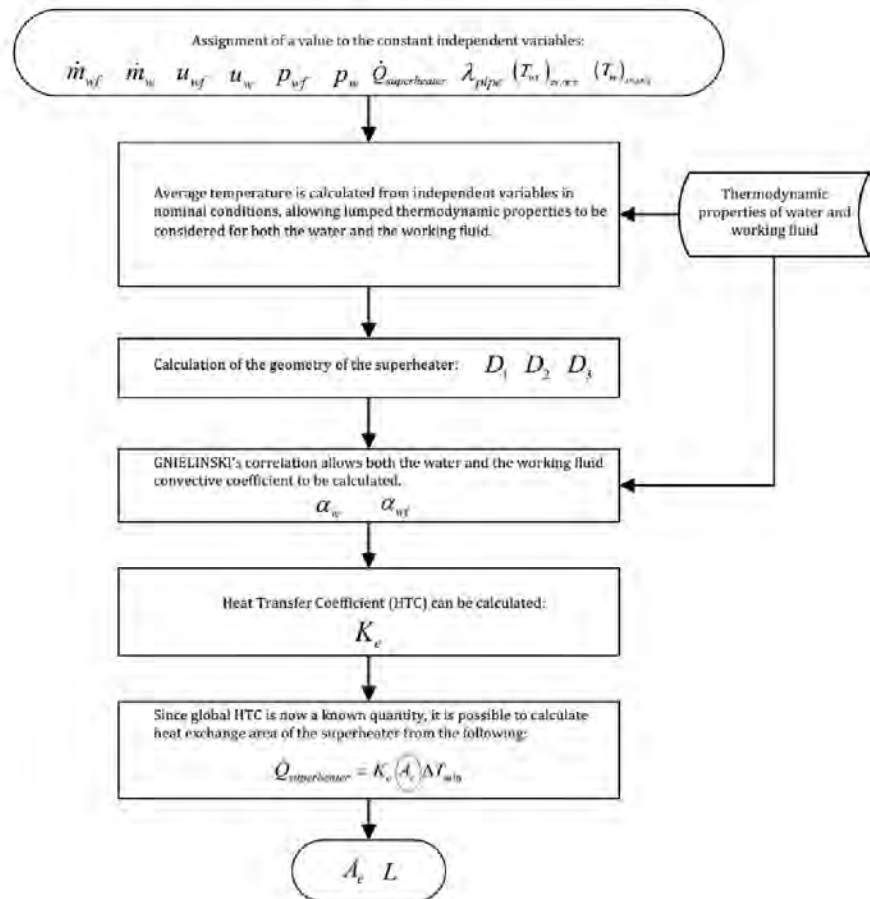


Figure 4.8  
Flow chart representing the design methodology of superheater.

Parameter	unit	R-134a
Single pipe length	m	1.167
Number of pipes	/	200
Internal diameter, inner pipe ( $D_1$ )	m	0.0095
External diameter, inner pipe ( $D_2$ )	m	0.0135
Internal diameter, outer pipe ( $D_3$ )	m	0.0287
Heat exchange area, referred to $D_2$	m <sup>2</sup>	9.9
Hot water overall mass flow rate	kg/s	196.36
Working fluid overall mass flow rate	kg/s	30.388
Working fluid inlet temperature	°C	67.8
Working fluid outlet temperature	°C	72.8
Hot water inlet temperature	°C	82.3
Hot water outlet temperature	°C	82.0
Working fluid pressure	bar	20.132
Hot water pressure	bar	3.15

Table 4.10  
Design characteristics and working parameters in nominal conditions for the high temperature superheater.

- Condenser

Condensation heat is rejected to cooling water through a counterflow pipe in pipe condenser.

Methodology followed to develop design model of condenser is similar to the one adopted for the evaporator. It is briefly described in Figure 4.9. Independent variables are set starting from the findings of Soffiato et al. [47], and an arbitrary number of lumped volumes is set to define the spatial discretization of the heat exchanger. Overall condensing heat flow in nominal condition is uniformly split considering the over mentioned spatial discretization, therefore it is assumed that each volume exchanges identical heat flow. In this case, no iterative solution procedure was necessary to size each lumped volume. As previously done for the evaporator, linearization procedure exposed in paragraph 3.3.2 was followed to define a smooth transition from single-phase to two-phase convective coefficients. Results of this first step of the design process were used in a second moment to define a new spatial discretization of the condenser, with lumped volumes characterized by an equal size. Table 4.11 presents main design characteristics and working parameters in nominal conditions for the condenser in both the R-134a and the R-245fa ORCs.

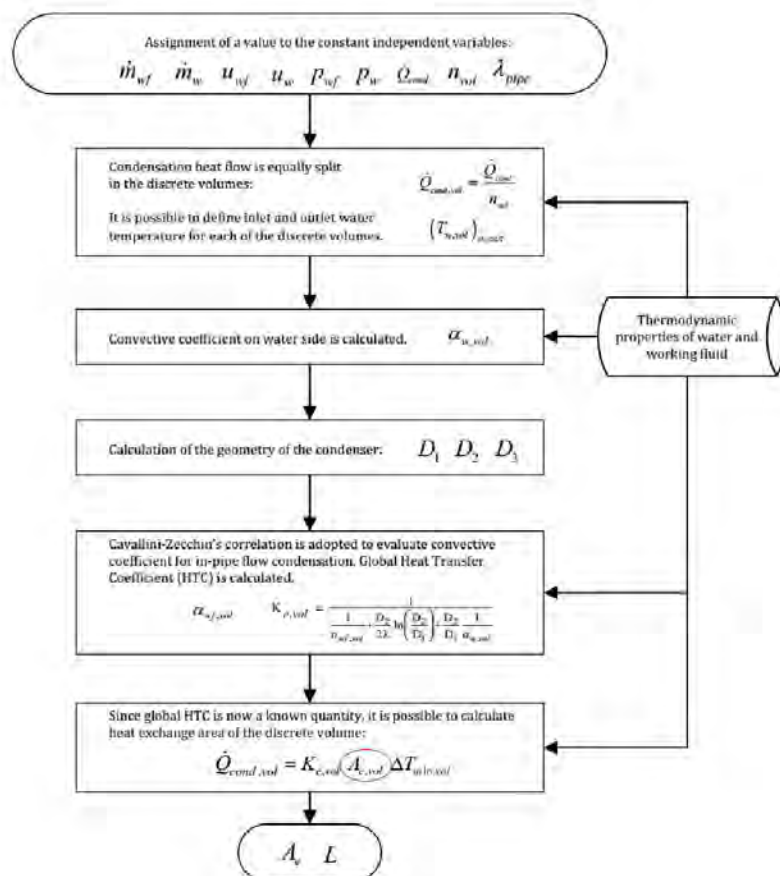


Figure 4.9  
Flow chart representing the design methodology of condenser.

<i>Parameter</i>	<i>unit</i>	R-134a	R-245fa
Single pipe length	m	14.82	14.13
Number of pipes	/	275	300
Internal diameter, inner pipe (D <sub>1</sub> )	m	0.01	0.01
External diameter, inner pipe (D <sub>2</sub> )	m	0.014	0.014
Internal diameter, outer pipe (D <sub>3</sub> )	m	0.0279	0.0267
Heat exchange area, referred to D <sub>2</sub>	m <sup>2</sup>	151	148.7
Cooling water overall mass flow rate	kg/s	251.34	242.55
Working fluid overall mass flow rate	kg/s	30.388	27.109
Working fluid inlet temperature	°C	34.1	39.2
Working fluid outlet temperature	°C	30.0	30.0
Cooling water inlet temperature	°C	15.0	15.0
Cooling water outlet temperature	°C	20.12	20.25
Working fluid pressure	bar	7.702	1.778
Cooling water pressure	bar	3.15	3.15

*Table 4.11*  
*Design characteristics and working parameters in nominal conditions for the condenser.*

### 4.3.2 Design specification of the capacities

Two capacities have been added to the plant layout in order to describe transient behaviour of the system and to evaluate pressure level in condenser and evaporator. A so-called hot drum is placed downstream the evaporator, while a cold drum is placed downstream the condenser. These storages are cylindrical shaped and main design characteristics are reported in Table 4.12.

<i>Parameter</i>	<i>unit</i>	R-134a	R-245fa
material	/	steel	steel
Internal volume	m <sup>3</sup>	8	8
Base internal diameter	m	1.596	1.596
Wall thickness	m	0.08	0.08
Height	m	4	4

*Table 4.12*  
*Design characteristics of hot drum and cold drum.*

### 4.3.3 Design specification of turbomachinery

Design specifications and performance of turbomachinery in nominal operation condition are presented for both the superheated R-134a and the saturated R-245fa ORCs in Table 4.13. The exposed data derived from the work of Soffiato et al. [47].

<i>Parameter</i>	<i>unit</i>	R-134a		R-245fa	
		pump	turbine	pump	turbine
Working fluid mass flow rate	kg/s	30.388	30.388	27.109	27.109
Working fluid inlet pressure	kPa	7.702	20.132	1.778	5.695
Working fluid outlet pressure	kPa	20.132	7.702	5.695	1.778
Isoentropic efficiency	/	0.7	0.7	0.85	0.85
Electrical/mechanical efficiency	/	0.9	0.9	0.9	0.9

Table 4.13  
Design characteristics of pump and turbine.

#### 4.4 Off-design dynamic model of the ORC bottoming ICEs with current configuration of the cooling systems.

This paragraph presents the overall dynamic models developed for the superheated R-134a ORC and the saturated R-245fa ORC. Dynamic models of single components, presented in Chapter 3, have been linked together in order to build the final configuration of the system model. According to the adopted sequential approach, capacities (hot and cold drum) and fluid flow blocks (pump and turbine) must be placed in series, in order to avoid algebraic loops that lead to a non-resolvable problem. As will explained in this paragraph, a similar problem occurs in the case of superheated R-134a ORC. In fact, static models of superheater and turbine have be placed in series, accordingly to the layout of the real plant. The resulting numerical issue have been solved by adding a Simulink® *memory* block to the overall model. Such a problem does not emerge in the model of saturated R-245fa ORC, because fluid flow blocks and capacities are all placed in series. Figure 4.10 reports the overall layout of superheated R-134a ORC dynamic model. Each numbered box referred to a specific component, which is described in Table 4.14. Links between different components correspond to congruence equations related to exchange variables. In other words, links represent the equivalence existing among output variables of a given block and input variables of the following block, which is linked to the former one. Links in question can represent mass flow rate, thermodynamic properties, power, heat flow and control signals.

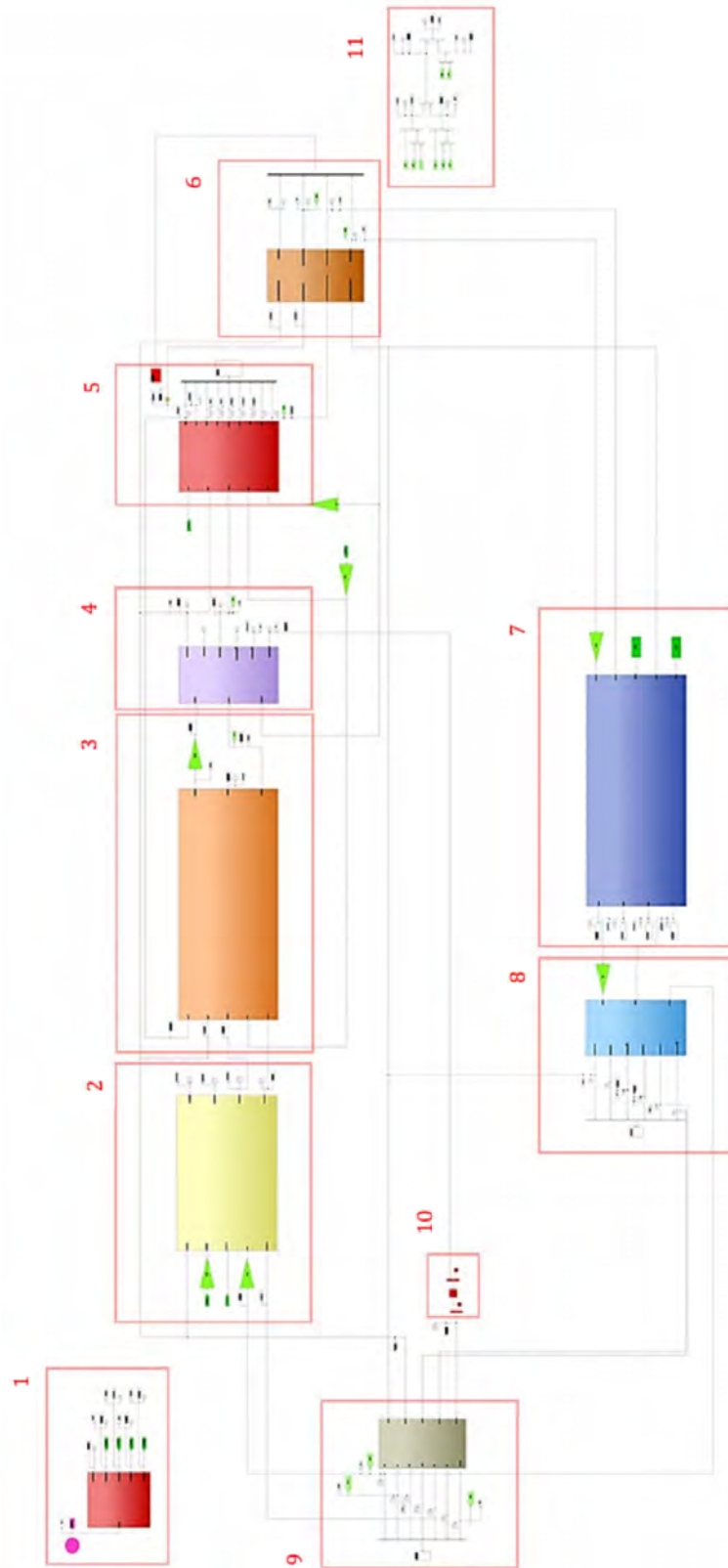










Figure 4.10  
Layout of the overall dynamic model of R-134a ORC

<p>1 <i>ICEs variable load look up tables</i></p> 	<p><i>INPUTS</i></p> <p><i>Simulation time</i></p>	<p><i>OUTPUTS</i></p> <p><i>ICEs load</i></p> <p><math>T_{wHTin}(t)</math></p> <p><math>\dot{m}_{wHT}(t)</math></p> <p><math>T_{wLTin}(t)</math></p> <p><math>\dot{m}_{wLT}(t)</math></p>	
<p>2 <i>Low temperature preheater</i></p> 	<p><i>INPUTS</i></p> <p><math>p_{wf}(t)</math></p> <p><math>\dot{m}_{wf}(t)</math></p> <p><math>T_{wf0}(t)</math></p> <p><math>p_{wLT}(t)</math></p> <p><math>\dot{m}_{wLT}(t)</math></p> <p><math>T_{w0}(t)</math></p>	<p><i>STATE VARIABLES</i></p> <p><math>T_{wf1N}(t)</math></p> <p><math>T_{w1N}(t)</math></p>	<p><i>OUTPUTS</i></p> <p><math>T_{wfN}(t)</math></p> <p><math>h_{wfN}(t)</math></p> <p><math>T_{wN}(t)</math></p>
<p>3 <i>High temperature preheater/evaporator</i></p> 	<p><i>INPUTS</i></p> <p><math>p_{wf}(t)</math></p> <p><math>\dot{m}_{wf0}(t)</math></p> <p><math>h_{wf0}(t)</math></p> <p><math>p_{wHT}(t)</math></p> <p><math>\dot{m}_{wHT}(t)</math></p> <p><math>T_{w0}(t)</math></p>	<p><i>STATE VARIABLES</i></p> <p><math>h_{wf1N}(t)</math></p> <p><math>T_{w1N}(t)</math></p> <p><math>\rho_{w1N}(t)</math></p>	<p><i>OUTPUTS</i></p> <p><math>\dot{m}_{wfN}(t)</math></p> <p><math>x_{wfN}(t)</math></p> <p><math>h_{wfN}(t)</math></p> <p><math>T_{wfN}(t)</math></p> <p><math>\rho_{wfN}(t)</math></p> <p><math>T_{wN}(t)</math></p>
<p>4 <i>Hot drum</i></p> 	<p><i>INPUTS</i></p> <p><math>\dot{m}_{wf1N}(t)</math></p> <p><math>\dot{m}_{wfOUT}(t)</math></p> <p><math>h_{wf1N}</math></p>	<p><i>STATE VARIABLES</i></p> <p><math>p(t)</math></p> <p><math>V_l(t)</math></p>	<p><i>OUTPUTS</i></p> <p><math>h_{wfOUT}</math></p> <p><math>p(t)</math></p> <p><math>V_l(t)</math></p> <p><math>T_{wfOUT}(t)</math></p> <p><math>\rho_{wfOUT}(t)</math></p> <p><math>l_l(t)</math></p>

5	<p style="text-align: center;"><i>Superheater</i></p> 	<p style="text-align: center;"><i>INPUTS</i></p> $p_{wf}(t)$ $\dot{m}_{wf}(t)$ $T_{wflN}(t)$ $p_{wHT}(t)$ $\dot{m}_{wHT}(t)$ $T_{wIN}(t)$	<p style="text-align: center;"><i>OUTPUTS</i></p> $T_{wfOUT}(t)$ $T_{wOUT}(t)$ $\rho_{wfOUT}(t)$	
6	<p style="text-align: center;"><i>Turbine</i></p> 	<p style="text-align: center;"><i>INPUTS</i></p> $p_{wflN}(t)$ $p_{wfOUT}(t)$ $T_{wflN}(t)$ $\rho_{wflN}(t)$ $h_{wflN}(t)$	<p style="text-align: center;"><i>OUTPUTS</i></p> $h_{wfOUT}(t)$ $T_{wfOUT}(t)$ $\dot{m}_{wf}(t)$ $P_T(t)$ $\eta_T(t)$	
7	<p style="text-align: center;"><i>Condenser</i></p> 	<p style="text-align: center;"><i>INPUTS</i></p> $p_{wf}(t)$ $\dot{m}_{wf0}(t)$ $h_{wf0}(t)$ $p_w(t)$ $\dot{m}_w(t)$ $T_{w0}(t)$	<p style="text-align: center;"><i>STATE VARIABLES</i></p> $h_{wflN}(t)$ $T_{w1N}(t)$ $\rho_{w1N}(t)$	<p style="text-align: center;"><i>OUTPUTS</i></p> $\dot{m}_{wflN}(t)$ $x_{wflN}(t)$ $h_{wflN}(t)$ $T_{wflN}(t)$ $\rho_{wflN}(t)$ $T_{wN}(t)$
8	<p style="text-align: center;"><i>Cold drum</i></p> 	<p style="text-align: center;"><i>INPUTS</i></p> $\dot{m}_{wflN}(t)$ $\dot{m}_{wfOUT}(t)$ $h_{wflN}$	<p style="text-align: center;"><i>STATE VARIABLES</i></p> $p(t)$ $V_l(t)$	<p style="text-align: center;"><i>OUTPUTS</i></p> $h_{wfOUT}$ $p(t)$ $V_l(t)$ $T_{wfOUT}(t)$ $\rho_{wfOUT}(t)$ $l_l(t)$




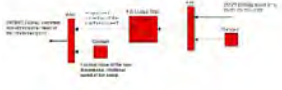

<p>9</p> <p style="text-align: center;"><i>Pump</i></p> 	<p style="text-align: center;"><i>INPUTS</i></p> $p_{wfIN}(t)$ $p_{wfOUT}(t)$ $T_{wfIN}(t)$ $\rho_{wfIN}(t)$ $h_{wfIN}(t)$	<p style="text-align: center;"><i>OUTPUTS</i></p> $h_{wfOUT}(t)$ $T_{wfOUT}(t)$ $\dot{m}_{wf}(t)$ $P_P(t)$ $\eta_P(t)$
<p>10</p> <p style="text-align: center;"><i>Control system</i></p> 	<p style="text-align: center;"><i>INPUTS</i></p> $l_l(t)$	<p style="text-align: center;"><i>OUTPUTS</i></p> $\frac{\omega}{\omega_{dp}}(t)$
<p>11</p> <p style="text-align: center;"><i>Performance calculation blocks</i></p> 	<p style="text-align: center;"><i>INPUTS</i></p> $\dot{Q}_{inputpr\ eLT}(t)$ $\dot{Q}_{inputpreHT}(t)$ $\dot{Q}_{inpute\ vHT}(t)$ $\dot{Q}_{inputshHT}(t)$ $P_T(t)$ $P_P(t)$	<p style="text-align: center;"><i>OUTPUTS</i></p> $P_{net}(t)$ $\eta_{el}(t)$

Table 4.14  
Overview of dynamic models that compose the overall dynamic model of superheated R-134a ORC.

Analogous considerations can be done about the saturated R-245fa ORC. The overall layout of this ORC system is presented in Figure 4.11, while Table 4.14 can be considered as reference for the description of each block of the model. To be noted that, as mentioned before, in this case superheater is not necessary.

Each block in Figure 4.10 and Figure 4.11 represents a Simulink® *subsystem*, created by means of the aggregation of user defined *m-Function* and default Simulink® blocks. This is particularly evident in the dynamic models of heat exchangers. Three main hierarchical levels can be observed in these components, passing from outside to inside. First, each component can be identified as a single block in the overall layout of the system. In second hierarchical level, the spatial discretization of the modelled component is defined. Finally, in the third level, subroutines developed to describe physical process occurring in each discrete volume are implemented.



*Figure 4.11*  
*Layout of the overall dynamic model of R-245fa ORC*

## 4.5 Summary

This chapter presented the optimal ORC solutions proposed by Soffiato [17, 47] and the design and off-design dynamic models of two ORCs.

ICEs and cooling systems have been briefly described, presenting their operation and performance in design and off-design conditions. Then, optimal design solutions for the ORC developed by Soffiato [47] were exposed. Design and off-design dynamic models have been presented for the superheated ORC with R-134a as working fluid, and the saturated ORC with R-245fa as working fluid.

# 5 OFF-DESIGN DYNAMIC SIMULATIONS

## 5.1 Introduction

This chapter presents the simulations of the ORC dynamic models described in Chapter 4. Dynamic simulations have been carried out to analyse transient behaviour of the ORCs during load variations of the topping ICEs, related to a change of the service speed of the ship. Dynamic models have been tested considering a mild variation (Test Case A) and a brutal decrement (Test Case B) of the service speed. A control strategy for the ORCs has been implemented and tested. Finally, the chapter exposes simulation results.

## 5.2 Off-design Hot Composite Curves

In order to evaluate transient response of the bottoming ORC, it is necessary to define in quantity and quality heat flux rejected by topping ICEs.

First, it is necessary to know the variation of service speed of the vessel, which influences the number of working engines and their load. A deceleration/acceleration ramp must be defined to set at any given time the value of the vessel's speed. The number of engines in operation and their load during this speed transient is given by Table 4.3 and Table 4.4, respectively in the cases of laden and ballast voyage mode.

Given the load of the engine in operation, Table 4.2 combined with equations from (4.4) to (4.12) allow the calculation of HCC during transient phase. Thus, water mass flow rate and inlet temperature in LT and HT circuits can be evaluated, defining inlet conditions of the heat source in the ORC heat exchangers.

## 5.3 Test cases for dynamic off-design simulations

Two different speed profiles have been considered to evaluate transient response of the investigated ORC system. First, a mild deceleration followed by a mild acceleration of the vessel have been simulated (Test Case A). The second test simulates a brutal decrease of the vessel's speed (Test Case B).

ORC with R-134a was tested with both the speed profiles, while ORC with R-245fa was tested only with Test Case B, due to its longer simulation time.

Subsequently, a control system have been added to the ORC model, in order to enhance the efficiency of the power plant during transient phase. Once again, ORC with R-134a was tested with both Test Cases A and B, while ORC with R-245fa was tested only with Test Case B.

### 5.3.1 Test Case A: mild variations of service speed

As mentioned before, this test case simulate a mild deceleration from 18.4 kn (service speed in nominal condition, point 1) to 16.5 kn (point 2). Then, a mild acceleration of the vessel is simulated, until service speed reaches 17.5 kn (point 3). During transient phase, overall heat available from the engine cooling systems drop from 9.785 to a minimum of 7.075 MW<sub>t</sub>. Figure 5.1 represents the profile of vessel's service speed during the transient phase. Figure 5.2 reports HCC related to initial (1), intermediate (2) and final (3) service speed values. Figure 5.3, Figure 5.4 and Figure 5.5 represent the main parameters that characterize the transient behaviour of both water HT circuit and water LT circuit.

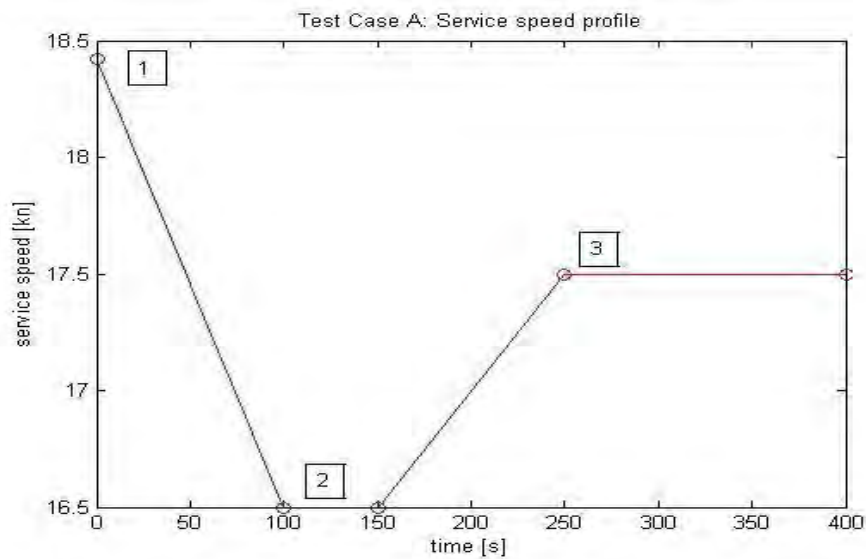


Figure 5.1

Test Case A: service speed profile of the vessel.

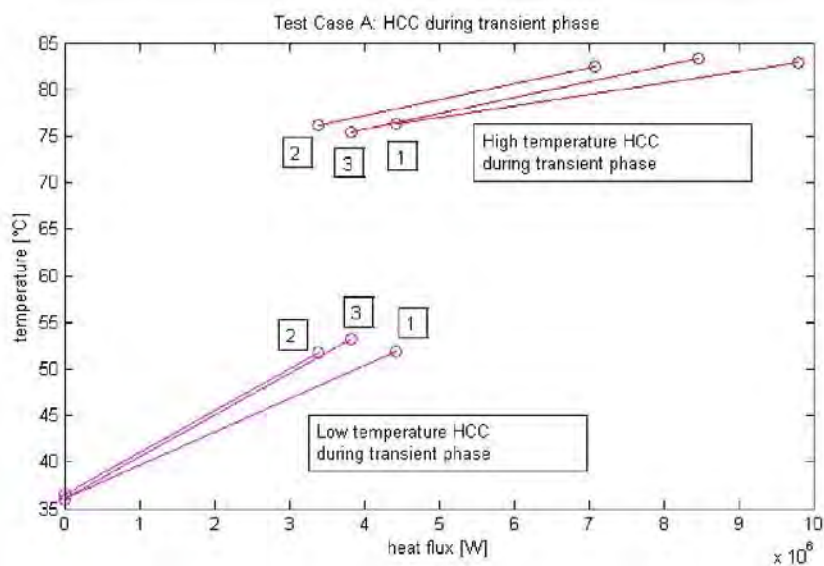


Figure 5.2

Test case A: HCC during transient phase.

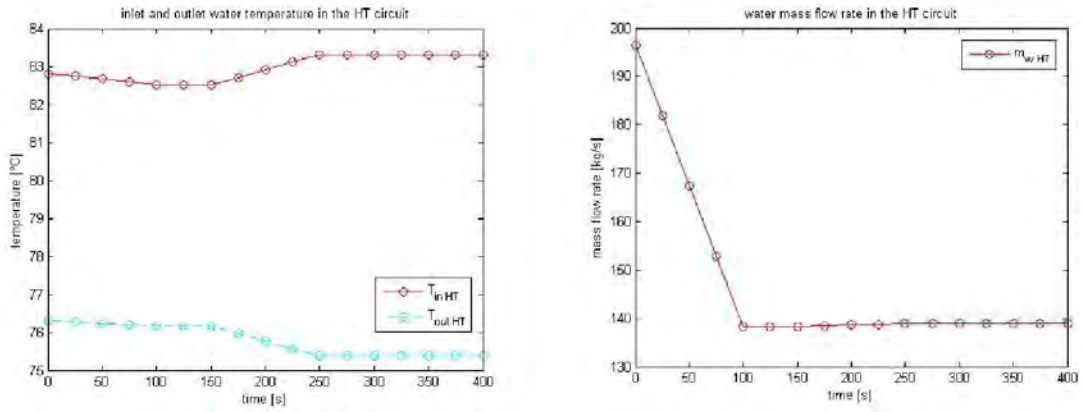


Figure 5.3

Test Case A: from left to right, profiles of water temperature and mass flow rate in the HT circuit during transient phase.

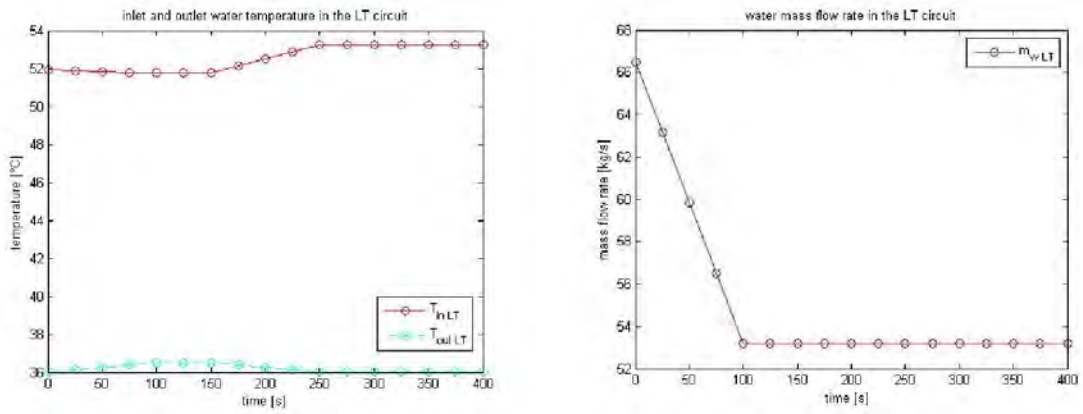


Figure 5.4

Test Case A: from left to right, profiles of water temperature and mass flow rate in the LT circuit during transient phase.

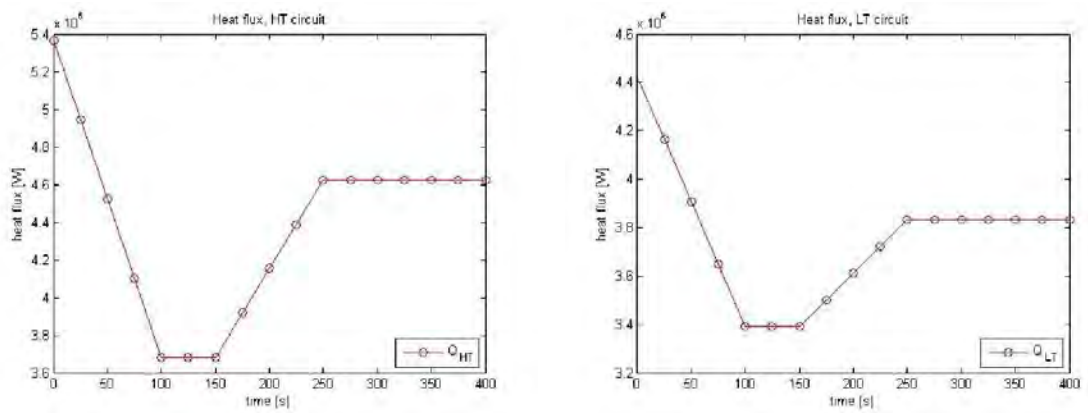


Figure 5.5

Test Case A: from left to right, profiles of heat flux available from water HT and LT circuit during transient phase.

### 5.3.2 Test Case B: brutal decrement of service speed

This test case simulate a significant reduction of the vessel's service speed, leading to an equally significant reduction of the heat flux exploitable by the ORC. Service speed of the ship drop from 18.4 kn to 12.5 kn in 120 seconds. Overall heat available from the engine cooling systems drop from 9.785 to 2.867 MW<sub>t</sub>. As previously done in paragraph 5.3.1, from Figure 5.6 to Figure 5.10 main parameters characterizing transient phase of the cooling system of the engines are exposed.

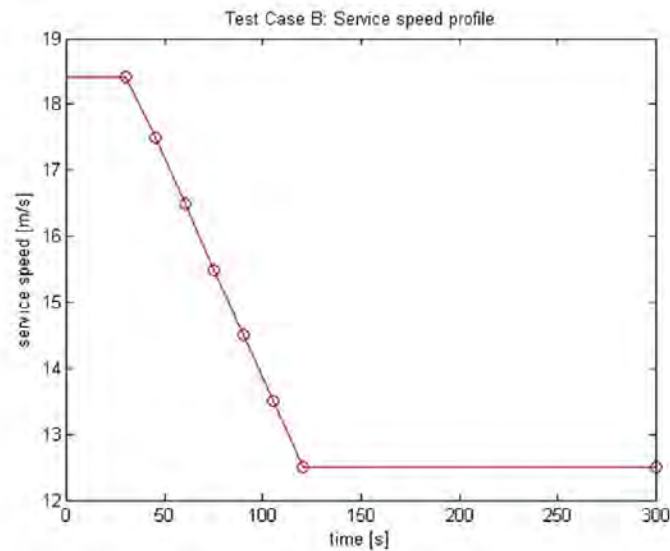


Figure 5.6  
Test Case B: Service speed profile of the vessel.

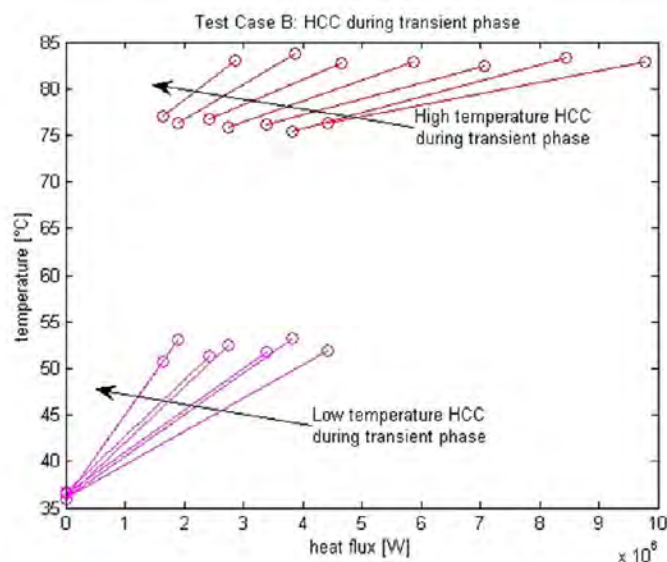


Figure 5.7  
Test case B: HCC during transient phase.

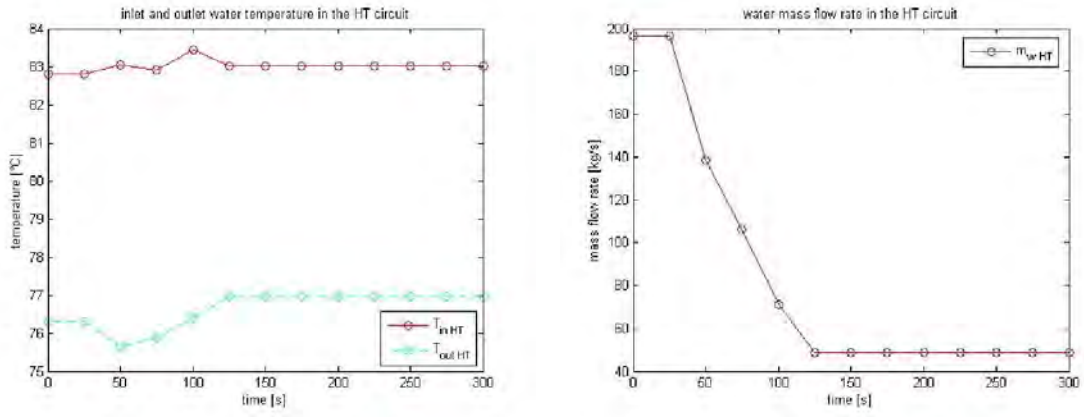


Figure 5.8

Test Case B: from left to right, profiles of water temperature and mass flow rate in the HT circuit during transient phase.

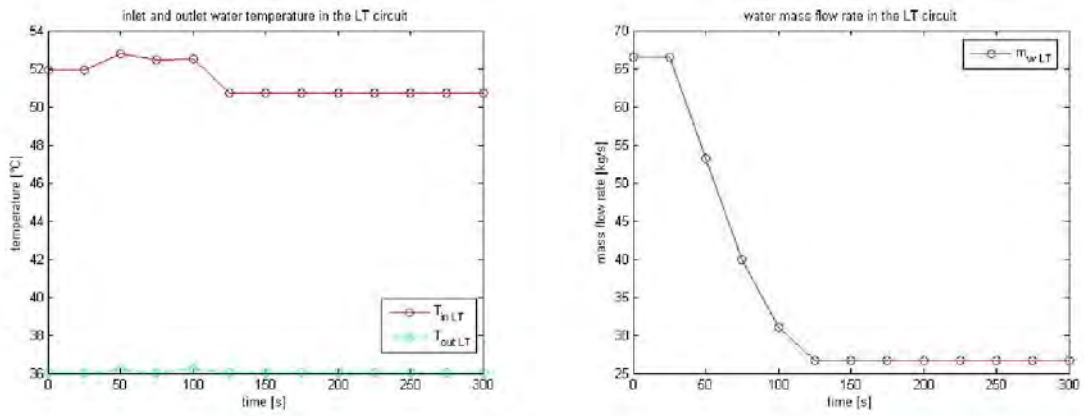


Figure 5.9

Test Case B: from left to right, profiles of water temperature and mass flow rate in the LT circuit during transient phase.

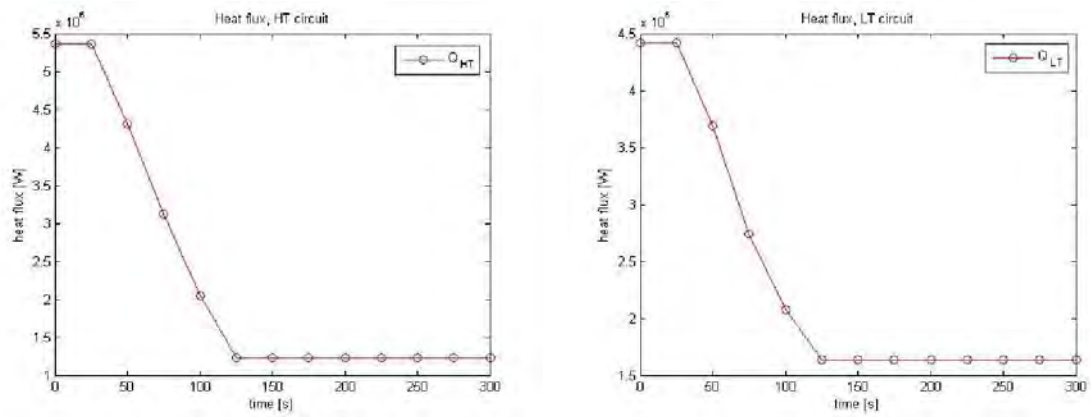


Figure 5.10

Test Case B: from left to right, profiles of heat flux available from water HT and LT circuit during transient phase.

### 5.3.3 Control system

To avoid complete emptying or filling of hot and cold drum, a control system governing rotational speed of the feed pump was developed. Liquid level inside the hot drum were chose as input signal for the controller. Rotational speed of the pump is reduced in the case of rising liquid level in the cold drum. Conversely, a decreasing liquid level in the hot drum lead to an acceleration of the rotational speed of the pump. Control system gives, as output signal, a proportional modification of the non-dimensional rotational speed of the feed pump, which leads to a modification of the characteristic maps of the component. In the following Figure 5.11, a schematic representation of the controller is reported.

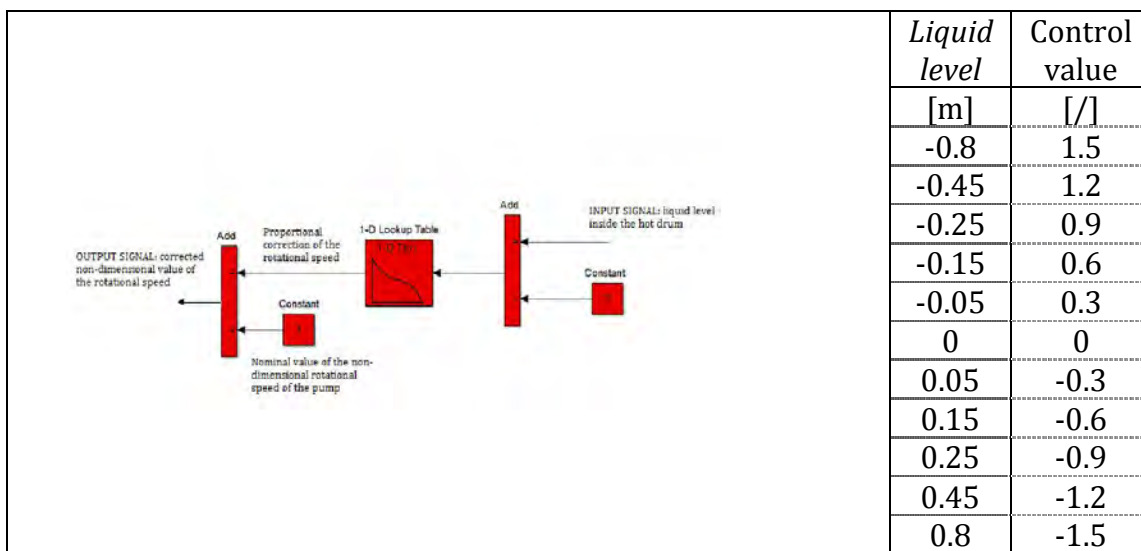


Figure 5.11  
Schematic representation of the implemented control system.

## 5.4 Simulation results

Following subparagraphs presents main results obtained with the dynamic model of the ORC. Classification takes into account the working fluid used in the power plant, the test case and if the control system was implemented or not.

### 5.4.1 R-134a ORC, test case A

Superheated ORC with R-134a as working fluid was tested with Test case A. First, a simulation without a control system was carried out. Main results are shown in the following Figure 5.12.



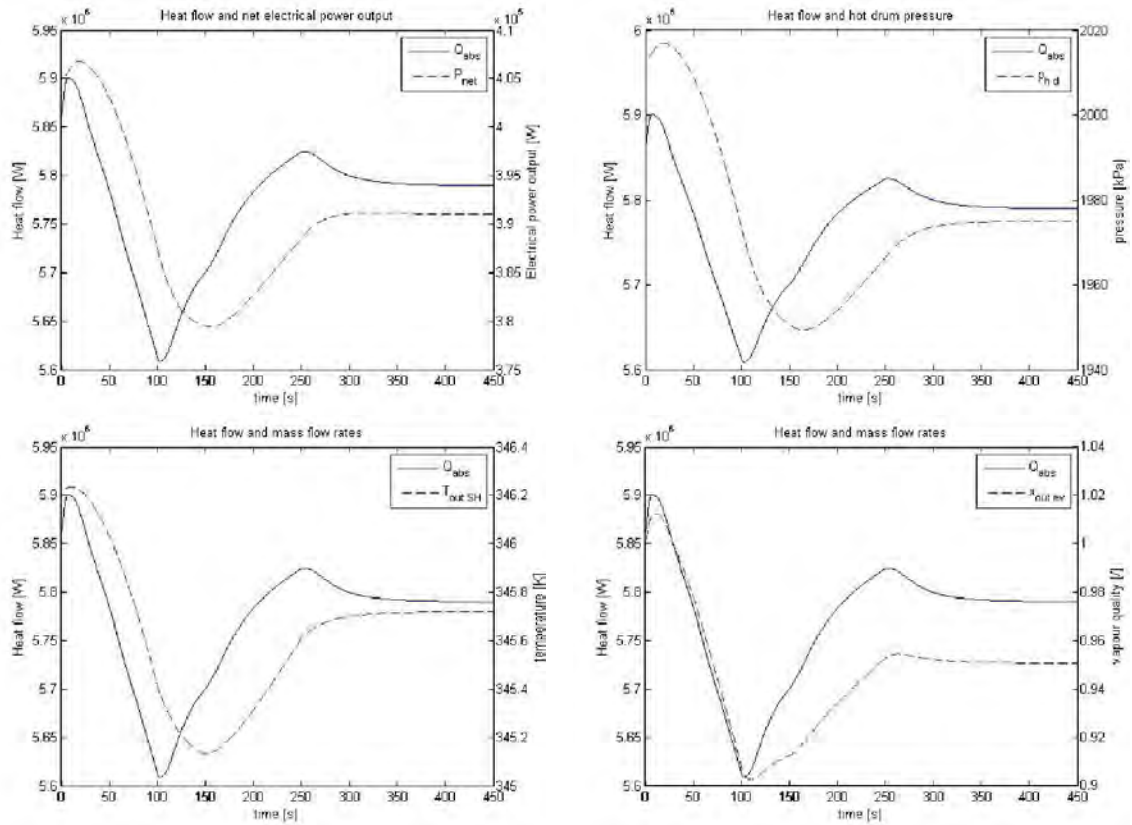


Figure 5.12

Clockwise, from upper left: Net electrical power output, evaporation pressure, superheater outlet temperature and vapour quality at the exit of the evaporator (green line). Blue line shows heat input of the ORC during transient phase. R-134a ORC, Test case A, No control.

The drop of the heat input of the ORC is reflected by a consequential drop in the electrical power output. The latter is slightly shifted respect the former, due to the thermal inertia of the system. The reduction in input heat flow is quite small (about 1.7% from initial to final state) but it strongly influences vapour quality at the exit of the evaporator and the turbine inlet temperature. The former undergoes a reduction of about 5%, while the latter passes from 346.2 K to 345.7 K.

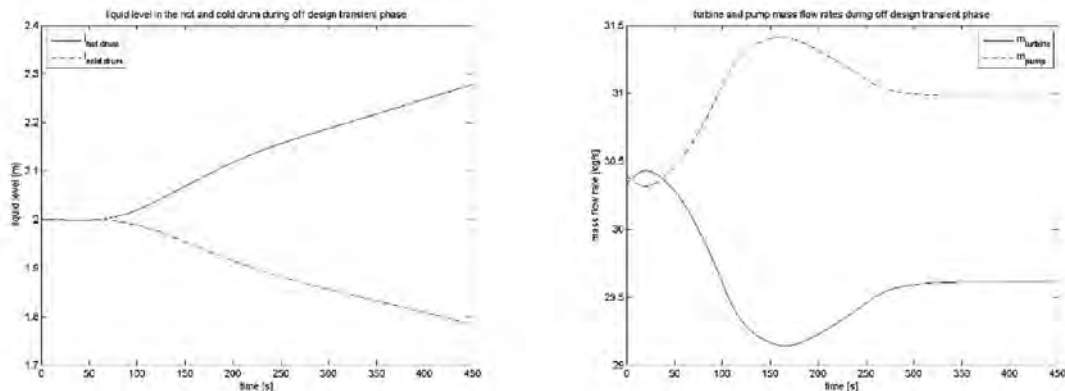


Figure 5.13

On the left: liquid level in the hot drum (red line) and the cold drum (blue line) during transient phase. On the right: turbine (red) and pump (blue) mass flow rate during transient phase.

During transient phase, pump and turbine experience an alteration of inlet and outlet pressure values. This leads to a discrepancy in the working fluid mass flow rate processed by the turbine and the pump. As a result, on the left of Figure 5.15, it is possible to note how capacities undergo an emptying or a filling process.

In order to avoid the total emptying, or filling, a control system was introduced. It controls liquid level in the hot drum acting on the rotational speed of the feed pump. Simulation results of Test Case A relative to the controlled R-134a ORC are exposed below, in Figure 5.14.

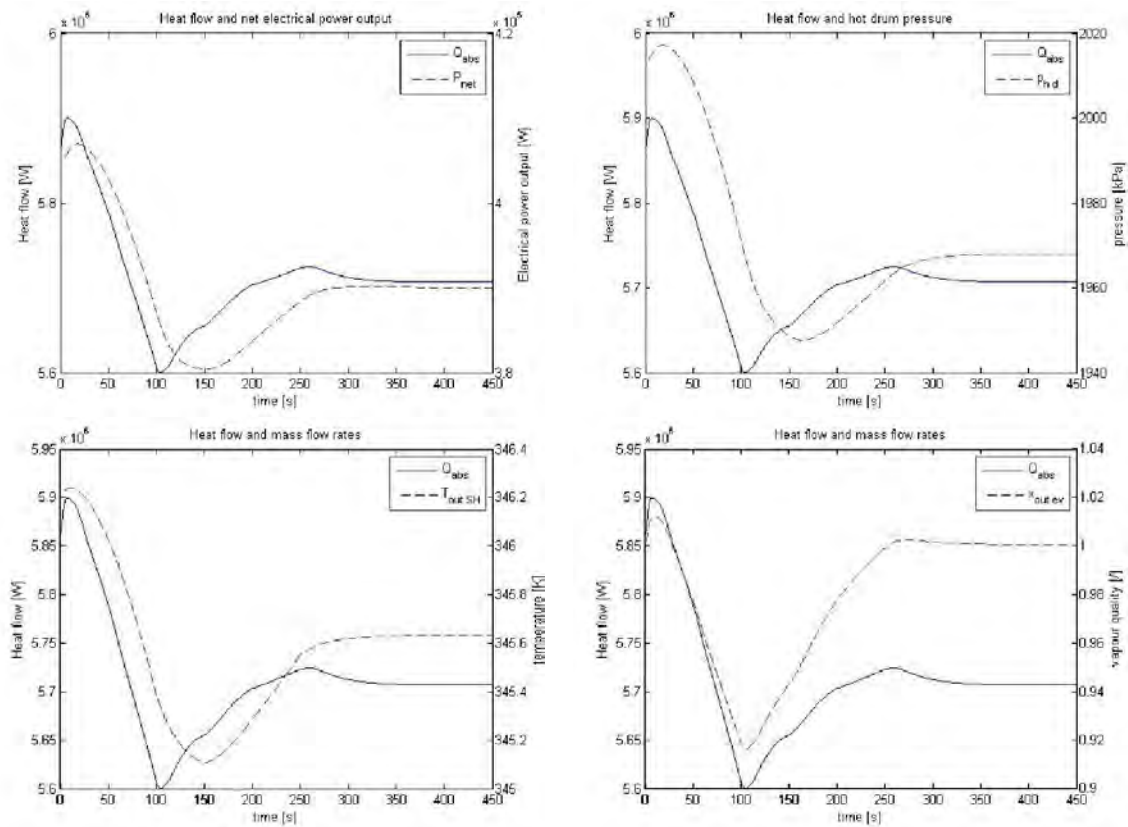


Figure 5.14

*Clockwise, from upper left: Net electrical power output, evaporation pressure, superheater outlet temperature and vapour quality at the exit of the evaporator (green line). Blue line shows heat input of the ORC during transient phase. R-134a ORC, Test case A, Controlled.*

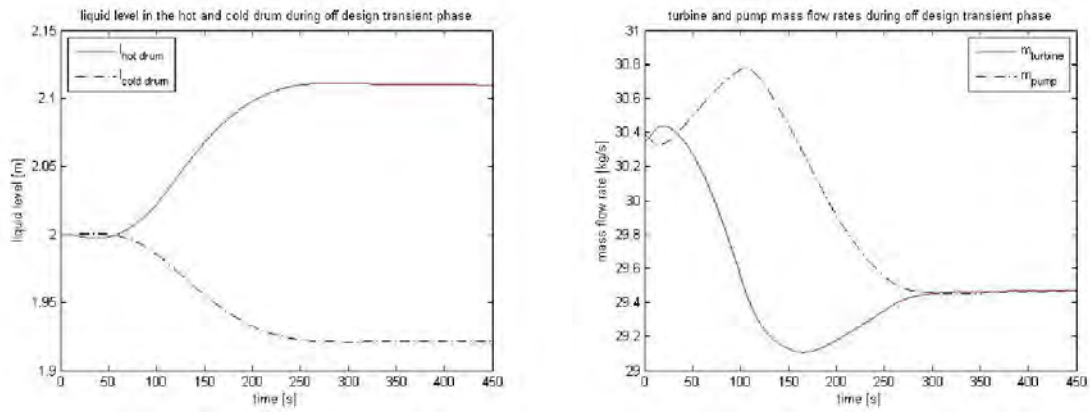


Figure 5.15

On the left: liquid level in the hot drum (red line) and the cold drum (blue line) during transient phase.  
On the right: turbine (red) and pump (blue) mass flow rate during transient phase.

As can be noted from Figure 5.15, the implemented control system allow reducing variations of liquid level inside hot and cold drum. However, further works should consider new and more effective control strategies which allow to enhance heat exploitation and electrical power production. In fact, simulation results show as this simple control strategy slightly disadvantages heat recovery and electrical power production.

#### 5.4.2 R-134a ORC, test case B

Superheated ORC with R-134a as working fluid was tested with Test case B. First, a simulation without a control system was carried out. Main results are shown in the following Figure 5.16.

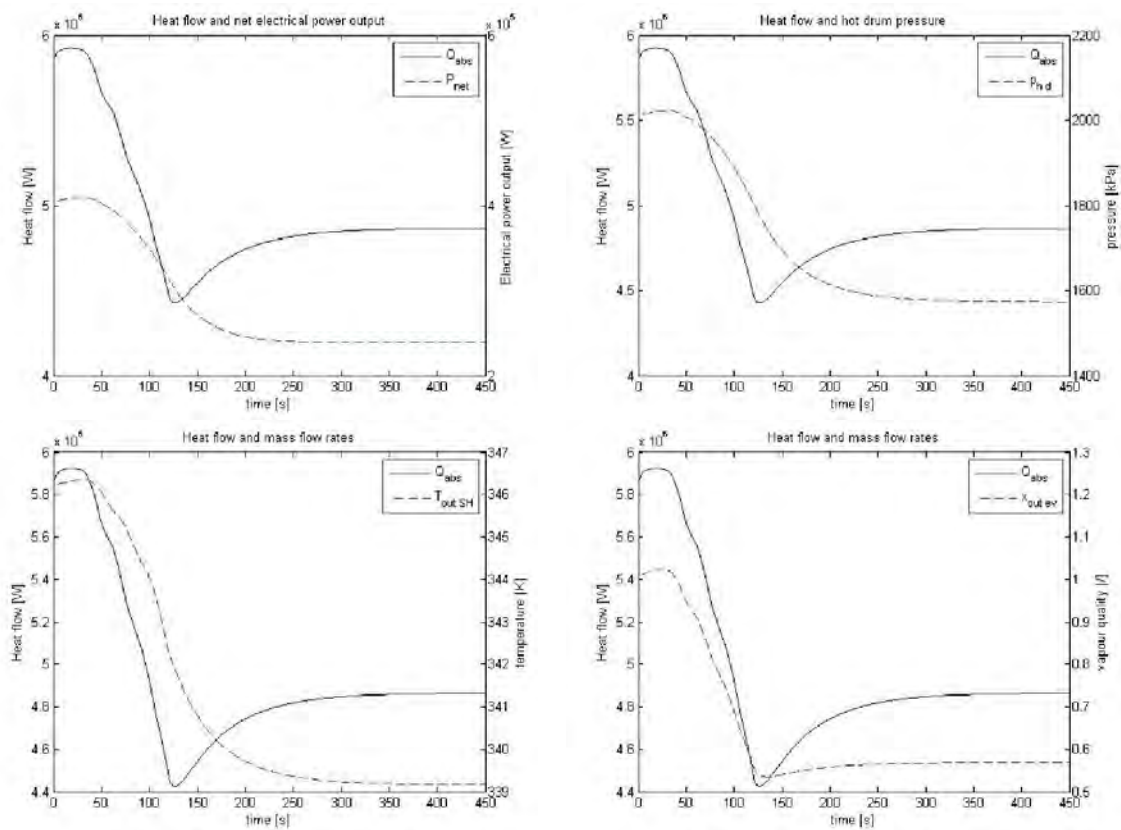


Figure 5.16

Clockwise, from upper left: Net electrical power output, evaporation pressure, superheater outlet temperature and vapour quality at the exit of the evaporator (green line). Blue line shows heat input of the ORC during transient phase. R-134a ORC, Test case B, No control.

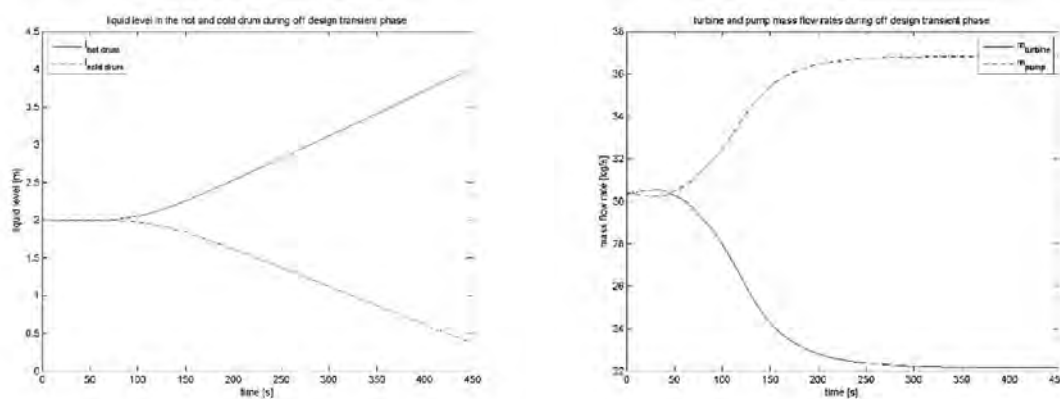


Figure 5.17

On the left: liquid level in the hot drum (red line) and the cold drum (blue line) during transient phase.  
On the right: turbine (red) and pump (blue) mass flow rate during transient phase.

Upper figure shows that a reduction of the service speed of the vessel from 18.4 to 12.5 kn (40% variation) leads to a reduction of about 18% of heat flow input of the ORC, which passes from 5.947 to 4.865 MW<sub>t</sub>. Net electrical power output collapses to 239 kW<sub>el</sub>, equal to 60% of nominal value.

As in the test case A, the hot drum experience a drastic increment of the liquid level, which is represented in Figure 5.17. Conversely, cold drum undergoes an emptying process. How can be note in Figure 5.18 and Figure 5.19, the application of the control system stabilizes liquid level in both the capacities, avoiding their complete emptying or filling. Furthermore, it allows a slightly increase of the electrical power output, which amounts at 252.7 kW<sub>el</sub> at the end of the transient phase.

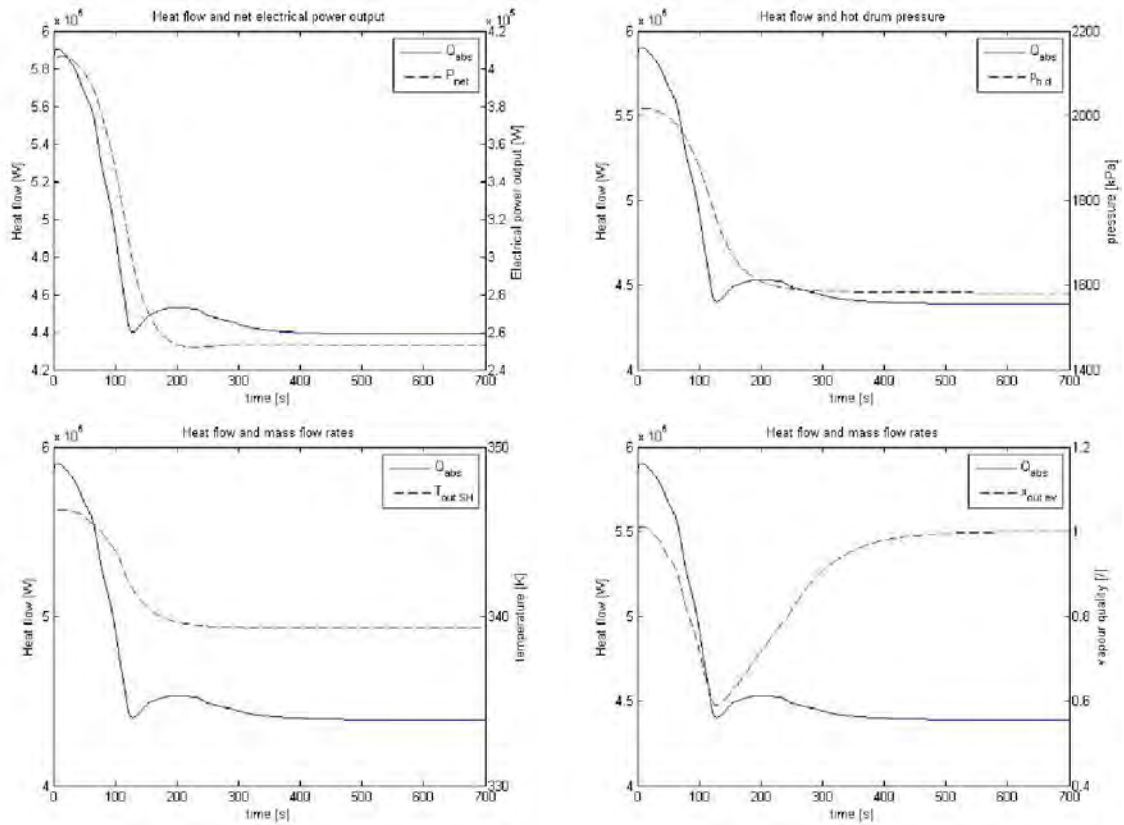


Figure 5.18

*Clockwise, from upper left: Net electrical power output, evaporation pressure, superheater outlet temperature and vapour quality at the exit of the evaporator (green line). Blue line shows heat input of the ORC during transient phase. R-134a ORC, Test case B, Controlled.*

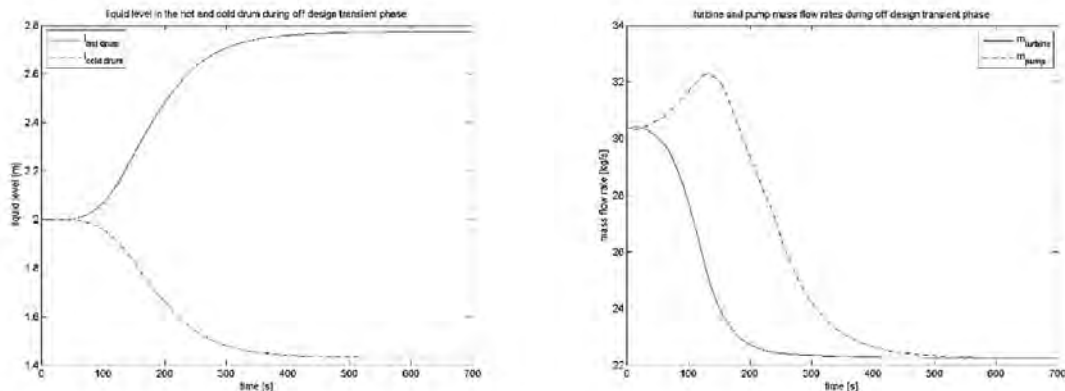


Figure 5.19

*On the left: liquid level in the hot drum (red line) and the cold drum (blue line) during transient phase. On the right: turbine (red) and pump (blue) mass flow rate during transient phase.*

### 5.4.3 R-245fa ORC, test case B

Saturated ORC with R-245fa as working fluid was tested with Test case A. First, a simulation without a control system was carried out. Main results are shown in the following Figure 5.20.

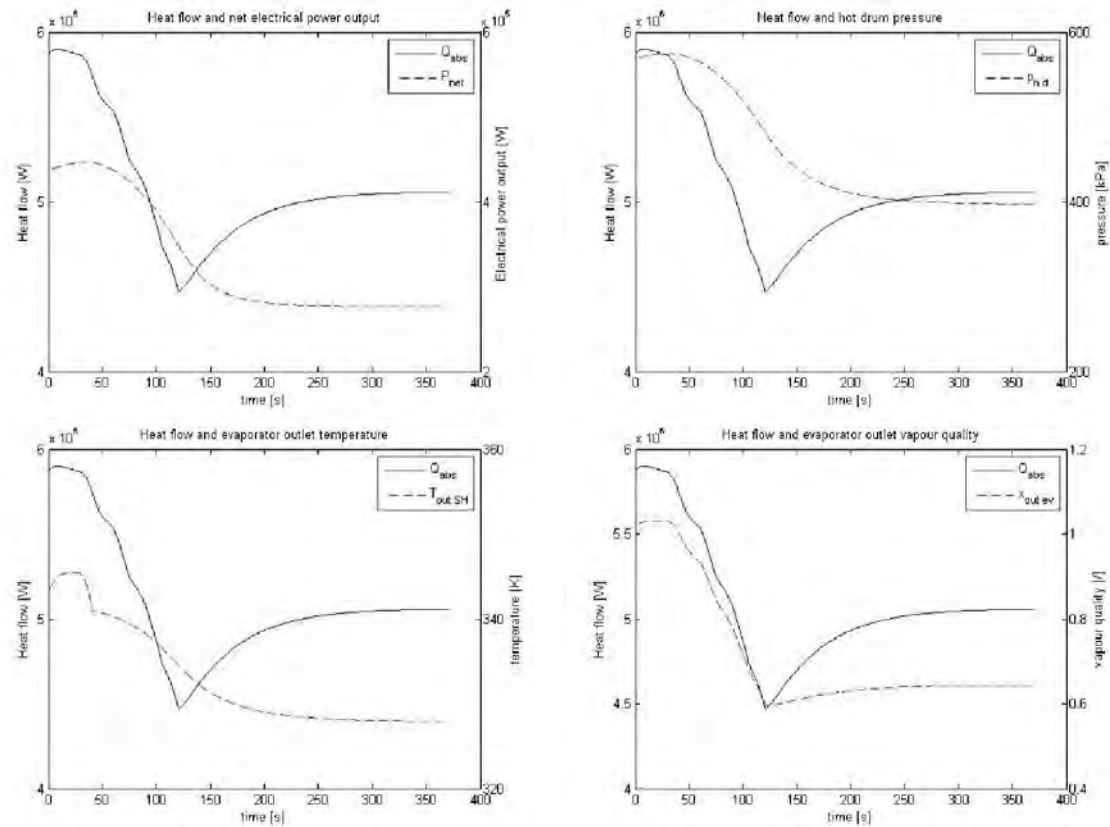


Figure 5.20

Clockwise, from upper left: Net electrical power output, evaporation pressure, evaporator outlet temperature and vapour quality at the exit of the evaporator (green line). Blue line shows heat input of the ORC during transient phase. R-245fa ORC, Test case B, No control.

Trends are similar to the ones characterizing dynamic simulations of the ORC with R-134a as working fluid.

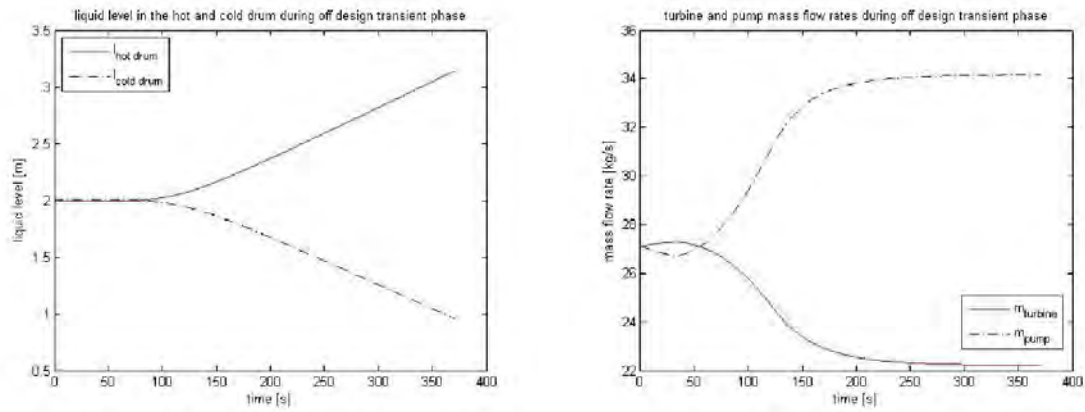


Figure 5.21

On the left: liquid level in the hot drum (red line) and the cold drum (blue line) during transient phase.  
On the right: turbine (red) and pump (blue) mass flow rate during transient phase.

As in the case of R-134a ORC, a control must be added to avoid complete emptying or filling of both the hot and cold capacity (see Figure 5.21). Simulations have been carried out, and main results are exposed in the following. To be noted that, due to the higher change of the service speed respect to test case A, a longer simulation time was necessary to reach a complete stationary condition of the system. Figure 5.22 exposes main simulation results.

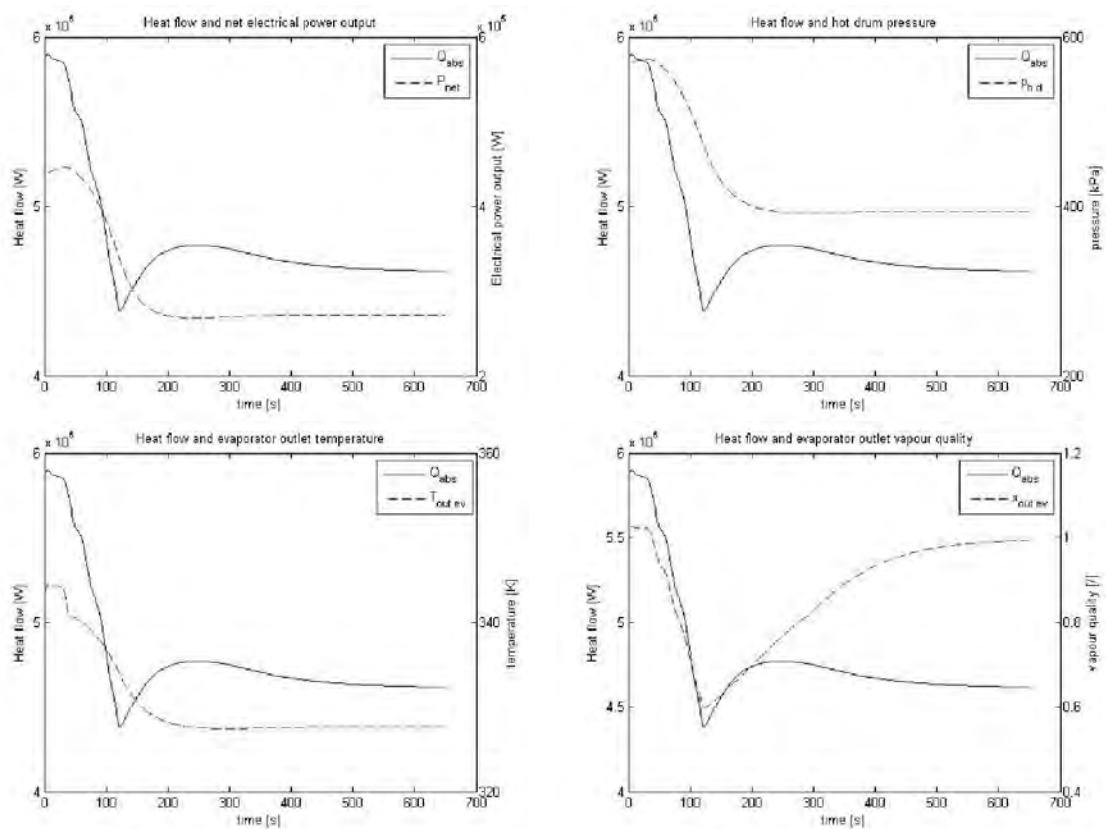


Figure 5.22

Clockwise, from upper left: Net electrical power output, evaporation pressure, evaporator outlet temperature and vapour quality at the exit of the evaporator (green line). Blue line shows heat input of the ORC during transient phase.  
R-245fa ORC, Test case B, Controlled.

Electrical power output passes from 437 to 272 kW<sub>el</sub>, which corresponds to the 62% of the nominal electrical output. Similar result emerges from uncontrolled model (276 kW<sub>e</sub>). As can be noted from Figure 5.23, control system allow avoiding complete emptying or filling of both the capacities.

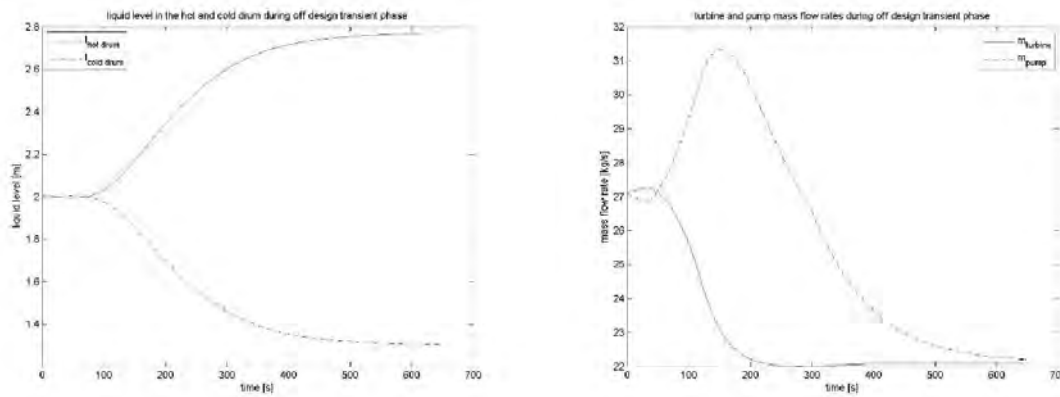


Figure 5.23

On the left: liquid level in the hot drum (red line) and the cold drum (blue line) during transient phase. On the right: turbine (red) and pump (blue) mass flow rate during transient phase.

## 5.5 Summary

This chapter presented test cases for the dynamic simulation of the dynamic models exposed in Chapter 4. Two test cases were defined: test case A simulate a mild deceleration of the vessel (from 18.4 to 16.5 kn in 100 seconds), followed by a brief steady-state condition (50 seconds) and a slight increment of the service speed (from 16.5 to 17.5 kn in 100 seconds). Test case B simulate a brutal deceleration ramp of the vessel's service speed, which decreases from 18.4 to 12.5 kn in 90 seconds. Basing on the work of Soffiato [17], the number of operating engines and their load during transient phase were evaluated, allowing the heat flow input of the bottoming ORC to be defined.

Simulations were carried out, and results show that the model can represent dynamic response of the bottoming ORC, allowing power output, electrical efficiency and main thermodynamic parameters to be estimated and monitored. Considering the system working without a control system, a significant filling of the hot drum and, conversely, emptying of the cold drum emerge. To avoid complete emptying or filling of the capacities, a control system acting on the rotational speed of the feed pump have been implemented. Liquid level inside the hot drum was choose as input for the control system. Simulation results show that control system allows the liquid level inside both the hot and cold drum to undergo a smooth variation, avoiding complete filling or emptying of the capacities.

Results also show that the implemented control strategy is not particularly effective in terms of thermal efficiency, since it does not enhance heat recovery and power generation during transient phases. Further works could deal with this issue: an



optimal control strategy that allows the heat recovery and the power output of the bottoming ORC to be maximized even during transient phases.

# CONCLUSIONS

## Results of the work

An off-design dynamic model of an Organic Rankine Cycle (ORC) exploiting low grade waste heat has been developed. A literary review of the numerical approaches to use in the modelling process has been first conducted, focusing on their application in dynamic modelling of thermal systems. Sequential approach has been chosen to numerically solve the model, allowing an object-oriented modelling process. Each component of the ORC system was modelled separately, as a single block. Overall model of the energy system derives from the interconnection of blocks referring to real components.

Some components have been modelled taking into account their capability of storing mass and energy, and differential equations have been set to evaluate the evolution in time of state variables. Capacities, such as the hot drum and the cold drum, and heat exchangers were modelled following this procedure. Great effort was dedicated to the dynamic modelling of the latter, particularly evaporator and condenser, since their behaviour strongly influences dynamic response of the overall system. Finite volume method was adopted to model heat exchangers. Time derivative of state variables were calculated from differential form of mass and energy balance equations. Subsequently, they were numerically integrated using proper Simulink® functions.

Turbomachinery, such as feed pump and turbine, have been modelled neglecting their storing capabilities. Characteristic maps have been used to define the performance of these components. Finally, also a static model of a single-phase heat exchanger have been developed basing on the effectiveness-NTU method. Time behaviour of these components has been described as a sequence of steady-state conditions, according to the quasi-steady approach.

The over introduced models have been used to analyse the dynamic response of two ORC power plant, which recover the low grade waste heat rejected by the main ICEs of a real LNG carrier. First configuration is a superheated ORC with an electrical output of 404.5 kW<sub>el</sub>, which uses R-134a as working fluid. The second one is a saturated ORC, with R-245fa as working fluid, which generates 424.6 kW<sub>el</sub>. Heat flow input of the bottoming ORC was varied in function of the service speed of the vessel, considering a mild (test case A) and a brutal (test case B) variation of the speed. First, simulations have been carried out without the application of any control system. Results showed that, during transient phases, a significant discrepancy between the mass flow rates processed by turbine and feed pump occurs, leading to the emptying, or filling, of the hot and cold drum. To avoid the complete emptying or filling of the capacities, a control system have been implemented. Such a controller acts on the rotational speed of the feed pump, receiving as input the liquid level within the hot drum placed downstream the evaporator. Simulation results show that control system allows the liquid level inside both the hot and cold drum to undergo a smooth variation, avoiding complete filling or emptying of the capacities. In the case of R-134a ORC, liquid level in hot and cold drum during the test case B simulation varied of about 37 % respect to the initial value. Similar results derived from analogous test case carried out with the R-245fa ORC model.

In summary, even if the models are not validated, they provide reasonable results. However, the aim of this work was not only to develop a dynamic model of a specific energy system, but also to create flexible and versatile models of some basic energy system's component. Subroutines developed for design and off-design dynamic models are easy to modify. Thus, new configuration of the system, different working fluids and characteristic maps for turbomachinery can be easily set.

## Notes for further works

Some simplifications have been introduced to develop the off-design dynamic model presented in this work. First, a simple counterflow pipe in pipe configuration was considered for the heat exchangers, even if heat exchangers used in real plants generally are shell and tube. Further works should also take into account head losses and the thermal inertia relate to the metal wall in heat exchange processes.

In order to model flow nucleate boiling and flow condensation, Chen's correlation and Cavallini-Zecchin correlation were adopted. Since developed model can be easily modified, more recent and more accurate empirical correlation could be implemented to describe heat transfer phenomena during phase-change processes. Analogous considerations are applicable to characteristic maps implemented in turbomachinery models: real maps can replace the ones implemented in the current model, enhancing its accuracy.

Simulations have been carried considering a variation of the input heat flow of the ORC, while mass flow rate and inlet temperature of the cooling water flowing in the condenser have been considered as constant value. Further works could investigate the effects on system's dynamics given by alterations of the boundary conditions at the condenser.

Since it was not the primary goal of this work, simple control system have been developed and implemented. It regulates rotational speed of the speed pump avoiding the complete emptying, or filling, of the hot and cold drum. However, simulation results show that such a controller does not improve significantly heat recovery, electrical power output or cycle efficiency. Thus, further works should deal with this issue, building-up an effective control system. This can significantly enhance the potential of these dynamic models.

Finally, due to the lack of experimental data, dynamic models were not validated. A validation process allows some, unavoidable, imprecisions to be corrected, enhancing the model's accuracy.



## References

- [1] B. F. Tchanche, G. Lambrinos, A. Frangoudakis and G. Papadakis, "Low-grade heat conversion into power using organic Rankine cycles - A review of various applications," *Renewable and Sustainable Energy Reviews*, no. 15, pp. 3963-3979, 2011.
- [2] S. Quoilin and V. Lemort, "Technological and Economical Survey of organic Rankine cycle Systems," in *Economics and Management of Energy in Industry, 5th European Conference*, Villamoura, Algarve, 2009.
- [3] C. Sprouse III and C. Depcik, "review of organic Rankine cycles for internal combustion engine exhaust waste heat recovery," *Applied Thermal Engineering*, no. 51, pp. 711-722, 2013.
- [4] y. Dai, J. Wang and L. Gao, "Parametric optimization and comparative study of organic Rankine cycle (ORC) for low grade waste heat recovery," *Energy Conversion and Management*, no. 50, pp. 576-582, 2009.
- [5] A. I. Papadopoulos, M. Stijepovic and P. Linke, "On the systematic design and selection of optimal working fluids for Organic Rankine Cycles," *Applied Thermal Energy*, no. 30, pp. 760-769, 2010.
- [6] V. Macián, J. R. Serrano, V. Dolz and J. Sánchez, "Methodology to design a bottoming Rankine cycle, as a waste energy recovering system in vehicles. Study in a HDD engine," *Applied Energy*, no. 104, pp. 758-771, 2013.
- [7] F. Casella, T. Mathijssen, P. Colonna and J. van Buijtenen, "Dynamic Modeling of Rankine Cycle power Systems," *Journal of Engineering for Gas Turbines and Power*, no. 135, pp. 1-12, 2013.
- [8] I. Vaja, "Definition of an object oriented library for the simulation of advanced energy systems: methodologies, tools and application to combined ICE-ORC power plants," *PhD Thesis*, 2009.
- [9] G. Manente, A. Toffolo, A. Lazzaretto and M. Paci, "An Organic Cycle off-design model for the search of the optimal control strategy," *Energy*, no. 58, pp. 97-106, 2013.
- [10] D. Wei, X. Lu, Z. Lu and J. Gu, "Dynamic modeling and simulation of an Organic Rankine Cycle (ORC) system for waste heat recovery," *Applied Thermal Engineering*, no. 28, p. 1216-1224, 2008.
- [11] J. Zhang, W. Zhang, G. Hou and F. Fang, "Dynamic modeling and multivariable control of organic Rankine cycles in waste heat utilizing

- processes," *Computers and Mathematics with Applications*, no. 64, p. 908–921, 2012.
- [12] H. Xie and C. Yang, "Dynamic behaviour of Rankine cycle system for waste heat recovery of heavy duty engines under driving cycle," *Applied Energy*, no. 112, pp. 130-141, 2013.
- [13] S. Quoilin, "Sustainable Energy Conversion Through the Use of Organic Rankine Cycles for Waste Heat Recovery and Solar Applications," *PhD Thesis*, 2011.
- [14] J. M. Jensen, "Dynamic Modeling of Thermo-Fluid Systems with focus on evaporators for refrigeration," *PhD Thesis*, 2003.
- [15] R. F. Boehm, *Design analysis of thermal system*, New York: John Wiley & Sons, 1987.
- [16] P. Colonna and H. van Putten, "Dynamic modeling of steam power cycles. Part I - Modeling paradigm and validation," *Applied Thermal Engineering*, no. 27, pp. 467-480, 2007.
- [17] M. Soffiato, "Design and performance evaluation of an ORC system exploiting the waste heat of the main engines of an LNG carrier," *Master Thesis*, 2014.
- [18] H. Chen, D. . Y. Goswami and E. K. Stefanakos, "A review of thermodynamic cycles and working fluids for the conversion of low-grade heat," *Renewable and Sustainable Energy Reviews*, no. 14, pp. 3059-3067, 2010.
- [19] I. Vaja and A. Gambarotta, "Internal Combustion Engine (ICE) bottoming with Organic Rankine Cycles (ORCs)," *Energy*, no. 35, pp. 1084-1093, 2010.
- [20] A. Shuster, S. Karellas and R. Aumann, "Efficiency optimization potential in supercritical Organic Rankine Cycles," *Energy*, no. 35, pp. 1033-1039, 2010.
- [21] F. J. Fernández, M. M. Prieto and I. Suárez, "Thermodynamic analysis of high-temperature regenerative organic Rankine cycles using siloxanes as working fluids," *Energy*, no. 36, pp. 5239-5249, 2011 .
- [22] D. Mikielewicz and J. Mikielewicz, "A thermodynamic criterion for selection of working fluid for subcritical and supercritical domestic micro CHP," *Applied Thermal Engineering*, no. 30, pp. 2357-2362, 2010.
- [23] T. C. Hung, T. Y. Shai and S. K. Wang, "A review of organic rankine cycles (ORCs) for the heat recovery of low-grade waste heat," *Energy*, vol. VII, no. 22, pp. 661-667, 1997.
- [24] D. Wang, X. Ling, H. Peng, L. Liu and L. Tao, "Efficiency and optimal performance evaluation of organic Rankine cycle for low grade waste heat power generation," *Energy*, no. 50, pp. 343-352, 2013.

- [25] W. C. Andersen and T. J. Bruno, "Rapid Screening of Fluids for Chemical Stability in Organic Rankine Cycle Applications," *Industrial and Engineering Chemistry Research*, no. 44, pp. 5560-5566, 2005.
- [26] J. M. Calm, "The toxicity of refrigerants," in *International Refrigeration and Air Conditioning Conference, Paper 317*, 1996.
- [27] P. S. Bundela and V. Chawla, "Sustainable development through waste heat recovery," *American Journal of Environmental Sciences*, vol. I, no. 6, pp. 83-89, 2010.
- [28] C. Sprouse III and C. Depcik, "Review of organic Rankine cycles for internal combustion engine exhaust waste heat recovery," *Applied Thermal Engineering*, no. 51, pp. 711-722, 2013.
- [29] I. Obernberger, H. Carlsen and F. Biedermann, "State-of-the-art and future developments regarding small-scale biomass CHP systems with a special focus on ORC and Stirling engine technologies," in *International Nordic Bioenergy 2003 conference*, 2003.
- [30] J. W. Lund, "Characteristics, development and utilization of geothermal resources," *GHC Bulletin, Geo-Heat Center, Oregon Institute of Technology*, 2007.
- [31] A. Bejan, G. Tsatsaronis and M. J. Moran, *Thermal Design & Optimization*, New York: John Wiley & Sons, 1996.
- [32] S. Rech, "Analisi e ottimizzazione della configurazione di un macrosistema di conversione di energia," *PhD Thesis*.
- [33] A. Lazzaretto and A. Toffolo, *Notes from the lectures of "Energy Systems"*, Padova: CUSL, 2012.
- [34] H. van Putten and P. Colonna, "Dynamic modeling of steam power cycles: Part II - Simulation of a small simple Rankine cycle system," *Applied Thermal Engineering*, no. 27, pp. 2566-2582, 2007.
- [35] S. Quoilin, R. Aumann, A. Grill, A. Shuster, V. Lemort and S. Hartmut, "Dynamic modeling and optimal control strategy of waste heat recovery Organic rankine Cycles," *Applied Energy*, no. 88, pp. 2183-2190, 2011.
- [36] K. J. Åström and R. Bell, "Drum-boiler dynamics," *Automatica*, no. 36, pp. 363-378, 2000.
- [37] C. Bonacina, A. Cavallini and L. Mattarolo, *Trasmissione del calore*, cleup editore, 1989.
- [38] F. Incropera and D. De Witt, *Fundamentals of Heat and Mass Transfer*, John Wiley & Sons, 2001.
- [39] E. W. Lemmon, M. L. Huber and M. O. McLinden, "NIST standard reference database 23: REFPROP - Reference fluid thermodynamic and transport properties," NIST Physical and chemical properties division, 2007.

- [40] L. Rossetto, Notes from the lectures of Applied Thermodynamics and Heat Transfer, 2012.
- [41] G. Comini e G. Cortella, Fondamenti di trasmissione del calore, SGEEditoriali Padova, 2005.
- [42] J. C. Chen, "Correlation for boiling heat transfer to saturated fluids in convective flow," *I & EC Process Design and Development*, vol. V, no. 3, pp. 322-329, 1966.
- [43] A. Dalkilic and S. Wongwises, "Intensive literature review of condensation inside smooth and enhanced tubes," *International Journal of Heat and Mass Transfer*, no. 52, p. 3409–3426, 2009.
- [44] A. Dalkilic and S. Wongwises, "Two-Phase Heat Transfer Coefficients of R134a Condensation in Vertical Downward Flow at High Mass Flux," in *Heat Transfer - Theoretical Analysis, Experimental Investigations and Industrial Systems*, In Tech, 2011.
- [45] R. Sánta, "The Analysis of Two-Phase Condensation Heat Transfer Models Based on the Comparison of the Boundary Condition," *Acta Polytechnica Hungarica*, vol. IX, no. 6, pp. 167-180, 2012.
- [46] G. Cornetti, Macchine Idrauliche, Torino: il capitello, 2006.
- [47] M. Soffiato, C. A. Frangopoulos, G. Manente, S. Rech and A. Lazzaretto, "Design and performance evaluation of an Organic Rankine Cycle system exploiting the low grade waste heat of the main engines in a LNG carrier," in *PROCEEDINGS OF ECOS 2014*, Turku, Finland, 2014.
- [48] Y. Dai, J. Wang and L. Gao, "Parametric optimization and comparative study of organic Rankine cycle (ORC) for low grade waste heat recovery," *Energy Conversion and Management*, no. 50, pp. 576-582, 2009.
- [49] T. Wang, Y. Zhang, Z. Peng and G. Shu, "A review of researches on thermal exhaust heat recovery with Rankine cycle," *Renewable and Sustainable Energy Reviews*, no. 15, p. 2862– 2871, 2011.
- [50] M. Soffiato, "Design and performance evaluation of an ORC system exploiting the waste heat of the main engines of an LNG carrier," *Master Thesis*, 2014.
- [51] W. F. Stoecker, Design of Thermal Systems, New York: McGraw-Hill, 1989.